Winter 2020

Using Strontium Coated Clay Nanoparticles For Bone Regeneration And Other Biomedical Applications

Anusha Elumalai

USING STRONTIUM-COATED CLAY NANOPARTICLES FOR BONE REGENERATION AND OTHER BIOMEDICAL APPLICATIONS

by

Anusha Elumalai MS, MS, MS, MS

A Dissertation Presented in Partial Fulfillment
of the Requirements of the Degree
Doctorate in Philosophy

COLLEGE OF SCIENCE AND ENGINEERING
LOUISIANA TECH UNIVERSITY

March 2019

LOUISIANA TECH UNIVERSITY

OCTOBER 21, 2019
Date

We hereby recommend that the dissertation prepared under our supervision by

Anusha Elumalai MS, MS, MS, MS

entitled **Using Strontium Coated Clay Nanoparticles For Bone Regeneration And Other Biomedical Applications**

be accepted in partial fulfillment of the requirements for the Degree of

Master of Science in Molecular Science and Nanotechnology

Supervisor of Dissertation Research

Head of Department

Department

Recommendation concurred in:

Advisory Committee

Approved:

Director of Graduate Studies

Approved:

Dean of the Graduate School

Dean of the College

GS Form 13
(8/10)

ABSTRACT

The aim of this project is to coat halloysite nanotubes (HNTs) with strontium in an eco-friendly, simple, and non-expensive process. These particles, when doped in calcium phosphate cements (CPC), are predicted to increase the osteoconductive and antibacterial properties of three dimensional (3D) printed bone scaffolds.

The purpose of the 3D printed bone scaffolds is to assume the same function as the bones they are replacing but with several additional functionalities. These biomaterials will have the ability to be resorbed as new bone is formed. Due to inherent osteogenic factors and antibiotics released from doped HNTs during the reparative process, it will also provide surgeons with a multi-functional construct for a diverse set of dental and orthopedic applications. The purpose of the 3D printed scaffolds will be to provide a microenvironment for normal cells along with the ability to release antimicrobial, chemotherapeutics or other drugs. The system will also enable growth factor release.

Material characterization was conducted to confirm the presence of Sr on the HNTs. Cellular characterizations studies assessed cellular impact and behavior and included cytocompatibility studies, osteogenic/osteoinductive, and differentiation effects on pre-osteoblast cells and stromal cells. Material characterization studies included material strength test of the SrHNT/CPC composites. Based on the results, fabrication methods in future will be modified as needed to obtain the ideal medical construct.

APPROVAL FOR SCHOLARLY DISSEMINATION

The author grants to the Prescott Memorial Library of Louisiana Tech University the right to reproduce, by appropriate methods, upon request, any or all portions of this Dissertation. It is understood that "proper request" consists of the agreement, on the part of the requesting party, that said reproduction is for his personal use and that subsequent reproduction will not occur without written approval of the author of this Dissertation. Further, any portions of the Dissertation used in books, papers, and other works must be appropriately referenced to this Dissertation.

Finally, the author of this Dissertation reserves the right to publish freely, in the literature, at any time, any or all portions of this Dissertation.

Author _____

Date _____

DEDICATION

This Dissertation is dedicated to my parents Mr. M. Elumalai & Mrs. Rama Malai and my brother Dr. Divya N. Elumalai for their support, belief, love, and encouragement.

TABLE OF CONTENTS

LIST OF FIGURES

ACKNOWLEDGMENTS

This project was possible because of my mentor Dr. David K. Mills for his belief in me and his unending encouragement even in dire research circumstances. I acknowledge the help of my labmates Dr. Yangyang Luo and Dr. Ahmed Humayun without whose support it would have been difficult to start in a new lab with such ease.

I acknowledge every person who has touched my life in some way and in doing so have contributed to my place here.

I hope that this research, a little drop in the vast ocean of Science and knowledge, holds the power of infinite possibility.

CHAPTER 1

INTRODUCTION

1.1 Use of Nanoparticles in Biomedical Engineering

1.1.1 Need of Medicinal Science

There is a rapidly increasing need in medicine for the development of technologies that can help with the treatment with personalized and specific to individual patient's needs which will include replacement of damaged tissues, drug delivery systems, and biocompatibility. Medicinal science has made advances in types and availability of drugs that can cure many different ailments. The issues surgeons and physicians face are the timely release of the drugs, the release of drugs in the required locations, and the appropriate quantity. In cases of organ or bone replacements surgeries a more biocompatible material is required which has inherent at antibacterial properties, patient specific, and easy availability which are cost effective prices.

Many medical conditions need treatments that can be delivered to the specific area of the ailment. Localized diseases can also be caused by bacteria or fungi. Especially in cases of implants the risk of infections is high. For example, in cases of knee or hip replacement surgeries the failure rate can be due to material tear, aseptic loosening, infection, and instability. For conditions such as advanced osteoarthritis of the knee where the patients loose knee function and are in extreme pain, total knee arthroplasty is the most common and effective surgical process. Although, over the years technology has

improved and reduced the cause of failure due aseptic loosening and material wear, the infection rate on the contrary is increasing [1]. Prosthetics surgeries can cost anywhere from $5000 to $50,000 [2]. Additionally, the prosthetics failures require hospitalization and additional procedure which can cost anywhere from $30,000 to $100,000 per patient [2]. Application of antibiotics can stop or slow bacterial growth and allows body's immune system to mobilize.

Cancer is another disease which has the focus of the scientific community. It is a disease which can be localized or become systemic after it metastasizes. There are many ways that are now being used to inhibit cancerous cells growth. One such treatment is chemotherapeutics which involves use of drugs such as 6-mercaptopurine, cytarabine, gemcitabine, and methotrexate, among many others.

1.1.2 Challenges in Treatment

Challenges in treatment of infections or cancerous diseases include systematic drug delivery. As of now we have many systematic treatments wherein the drug is delivered to the entire body. Hence a much larger dose of drugs is needed which can in turn in then lead to side effects such as hepatotoxicity or nephrotoxicity [3]. If we can assure a localized treatment with the specific disease treating drug then we can prevent the negative side effects. Targeted drug delivery can provide more drugs to be effective for treatment that are found to be toxic or with lower levels of efficiency due to their distribution in the entire body. Recent researches have shown the efficacy of such techniques such as carrier proteins, lipid coats or antibodies.

Biomaterials are latest area of research and medical interest that has led to many innovations. Materials such as bone cements which were approved in the 1970s are now improved by inclusion of smart biomaterials. The additional properties to biomaterials include features like localized drug delivery or sensors to monitor patients' specific conditions. These smart materials are described in a new emerging field of Nanotechnology which is now being increasingly integrated in medical research for targeted drug deliveries or for creation of biomaterials in increased beneficial and novel properties [1-5]. A cheaper version of carbon nanotubes are Halloysites (HNT) which is now showing promise as a novel drug delivery carrier and for creating biomaterials like calcium phosphate cements (CPC) with improved strength. Through added layers deposited onto the HNTs, the pattern of released substances can be further controlled, enabling delayed or inhibited release [5]. These layers can be metal deposits like Gold, Silver, Copper, Platinum, Strontium etc.

1.1.3 Grand Challenges

Grand Challenges was developed in 2008 by the United States National Academy for Engineering based on humanitarian needs and technological developments [6]. The challenge included needs such as affordable solar power, advance health informatics, engineer of better medicines, access to clean water, etc. Three of these challenges related to general health needs good health informatics, better medicines, and clean drinking water. These challenges are interrelated and can lead to better quality of healthcare and personalized medical care. The creation of nanoparticles without producing any toxic waste for enhancing the quality of biomaterials would be a novel process integrating these three challenges and bring positive effect in the quality of medical care.

1.2 Objectives

This research will have a range of objectives with a single goal of advancing the properties of biomaterials by optimizing the use of harmful chemicals or products to make the raw material. The objectives are:

1. To formulate and fabricate green Sr coated HNTs and to evaluate any cytotoxic effect on pre-osteoblast cells.
2. To formulate and fabricate nano-enhanced calcium phosphate cement and to evaluate the mechanical, osteoconductive and osteo-inductive properties
3. To evaluate our green SrHNT for antibiotic activity and effective drug delivery

1.3 Research Need

Metal acetate and metal salts are some of the substances used to deposit metals on the surface of HNTs which possess a negative charge. many processes use chemicals to modify the surface for a modified attachment of metal ions [7]. Many coatings are principally done through a wet chemical process. The majority of these methods are limited in their use of desired chemicals, due to the polarity of the halloysite [7-9]. Additionally, this constraint in the type of chemicals used frequently involves the use of additional toxic chemicals in place of greener options, and characteristically necessitates the use of a significantly longer chemical process to achieve the desired coating. In this study, we will develop an HNT coating method that is simple, efficient and requires no post-processing.

We proposed that HNTs can be coated with metal carbonates compounds, as metal ions donor, and as NMR shift reagents—through a simple breakdown of the salt in

water. This method will result in a free positively-charged metal ion that can readily bond to the negatively-charged HNT exterior, resulting in metallic coatings forming on the HNT surface. In future our coating method may enable greater deposition of coated material onto these nanotubes for the desired application. Furthermore, the use of chemical processes using toxic chemicals is not required, thus eliminating exposure to toxic chemicals and costs associated with the disposal of the resultant chemical waste.

The objective of this study is to improve the anti-infective and mechanical properties of CPCs by embedding them with Sr coated HNTs to incorporate the mechanical strength and drug loading capacity of HNTs and the dual action of osteoconductive, osteoinductive, and antibacterial properties of Sr. We also focused on using SrHNT as cancer and antibacterial drug carriers.

CHAPTER 2

BACKGROUND

2.1 Nanoparticles

We are now in the age of medicinal and technological revolution. From 3D printing a car, silicon chips, to nanotubes we have come a long way. Medicine has also seen that exponential progress which can be seen as increased survival rate and the higher average death age in *Homo sapiens* aka modern man. In spite of all the advancements we still have cases of infection after surgeries in sterile and aseptic environment. An addition understanding in additive manufacturing and recent advances in nanotechnology is vital to comprehend their capabilities in the area of medicine. Nowadays nanoparticles are used as vehicles for drug delivery. HNTs are used as biosensors and drug carriers. Addition of nanoparticles and HNTs to polymeric matrices has also led to improved mechanical strength [1].

2.1.1 Halloysite

Halloysite nanotubes (HNTs) are a form of aluminosilicate with the chemical formula $Al_2Si_2O_5(OH)_4.nH_2O$ [2-4]. They are a naturally occurring clay mineral with a tubular structure and an inner diameter of 10-15 nm and the outer diameter of 50-70 nm, with average linear dimensions of 50-70 nm [1] and are chemically similar to kaolinite [5]. It takes millions of years of hydrothermal process and weathering that result in HNTs from kaolinites [8-9]. Named after Omalius D'Halloy, HNTs was extensively used in the

ceramics industries. HNT was first discovered around 18th century [10-11]. The unique crystalline structure was identified after the invention of X-ray analysis and gained popularity in the field of nanotechnology due to its tubular structure. HNTs have been researched extensively as a delivery system for different chemicals, antibacterial and anticancer drugs, as an adsorbent, and as a nanofiller to improve mechanical and thermal properties, etc. [11-12].

HNTs are structured two layered nanotubes in a dehydrated state forms a hollow lumen. The thickness of the layers depends on the state of hydration such as during hydrated state it is 10Å and 7Å during dehydrated state. The silica layer is on the outer side of the tube and the alumina layer is on the inner lumen surface as seen in **Figure 2-1**. The inner surface of the lumen is positively charged with an external negative surface [14]. The outer surface has low hydroxyl density which is the target for attachment of metal ions for specific applications such as modified surfaces using surfactants, coupling agents, electrostatic adsorption or layer by layer coatings [14-15]. Substances with an overall positive charge such as antibiotics, growth factors, and hormones can be loaded inside the lumen [15-16].

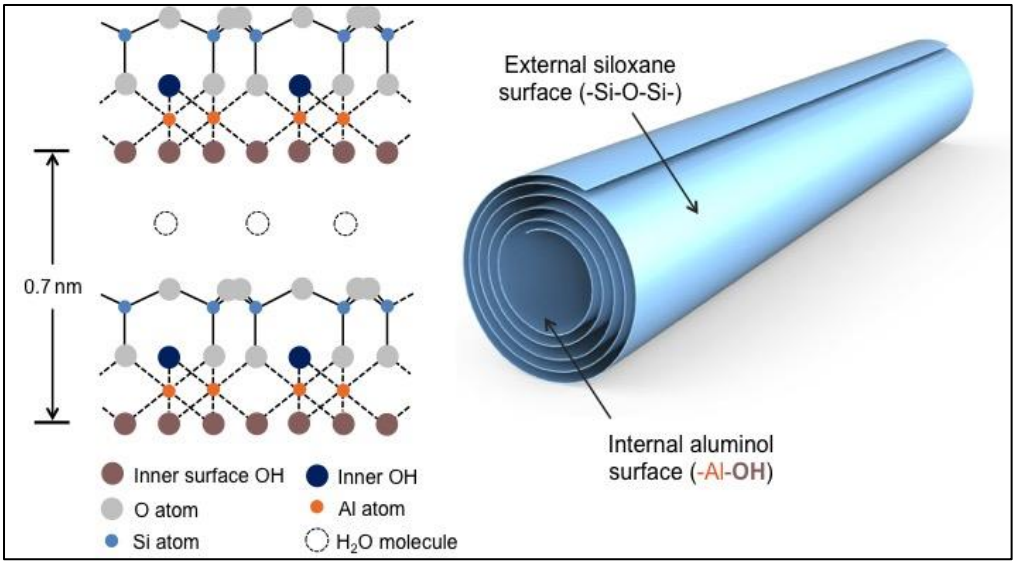

Figure 2-1: Structure of halloysite showing the inner hydroxyl (-Al-OH) surface.

2.1.2 Halloysite Structure Related to Release of Bioactive Agents

The difference in the chemical composition on the different sides of HNT makes it unique among other nanotubes. Both inner and outer surfaces have different ionization and dielectric properties. Both sides can be modified selectively and have many beneficial applications. One of the properties of the HNT based on the charge of the lumen and its diameter is the capability to encase macromolecules including proteins drugs, and Di oxy ribonucleic acid (DNA) [18]. The lumen of HNT is wettable with high capillary force allowing the filling of lumen. The loading of DNA in HNTs probably occurs in the lumen as its cationic and DNA is anionic comparatively [19]. Such loaded HNTs can be used for external applications. The diameter of the lumen makes it a good container for protein molecules. Since the lumen has a positive charge the proteins with high isoelectric points can be efficiently be loaded in the lumen. In some cases, research have shown non-specific protein and lipid adsorption [20]. HNTs easily adsorbs

polyallyamine hydrochloride, chitosan, etc. [21]. Due to biocompatibility and high loading capacity, HNTs make good carriers as drug delivery vehicles.

2.1.3 Drug Delivery Strategies Using HNTs

There are two ways to administer drugs by conventional methods, orally and through injection.

Insulin administration is affected by its digestion by proteolytic enzymes, speedy degradation, or inactivation along with poor permeability results in low availability [22]. These are suggested to be overcome by loading it in HNTs. Research has shown that drugs such as furosemide, dexamethasone, and niferadine show a pattern of slow release when loaded in HNTs [23-25]. The hollow cylindrical lumen of HNT when loaded by vacuum cycling results in extended drug delivery over time [25]. Due to pressure the chemicals are loaded in the lumen but these chemicals can be coated externally also. For the drug release the desorption of the active agent from the outer surface and ends of the tubes occurs first, then the drugs inside the lumen are released more slowly through pore diffusion. Research has shown that loaded HNT show a 5-10% initial burst release followed by a slower release rate [26]. Through added layers deposited onto the HNTs, the pattern of released substances can be further controlled, enabling delayed or inhibited release [25-26]. HNTs used as filler enhances the mechanical properties of various biomaterials. When these HNTs are coated with metal then their ability to increase the material properties for the biomaterial also tends to show an increase.

2.2 Metal Nanoparticles

Metal nanoparticles have been commonly used in the labeling and tracking of stem cells [27]. Magnetic nanoparticles (MNPs) are currently being explored as a means for manipulating stem cell commitment, in particular, for the regeneration of bone and cartilage to combat various orthopedic diseases [28]. Gold and silver nanoparticles have seen considerable interest as nanoparticles for a range of biomedical applications in the areas of microbial resistance, anti-cancer, drug delivery, and bioengineered reparative tissues.

2.2.1 Iron Oxide Nanoparticles

Iron oxide nanoparticles, as seen in non-regenerative studies, have been use the labeling and tracking of stem cells [29-30]. Mechanical stimulation (through mechano-transduction) can be used to facilitate stem cell proliferation, differentiation into different lineages, and migration of stem cells bound to RGD receptors on the surface of osteoblasts and with applied cyclical magnetic stimulation over a 3-week period [29-30]. Osteoblasts upregulated osteopontin, a key bone cell marker, and indicator of osteoblast differentiation, maturation, and matrix mineralization [30]. A recent interesting study supports the potential of iron oxide MNPs to promote osteogenic differentiation of human bone marrow-derived using the MAPK pathway [31].

2.2.2 Silver Nanoparticles

Silver nanoparticles possess several unique characteristics including a potent and broad-spectrum level of antimicrobial activity [31]. AgNPs showed enhanced proliferation and osteogenic differentiation of various animal-derived MSCs and promoted fracture healing [33-34]. As an implant coating, AgNPs have also been

effective in promoting bone tissue formation and mineralization on various surfaces [34-35].

2.2.3 Gold Nanoparticles

Gold nanoparticles (AuNPs) have also attracted much attention recently in biomedicine for uses in anti-cancer applications, drug delivery, and regenerative medicine. This is ascribed to its relatively low toxicity compared to other NPs [36]. AuNPs have been shown to regulate MSC differentiation various cell types, such as osteoblasts [37-38], cardiocytes [39], and neuronal cells [40]. AuNPs have also been used to direct stem cell differentiation. AuNPs act on MSCs to activate the Wnt/β-catenin, ERK/MAPK, and p38 MAPK pathways, resulting in the activation of the transcription factors for the osteogenic differentiation [40].

2.2.4 Magnesium Nanoparticles

Magnesium (Mg) is a divalent ion found abundantly in the body and plays an important role in many cellular processes. It is used in human body as activator of enzymes, regulation of neuromuscular activities and central nervous system, synthesis of protein, myocardial contraction and regulation of temperature. Mg is biocompatible and biodegradable and can play a potential role as an implant material [41]. Mg in alloys have been shown to be an excellent candidate for vascular stents, biodegradable orthopedic implants and hyperthermia [42]. Mg has certain advantages over gold nanoparticles such as lower density (1.7 g/cm^3) and hence easier loading on the target site [41]. This density almost mimics the density of human bones. Due to the abundance of this metal, it can be cost effective for clinical use. When MSCs are cultured in presence of magnesium, research has observed a decrease in calcium influx and intracellular calcium

concentration [42]. Mg has been shown to have a positive effect on cell coverage of H9-OCT4ESCs [44]. Osteoporosis and osteopenia have been associated with low concentration of Mg. Since Wnt/β-pathways and activation of Notch signaling are related to bone marrow MSCs osteogenesis, Mg can enhance proliferation in these MSCs and herby increase osteogenesis [45]. Integrins play an important role in activation of intracellular pathway and cell differentiation. Research showed that magnesium improved the attachment of synovial MSCs to osteochondral defect through integrin α3β1 [46]. Increase in concentration of Mg can also stimulate gene expression of TRPM7 to promote osteoblasts proliferation [47].

2.2.5 Zinc Nanoparticles

Zinc has multitude of physiological functions in human body. Zinc and alloys using zinc are progressively promising biomaterials for orthopedic and dental applications [48]. The use of Zinc alloys as biomaterials for making scaffolds mimicking mammalian bone. Zinc leads to an increased ECM mineralization in MSCs and there is a concentration dependent regarding SMCs [48]. Studies have shown that cells preferred Zn ions on the interface of biomaterials rather than it being in diffused state when measured as an expression of Zn transporters (ZnT1 and ZIP1) [50-51]. Further research on zinc supplementation in osteogenesis in MC3T3-E1 cells showed increased collagen deposition and mineralization [51]. Zinc phosphate has shown potential anti-bacterial properties and helped in preventing bacterial colonization, when loaded on barrier membranes. For osteoblastogenesis these actions can be regulated by zinc through the TGF-β/Smad signaling pathway [52]. The increased osteogenic differentiation and mineralization Zinc makes for an excellent candidate as coatings on implants to promote

integration. Adipose derived (AD) MSCs can differentiate into chondrocytes, osteoblasts and neuron like cells. Supplementation by Zn can increase AD-MSCs proliferation and neutrite growth. ERK1/2, BDNF, and JMK are some of the potential molecules involved in the action and regulation of Zn [53]. Wang et al. (2007) reported that Zn^{2+} decreased adipocytic cell formation in mouse bone marrow stem cells leading to mineralization, osteoblast proliferation, bone formation, and inhibition of bone resorption [54].

2.3 Strontium

Strontium (Sr) nanoparticles have been established as metal ions that can lead to a significant improvement in the biological and mechanical properties of many polymers. The growing interest of strontium and nanoclays as implants is based on the effects of Sr on cells to induce osteogenic and osteoinductive properties. Sr is now used in dental implants and orthopedic coatings. Sr may also lead to bone healing process after further remodeling [55].

One of the primary methods to advance the properties of biomaterials is by adding trace quantities of metal elements. These elements play a significant role in enhancing the biological response, increase in mechanical properties, drug release, and control of the degradation rate of biomaterials. There is an increased interest developing over the years for the use of Sr as the additional element. Information about Sr gained momentum in the mid-19^{th} century with an early review published in 1964 [56]. The signaling of vascular endothelial growth factor is essential for stem cell commitment. Research found that Sr triggered the secretion of these growth factors which were associated with RhoA/Rac 1 activation and thereby repressing adipogenesis and activating osteoblastogenesis in gravity induced alteration of cell commitment [57-58]. Sr treated MSCs was reported to

increase phosphorylation of MAPK ERK1/2 and p38 along with osteogenic differentiation [59]. One of the members of the MAPK family is the ERK1/2 (Extracellular signal related kinase) involved in cellular response to apoptotic promoting signals [59]. Strontium ranelate in lower doses can enhance hASC osteogenic differentiation but higher doses can cause hASC apoptosis by activating ERK signaling pathway [60]. This information lay a solid foundation for Sr containing scaffolds for use in bone engineering.

2.3.1 History of Strontium

Strontium was first discovered in a mine in 1790 and isolated in 1808 [56]. A soft silver-white chemical element with an atomic number of 38, strontium (Sr) is an alkaline earth metal which is not hazardous when occurring in a naturally stable form [61]. It readily oxidizes to form an oxide yellowish in color. It comprises only 0.02-0.03% of the earth's crust and is widely available. It occurs naturally on earth and found mainly as carbonate ($SrCO_3$) and sulfates. Sr in plants acts as a growth stimulant and in Chorella plant Sr can replace Ca requirements [61]. Sr is not a highly essential element in our body but can prevent caries in rats when administered in moderate amounts. Research has shown that Sr taken as Sr ranelate increase bone Ca and reduces fracture percentage in osteoporotic patients [62-62]. Data on the requirements of Sr in bones is scarce and more research is needed in that aspect of bone repairs, since research has shown Sr is the only trace metal that correlated with bone compression. Excessive amounts of Sr or Sr overdose causing toxicity in humans have not been reported yet. However, if high quantities of Sr are delivered intravenously, it has shown to result hypocalcemia due to renal secretion of Ca [64-65]. Research has shown that dietary digestion of large amounts

of Sr varies in hens and pigs [66-67]. Till date only known genotoxic carcinogen is Strontium chromate [68-69]. Human body differentiates the use between Ca and Sr based on the body functions for example mammary secretions, renal absorption, and gastrointestinal absorption [70]. Though Sr absorption decreases with age, consumption of Vitamin D promotes the intestinal absorption. This difference in the absorption rates of Sr and calcium can be attributed to the smaller size of Ca atom. In recent times Sr is being investigated as pharmacological substance in cells and organs mimicking the actions of Ca although the stimulated response is comparatively weaker [70]. Research showed that Sr ions were effective in insulin mediated glucose cell uptake when there was a Ca and Mg ions deprivation to a certain extent [68].

2.3.2 Strontium versus Calcium

Sr can form divalent cations in biological fluids and has protein binding capacity in plasma or serum similar to calcium. Sr falls after calcium in the periodic table and shares many similar properties. It is softer than calcium with a lower melting point of 777^{o}C and a boiling point of 1655^{o}C comparatively [72]. Sr forms coprecipitates such as anhydrite and calcite in presence of calcium and a slightly higher pH [72-73]. The density of Sr is 2.64 g/cm^{3} and is very close to calcium with a density of 1.54 g/cm^{3} [73]. The amount of Sr in human skeleton is about 0.035% of the total Ca content [66]. RadioSr does not stay in the body for a long time and is cleared immediately after it is injected. By the process of diffusion Sr transverses, the walls of the Harvesian capillaries and reaches the extracellular fluid of bones. Due to its similarities with calcium, Sr is incorporated in bone repair as Sr^{2+} (ions) are bone-seeking and can stay in the body for a long time [74]. The response of signaling principle and metabolic pathways for calcium

follow Sr albeit the effects are weaker but have almost similar protein binding capacity [74]. The important difference in the response of Sr and Ca to accumulation in the bone is due to the fact the amount of Sr is less compared to Ca. Sr has been shown to have a dual effect of the development and inhibition of degradation by enhancing osteoblast and inhibition of osteoclast activities. Researchers have proposed that Sr turns on the signaling pathway associated with calcium-regulated bone metabolism by acting on the calcium-sensing receptor (CaSR) of bone forming cells [75]. It has been shown that under the effect of Sr there is a decrease in inhibitors of Wnt-pathway and increase in β-catenin expression marking an increase transcription of osteogenic factors and prostaglandin expression [76]. Some animal studies show that Sr can substitute Ca in some physiological process like blood clotting and muscle contraction although to a lesser extent. It may be due to its smaller size, Ca is transported more easily than Sr in lactation, renal excretion, placental passage, and gastrointestinal absorption [74]. The toxicity of Sr in human body is not very pronounced [68-69], hence supervised administration of Sr is possible without any deleterious effect on physiological functions and human organ systems. The capacity of CPC to host ions like Sr^{2+} can lead to bone cell response over the generally used growth factors have an impact on bone healing therapeutic methods of modern regenerative medicine.

2.4 Metal Coating Procedures

Halloysite is an abundant natural nanomaterial with deposits in France, China, Belgium, and New Zealand. Due to the ease of availability, functionalization, and defined structures, HNT based nanocomposites is now being researched for many decades owing to their tubular structure, hydrophobicity, ion exchange, and physiochemical properties

[77]. HNTs have also been used for catalytic [77], antibacterial [78], magnetic [79], electrical [80], and energy storage applications [75-78]. Recent research has also focused on interfacial relationship of these nanoparticles. Based on those results surface modification of HNT is gaining prominence as a host for different functional compounds such as drugs and bio-molecules. Most research on metal deposition on HNT focus on transitional metals such as Ag, Au, Pt, Ru, and Pd. Some of the methods used are Solvothermal method, Dry sintering, Silanization, etc.

2.4.1 Solvothermal Synthesis

Solvothermal is a system dependent process method is a chemical reaction occurring at high temperatures and pressures which changes the fundamental properties of the solvent [81]. Since density, ionic product, viscosity, dielectric constant, thermal conductivity, and heat capacity are temperature and pressure dependent, the solvent properties can be adjusted based on these two parameters [81-82]. For example, when the temperature increases the dielectric constant decreases resulting in a solid phase precipitate of ionic species. Similarly, the Sol-gel process involves a wet chemical method where formation of a sol (inorganic colloidal suspense) and the gelation of the sol in a gel (continuous liquid phase) to form a 3D network structure [83]. Sol-gel is performed at low temperatures and an acid or base is used to catalyze the reaction which can alter the hydrolysis and condensation [83-84]. The specific interaction between the drug, adsorption solvent and the sol-gel interface determine the deposition of the kind of molecules adsorbed on the HNTs [84]. The advantages of solvothermal process is that it is a one step process, it has pH sensibility, and high photocatalytic activity [85]. The disadvantages of such a method is the use of acids, bases or other harsh chemicals as

solvent or catalyst, specific requirements for oven for creating an atmosphere of high temperature, it is time consuming, and not cost effective.

2.4.2 Silanization of HNT

Aminofunctional silane can be applied to nanoparticles to improve adhesion thus control and increase the amount of metal on the surface. Due to the absence of chemical bonding, the naturally treated HNT have low adhesion to certain metals. Modified HNT surface with an organo-silane finds uses in fields of anticorrosion, enzyme immobilization, and nanocomposite materials [86]. In silanization method the surface of HNT is modified by using γ-aminopropyltriethoxysilane (APTES) which leads to Pd/NH^2-HNT as seen in **Figure 2-2** [75].

APTES is a toxic substance (MSDS health score=3) The chemical is carefully used under hood since it creates fumes which are destructive to the upper respiratory tract and mucous membranes. This compound acts on the kidneys, liver, and nerves hence the use of APTES is done under extreme precaution.

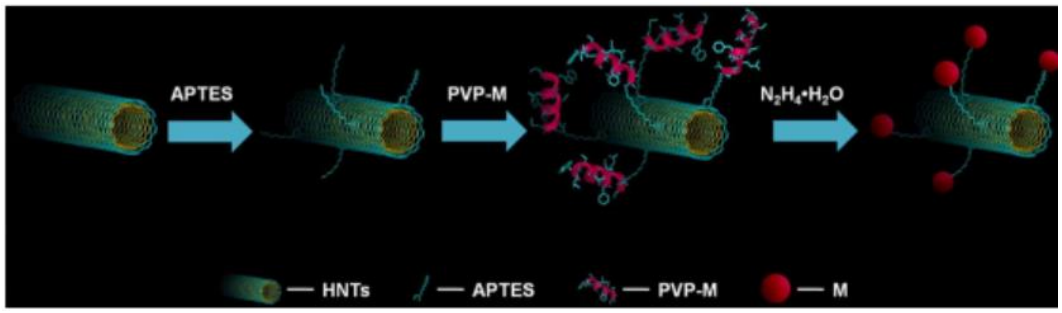

Figure 2-2: Palladium (Pd) nanoparticles deposited on the surface of halloysite nanotubes (HNTs) modified with γ-aminopropyltriethoxysilane (APTES) to produce Pd/NH^2-HNTs nanocomposites.

The advantages of this method are that the surface property of the NH^2-HNT is beneficial in improving the dispersion and loading of Pd which can be uniformly distributed with smaller particle size. This can lead to higher catalytic activity of the product. The disadvantages of this method are it requires very specific binding which uses very toxic and harsh chemicals. It is a cumbersome and expensive process.

2.4.3 Dry Sintering Method

For coating of the HNT surface, a layering method is commonly used to achieve the desired coatings onto the exterior surface, using the inherent charge differential between the layers of the nanotubes as the basis for these coatings [88]. In Dry sintering method, metal acetylacetonates—compounds primarily are used in the synthesis of nanoparticles, metal catalysts, and as NMR shift reagents. This method is capable of thermally decaying the metal acetylacetonate molecules, resulting in a free positively-charged metal ion that readily bonds to the negatively-charged exterior of the HNT [86]. Most metal acetylacetonates degrade completely at 300 ◦C, outgassing acetone and carbon dioxide and leaving behind positively-charged metal ions. Due to the negatively-charged outer lumen of the halloysite, these metal ions should readily bond to the outer surface, allowing for a one-step sintering coating [86].

The advantages of this process are it's a simple process with simpler fabrication conditions, environmentally safe, and does not require the use of any caustic material. The disadvantage of this method is that it is not very cost effective as it requires an energy source for operating the oven to keep it going at 300◦C.

The objective of this research was to come up with a single step low cost, environmentally friendly and safe method to coat Sr on HNTs without producing any toxic waste or the use of any harsh chemicals.

CHAPTER 3

BONE CEMENT

3.1 Bone Cement

Today in orthopedic surgeries the most widely used biomaterials are metal implants and bone grafts. Chronic health conditions, such as osteoporosis and bone fractures and injuries, can be treated with surgery only and medications can help only provide so much relief. This method of using tissue engineering methods and implants to restore bio-functionality is defined as regenerative medicine [87]. The best examples of these are the allografts and autografts of bones. The availability of the right size, appropriate shape, with desired bio-functionality, antibacterial properties, biocompatibility and biodegradability is scarce [88].

The biomaterials used in most orthopedics surgeries are bone grafts, metal implants, and bone cements. The intended role of these biomaterials is to restore the functionality of the body part where they are inserted. Bone is capable of repair small injuries but those severe injuries caused by disease like gout, osteoporosis, rheumatoid arthritis, osteo sarcoma, and bone fractures can be repaired by surgeries and medicine only. This restoration of body functions by implants, bone grafts, allografts, or autografts is a good example of Regenerative Medicine [89]. It is often rare to find the biomaterial of right size and shape and results in additional post-operative complications and care. In

such cases bone cements are usually employed in treating joint replacement surgeries and fractures. For example, Arthroplasties surgeries involve complete or partial joint replacements [90]. Such surgeries use industrial built metal implants which are supported and held in place by the surrounding bones and bone cement. This supporting cement is under flexural and shear forces as seen in **Figure 3-1**.

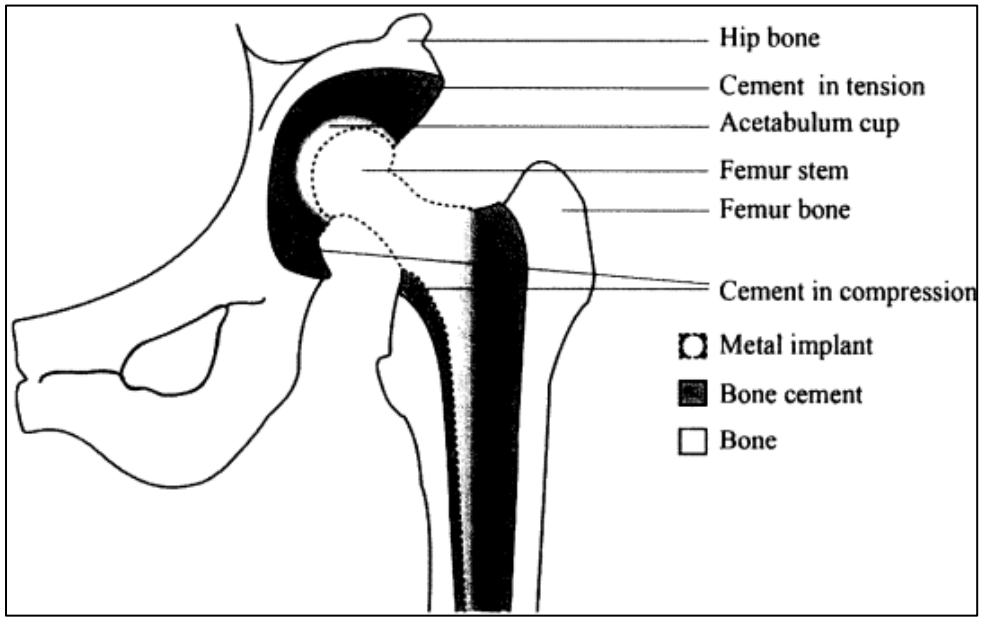

Figure 3-1: Illustration of total hip replacement implant and various forces acting on the cement.

In surgeries like kyphoplasty, vertebroplasty, and compression fractures in the vertebral column, using percutaneous injection the bone cement is injected into the fractured bone [91].

The most widely used commercial bone cement is polymethylmethacrylate (PMMA) [92]. The usual application method is by dry mixing of the bone cement with the drugs and then administered to the body. These cements have an exothermic setting temperature ranging from 70 -120^{o}C during implantation [92-93]. These cements have

other disadvantages such as the addition of antibiotics decreases the mechanical strength and are released quickly but not completely [94]. The methyl methacrylate monomers damage the surrounding tissue as they are toxic in nature and are released at the bone cement interface [94].

Polymeric materials loaded with HNTs have shown an increase in mechanical and material stability and performance [95]. Along with the material properties, these HNTs can enhance the chemical, biological and thermal properties. In recent times HNTs have been used to impart high surface reactivity, increase surface area, mechanical strength, toughness, and thermal stability at a relatively low cost [95-97]. Biomaterials in contact with bone have a fundamentally strong interface to support the mechanical integrity of the supported bone [98]. The mechanical and biological properties of biomaterials like CPCs can also be enhanced using metal coated HNTs.

3.1.1 Calcium Phosphate Cement

CPC in different companies use different forms and ratios of calcium and phosphate salts such as calcium monobasic phosphate, anhydrous calcium diphosphate, calcium diphosphate dihydrate, calcium tri phosphate, tetra calcium phosphate, etc. The cement is usually prepared by mixing two of such calcium salts and making it to a paste by adding a setting liquid. Different researches and companies use various setting liquid such as water, disodium phosphate, saline solution, and chitosan [98]. The calcium and phosphate salts precipitates as crystals of dicalcium phosphate or hydroxyapatite and along with the setting liquid sets into a hard cement mass. Here we use tetra calcium phosphate and di calcium phosphate. The structural formula is seen below in **Figure 3-2**.

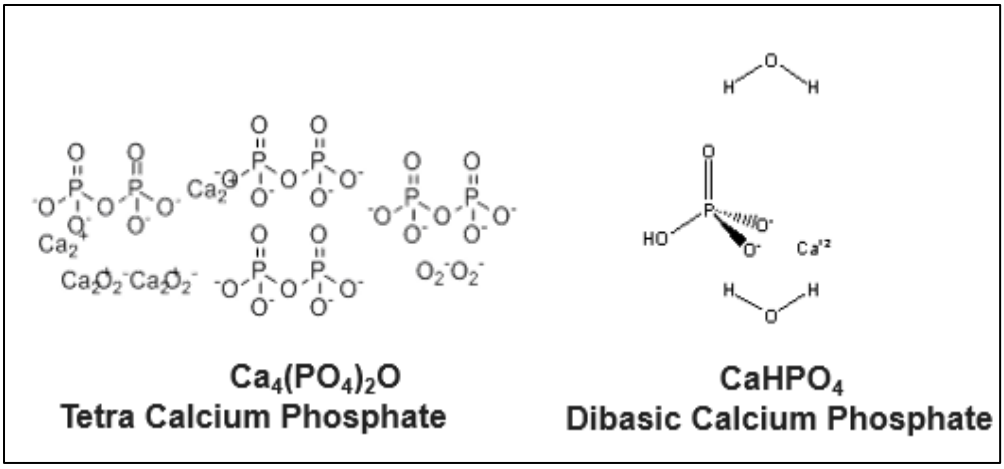

Figure 3-2: Chemical structure of the two calcium phosphate salts used to make CPC in this lab.

Depending on the salts used and the final product the cements are classified in two categories Brushite or Apatite. The difference in these categories is that Apatite, result in HA, are stronger and degrade slowly. Whereas Brushite has anhydrous calcium phosphate as the setting result and it degrades faster comparatively [99].

3.1.2 Chitosan

For our research, we used chitosan as the setting liquid based on the established protocol by previous research conducted in this lab by Uday et al (2017). It is a biodegradable, osteoconductive, and biocompatible polysaccharide, promotes cell attachment and proliferation hence is widely use in bone and tissue engineering. Processed crustacean shells produce chitin which is further processed by deacetylation to produce chitosan. It is a polymer of glucosamine as seen in **Figure 3-3**.

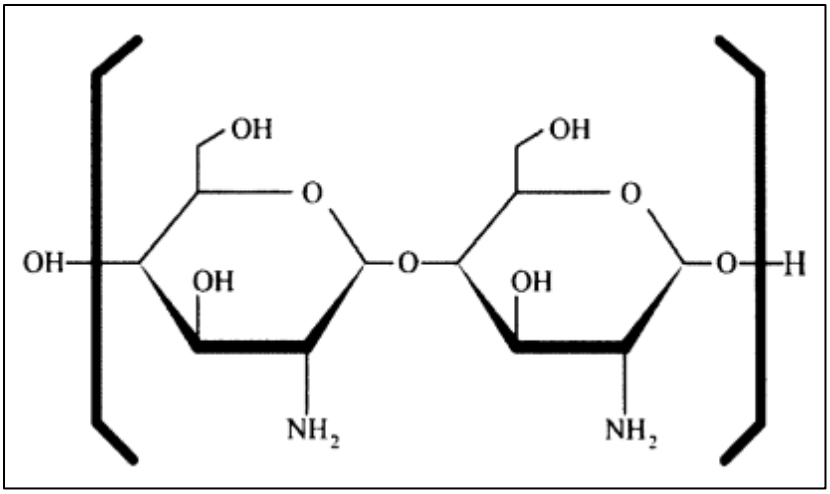

Figure 3-3: Chemical structure of chitosan showing the monomer unit of D-glucosamine

Addition of chitosan in CPC as a setting liquid improves the flexural and compressive strengths [99], also decreases the setting time [98]. The addition of Chitosan reduces or prevents CPC from precipitating or washing out [98]. This property is called cohesiveness or anti washout [98].

3.1.3 Addition of Nanoparticles

CPC are osteo-conductive and biocompatible but with low mechanical properties. Many fillers or polymers can be added to the paste to enhance the mechanical properties. CPCs have numerous advantages over PMMA such as durability, formability, low shrinkage, dense, and a porous nature [94-98]. Research is now being directed to enhance the mechanical and biological properties of CPCs. The addition of HNTs and other nanoparticles have been used as additives and have resulted in improving the mechanical stability of the material and also serving as a drug carrier [94]. Currently, CPCs used in regenerative medicine and orthopedic surgery is restricted to non-load bearing regions such as craniofacial and maxillofacial surgeries only [88]. There is a high demand for developing osteoconductive and osteogenic CPC which have a good load bearing

capacity for 3D printing bones for transplantations [94]. The use of strontium for bone regeneration has garnered significant interest over the past years due to its beneficial properties in treating bone loss associated with osteoporosis [100].

Since Sr and calcium share many chemical similarities, incorporating Sr coated HNTs (SrHNTs) in bone structure will result in a strengthening of the bone and induces bone formation by osteoblasts while reducing bone reabsorption by osteoclasts along with anti-bacterial and drug loading capacity.

CHAPTER 4

DRUG LOADING

4.1 Effective Drug Loading

The worldwide escalation of bacterial resistance to conventional medical antibiotics is a serious concern for modern medicine. High prevalence of multidrug-resistant bacteria among bacteria-based infections decreases effectiveness of current treatments and causes thousands of deaths. New improvements in present methods and novel strategies are urgently needed to cope with this problem. Owing to their antibacterial activities, metallic nanoparticles represent an effective solution for overcoming bacterial resistance. However, sometimes metallic nanoparticles are toxic, which causes restrictions in their use. Recent studies have shown that combining nanoparticles with antibiotics not only reduces the toxicity of both agents towards human cells by decreasing the requirement for high dosages but also increases their bactericidal properties. Combining antibiotics with nanoparticles also restores their ability to destroy bacteria that have acquired resistance to them. Furthermore, nanoparticles tagged with antibiotics have been shown to increase the concentration of antibiotics at the site of bacterium-antibiotic interaction, and to enable binding of antibiotics to bacteria [101]. Several strategies have used in implants such as surface modification or coating with antimicrobial agents to prevent bacterial colonization and biofilm formation [102-103].

The antibiotics used to treat bone infections are given intravenously or orally, through antibiotic-releasing bone cement, or collagen sponges [104-105]. Antibiotics currently used suffer from systemic toxicity, short half-life, and may lead to an increase in antibiotic resistance [106]. Collectively, these approaches have shown limited effectiveness due to the lack of site specificity, uncontrolled release, and ineffective control over microbial growth. Metal nanoparticles are gaining interest as they are effective in controlling pathogenic bacterial and microorganism growth due to targeted delivery [104].

4.1.1 Metal Nanoparticles

Antimicrobial effect of heavy metals has been known and utilized since centuries. Silver was used in wound care and as self-sanitizing cutlery similarly copper has been used in brass for storing water, gold has been used in dental fillings, arsenic has been used in treatment of syphilis [106]. The use of metal can be attributed for causing damage to bacterial cell by production of reactive oxygen species, protein denaturing, and cell membrane damage [107]. Additionally, metals such as silver, copper etc. exert toxicity at low concentrations which is nontoxic to mammalian cells. Reduction of the metal particle size amplifies the toxicity even at low level and in this regard, nanotechnology holds great promise. Silver, copper, zinc, titanium oxide nanoparticles have shown increased efficacy against prokaryotes [108]. Metal nanoparticles find utility in various potential medical applications as biofouling surfaces, implants, topical agents etc., they have the potential to act as a structural reinforcer, stimulate angiogenesis, promote extracellular matrix synthesis, inhibit bone resorption and many have an inherent antimicrobial activity [109]. Multiple factors affect the success of antimicrobial

device including osseointegration, degradation, anti-biofouling, and angiogenesis capability [110]. Incorporation of several metallic nanoparticles having an inherent antimicrobial activity such as silver [110], strontium [111], zinc oxide [112], and copper [113] have been shown further help improve implants by exhibiting anti-biofouling effects.

Metal nanoparticles at higher concentrations exhibit bactericidal effect but toxicity to eukaryotic cell lines as well. Several studies have reported that combinations of the metal nanoparticles can lower the lethal concentration level [114]. Combination of silver, copper, zinc, nanoparticles has shown to exhibit synergistic antimicrobial activity, which can be attributed to increased prokaryotic cell permeability [115-116]. Further, metals when combined with antibiotics, have shown similar augmented antimicrobial effect [117-118]. Metal nanoparticles have been combined with support surfaces such as polymers, ceramics, clay nanoparticles [119]. Metal nanoparticles deposited on halloysite outer surface have also shown enhanced antimicrobial activity [120]. Hydroxyapatite (HA), a widely studied calcium phosphate and bioactive glass suffer drawbacks such low biodegradability and mechanical qualities making them impractical candidates for such applications and require structural modification. These shortcomings can be improved by blending/modification with metal nanoparticles that act as a structural reinforcer, stimulate angiogenesis, promote extracellular matrix synthesis, inhibit bone resorption, and importantly have an inherent antimicrobial activity.

The successful regeneration of bone requires a ‘complete package’ consisting of three integral components: osteoprogenitor cells, osteogenic factors, and osteoinductive/osteoconductive scaffolds [121]. Inherent in any bioengineered design

are these requirements in the scaffold structure: interconnected porosity, adequate mechanical properties, and stimulating healing by inducing chemotaxis, proliferation, and osteoblast differentiation [122-123]. A significant issue with the use of growth factors is specific delivery to the target site and in the required amounts. Many antibiotics or chemotherapeutics are delivered systemically, but their efficacy is limited due the insufficient quantities of drug reaching the affected site [124]. Previous studies have shown that HNTs can stimulate chemotaxis, proliferation, and osteoblast differentiation [125-127], and can be doped with antibiotics, chemotherapeutics, and steroids, and 3D printed into various devices [128]. HA incorporated with strontium [113], zinc [114], silver [119], iron [118], and titanium [112] nanoparticles respectively show improved tensile properties after their addition. Metal nanoparticles including copper [115], strontium [113], and cobalt [118] have also shown strong angiogenic effects.

4.1.2 Antibiotic Delivery

Antibiotics can be delivered either systematically or locally. Local administration has many advantages over systemic such as lower risk of toxicity, low cost, and high concentrations of antibiotics at the targeted site [129]. Loading metal coated HNT can lead to a systemic release locally. It can reduce the drawbacks of systemic delivery and also development of resistant strains. Local delivery of drugs has applications in orthopedics and dentistry. To prevent a cytotoxic effect of the drug it must have a critical concentration of 8-16 μg/ml to 100 μg/ml [129-130]. CPC have been loaded with vancomycin and gentamicin to reduce bone infections in orthopedics

surgeries [131]. Antibiotics have been added to the cement in solid or liquid phase [132-134].

4.1.3 Use of Gentamicin

Gentamicin sulphate is one of the most commonly used antibiotics in cranioplasty. It is highly efficient against infections, although it has shown to have negative influence on cell proliferation [135]. It is important to understand the concentration of use of gentamicin. Gentamicin is an aminoglycoside antibiotic, as seen in **Figure 4-1**, which is not absorbed by the gut when it is administered orally [136]. Hence it is administered through intravenous, or intramuscular injection. It can cause dose related negative side effects such as irreversible hearing loss or nephrotoxicity [135].

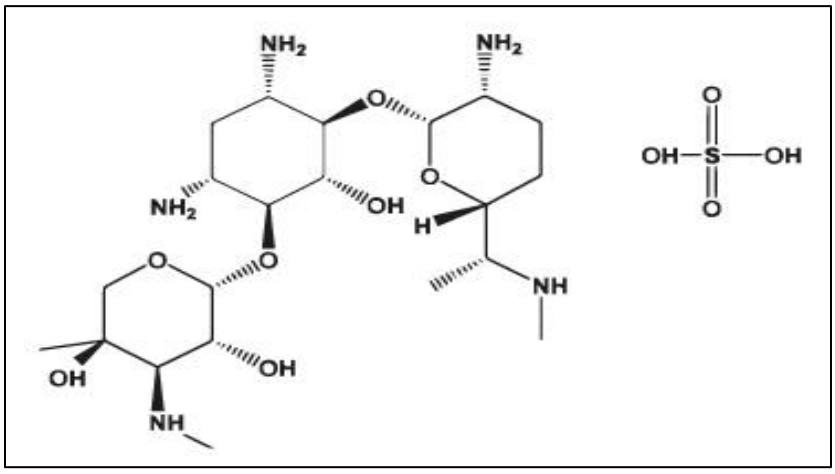

Figure 4-1: Schematic representation of Gentamicin sulphate.

It is impertinent to ensure that the patient does not receive high dose in an instant. Aminoglycosides act on some gram-positive and gram-negative bacteria by inhibiting protein synthesis. Inside the bacterial cell gentamicin binds to the 30S subunit of the

ribosome resulting in the misreading of mRNA causing interruption in normal protein synthesis [137]. Gentamicin is given in slow dose three minutes by bolus injection or over thirty minutes via intravenous injection [138]. The dose also depends on the body and body mass index of the patients. Gentamicin is easily cleared by the kidneys [138]. But it is important to ensure the healthiness of the renal system before administration of this drugs.

4.1.4 Methotrexate

Methotrexate was developed in 1940s as a cancer drug where it effectively stops malignant cells from proliferation and blocks the access of the cells for folate needed by the such cells to survive [139]. The chemical representation of Methotrexate is seen in **Figure 4-2**.

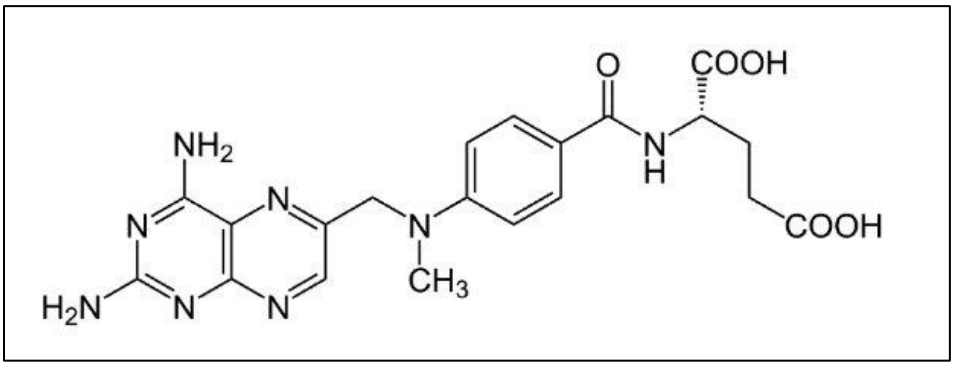

Figure 4-2: Schematic representation of Methotrexate

More recent use of Methotrexate is for treating rheumatoid arthritis and other types of inflammatory arthritis [140]. The dose concentration of this drug is between 10 to 25 mg/week whereas the dose for certain types of cancer is hundreds of times higher [140].

4.1.5 Strontium and Drug Loaded HNT

Based on the promising data that demonstrated the synergistic effects of antimicrobial agents with nanoparticles, we believe that this combination is a potential candidate for more research into treatments for antibiotic-resistant bacteria and other disease. We used this knowledge in creating a complete delivery package that includes antibiotics, or cancer medication to support bone tissue regeneration directly to the infected part by loading SrHNTs with the drugs by vacuum loading.

CHAPTER 5

METHODS

5.1 Materials

5.1.1 To Prepare Sr Coated HNTs

We ordered HNTs from Sigma Aldrich and coated with Sr by adding the HNTs and Strontium carbonate ($SrCO_3$) from Sigma Aldrich in same quantities in distilled water as seen in **Figure 5-1**. The even distribution and preventions of clot formation was done using a sonicator. The reaction mixture (Rm) was sonicated at regular intervals for a duration of 30 minutes for 3 days. The Rm was exposed to three different temperatures. One set was kept at room temperature (25°C), another in incubator (60°C) and the third one was microwaved till boiled.

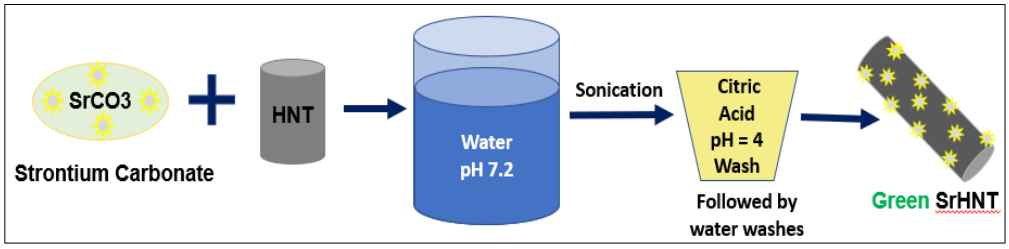

Figure 5-1: Schematic representation of the process to make Green SrHNT

The precipitate obtained was washed in citric acid (pH=4) to remove excess CO_3^{2-} ions and water washed 3 times. The precipitate was collected and dried.

5.1.2 Calcium Phosphate Cement

Two calcium salts were used calcium phosphate dibasic anhydrous (DCPA-$CaHPO_4$) from Sigma Aldrich, St Louis, MO and Tetra calcium phosphate (TTCP-$Ca_4(PO_4)_2O$) was ordered specifically from CaP Biomaterials, E. Troy, WI, for a specific particle size. Chitosan Oligosaccharide Lactate was brought from Sigma-Aldrich, St Louis, Mo. The ratio of the mixture was the one used from previous work which showed the best compressive strengths and anti washout property.

For all the tests four groups of samples were made.

Group 1: CPC

Group 2: CPC with 1% wt HNT, $SrCO_3$, and SrHNT each

Group 3: CPC with 5% wt HNT, $SrCO_3$, and SrHNT each

Group 4: CPC with 10% wt HNT, $SrCO_3$, and SrHNT each

5.2 Material Testing

5.2.1 Compression Test

Cylindrical shaped specimen was made of 12 mm x 6 mm (Length x Diameter) in accordance with the ATSM F-451 standards. Since this project was an extension for the previous work done in this lab, these standards were chosen. The specimens were tested using CellScale UniVert testing equipment with a load speed of 1 mm/min.

5.2.2 Flexural Testing

Cuboid specimen was made of 65 x 10x 4 mm was made using a 3D printed mold to maintain the size and shape of the specimens and subjected to a 3-point bend test. Load speed was 1 mm/min using CellScale UniVert testing equipment. Flexural strength of the CPCs was tested using the following formula.

$$\frac{3FL}{2bdxd} = \sigma$$

Where σ is the Flexural strength, *F* is the peak force, *L* is the distance between the 3 points, *b* is the width of the sample, and *d* is the height of the sample.

5.2.3 Scanning Electron Microscope (SEM)

Sample preparation for SEM was used to analyze the surface of CPCs. S4800 Field Emission SEM, HITACHI was used. The high magnification attained by SEM allowed for a close comparison of the surface morphologies of the HNTs, SrHNTs and the four groups of CPCs.

5.2.4 Energy Dispersive Spectroscopy (EDS)

SEM EDS was performed for HNTs and SrHNTs with the help of EDAX dispersive X-ray analyzer attached to the HITACHI S-4800 SEM to evaluate the elemental composition and weight percentage of Sr on the HNTs. EDS was done at distance of 15mm with an acceleration voltage of 15kV and the spectra was analyzed using the EDAX Genesis software.

5.2.5 X-Ray Diffraction (XRD)

XRD for HNT and SrHNT was done using Bruker D8 Venture diffractometer (Brunker, Karlsruhe, Germany). The scan speed and step size used was 2s and 0.02°. The diffraction patterns were recorded using a Philips PW 1710 X-ray powder diffractometer over 2Θ within 3° and 85°.

5.2.6 Fourier Transformation Infrared (FT-IR) Spectroscopy

FT-IR was done of HNT, $SrCO_3$, SrHNTs discs and the discs of groups 1 and 4, to analyze the composition of the powders using the Attenuated Total Reflection (ATR) method. IR Spectroscopy is usually used for qualitative identification of organic and

inorganic compounds. This method is used for checking presence of functional groups in organic compounds. ATR method was used as it's a more efficient method to analyze a sample to give a more accurate result and has low signal to noise ratio. The discs were prepared by the same procedure.

5.2.7 Multi BET/ Pore Size Testing

Pore size is very important aspect of tissue engineering especially for bones. The large pore size can result in smaller surface areas which can reduce space for cell attachment. Very small pore size will inhibit the migration of cells towards the center and also limit the diffusion of nutrients or removal of waste. The pore size of the different CPCs samples was measured for 1 gm of samples in NOVA 2200 surface area and pore size analyzer. The measurements were done for 0.200 gm first. Since the measurements are more accurate for large quantities the measurement was repeated 2 more times for 1 gm of samples.

5.2.8 Bio-Degradability Test

Stimulated body fluid (SBF) is a fluid created in the lab that mimics the ion concentrations approximately equal to human blood plasma. SBF has been used for invitro assessment to measure biodegradability of many materials. The samples from the four groups of CPC were tested for bio-degradability by comparing the weight reduction over a period of six weeks. The discs were soaked in SBF and stored at 37˚C. The media was changed every two days. The weight of all the samples was measured as dry samples, after soaking, and every week for six weeks.

5.3 Cell Culture

All cells came cryopreserved from ATCC. Cryovials were thawed and allowed to equilibrate in a water bath, all the cells were cultured in 25 cm^2 tissue culture flask and incubated at 37°C under humidified 5% CO_2 and 95% air. Pre-osteoblast and BSC cells were incubated in complete alpha-MEM and Dulbecco's Modified Eagle medium respectively, containing 10% FBS and 1% penicillin. Sub-confluent cells were passaged with 0.25% trypsin, collected by centrifugation, suspended in cell culture medium and cultured at a 1:4 split into 25 $cm.^2$ tissue culture flasks. Cell count was same in all the wells during each testing. The cells went through passage four before use.

5.3.1 Cell Culture and Staining

Mouse pre-osteoblast cell lines MC3T3-E1 (ATCC® CRL-2593™) were obtained from ATCC (Manassas, VA.). These cells were used to evaluate the cytotoxicity and proliferation of all the samples. Proliferation tests for four groups of CPCs was dome on day 1, 7, 14, 21, and 28. Mouse bone marrow stromal cells (BSCs) (ATCC® Crl-12424™ was used. Both the cells lines were seeded in 48 well plates which had 40 mg of the samples on each well. Both cells lines were used to analyze for collagen, acidic mucopolysaccharides and ALPase activity. Osteoconductive tests was done on Day 1, 7, 14, and 21 and osteoinductive tests was done on Day 1, 7, 14, 21, and 28 days. The control was just cells. Cell culture and lab plastics were obtained from MidScientific, St. Louis, Mo. Alpha minimal essential medium (α-MEM) and Dulbecco's DMEM were obtained from GIBCO Invitrogen, Grand Island, NY. Fetal bovine serum and penicillin were purchased from Phenix Research Products (Candler, NC). TryplE, an animal-free

trypsin substitute, and Trypan blue were obtained from GIBCO Invitrogen, (Grand Island, NY).

5.3.2 Cytotoxicity Testing

Live/Dead as a means for estimating the cell viability after exposure to HNTs, SrHNTs and the Four groups of CPCs were assessed by MTS assay. Cells were seeded into 48-well plate at a concentration of 1 X 10^5 cells/ well and cultured for 24 hours. Different amount of pure HNTs or functionalized HNTs were added into cell culture plates (0, 25 and 50 μg/ml). 40 μg of the four groups of samples was added to each well of the 48 well plate. The assay was performed using Biotium cytotoxicity kit. The live/dead assay was performed on day 1,3, and 7. The fluorescence images were taken using Olympus Florescence microscope fitted with a Nikon camera

5.3.3 Cell Proliferation Assay

Cell proliferation ability affected by HNTs and SrHNTs were assessed by MTS assay. Different amount of pure HNTs or SrHNTs were added into cell culture plates (0, 25 and 50 μg/ml). Proliferation assay was conducted on day 1, 3, and 7 days. 40 mg of the four groups of samples was added to each well of the 48 well plate. Proliferation assay was conducted on day 1, 7, 14, 21, and 28 days. Cells were seeded into 48-well plate at a concentration of 1 X 10^5 cells/ well and cultured for 24 hours. 40 μl MTS stock solution were added to each well and cultured for 2 hours at 37°C in darkness. 200ul of supernatant of each sample were transferred to 96-well plates and read absorbance values at 490nm by microplate reader.

5.4 Cell Staining

5.4.1 Picosirus Red Staining

Media was removed from the wells and washed with Phosphate Buffer solution from Dulbecco's (PBS)to quantify the collagen content. The cells were fixed with 95% ethanol for 10 minutes. The cells were washed again with PBS twice. The staining kit had two solutions, the Picosirus stain (PRS) and acetic acid 0.5% (AA). These cells were then stained with PSR for 60 minutes and then washed with AA to remove excess staining. 7% v/v aqueous solution of Glacial acetic acid was used for de-staining. To quantify, the de-staining liquid was measured for staining concentration using Thermo Scientific spectrophotometer at 490 nm.

Since PRS stain showed maximum absorbance at that wavelength. This staining procedure was also used on Pre-osteoblast cells and the images were taken over a period of 28 days under contrast microscope.

5.4.2 Alcian Blue Staining

Cells were fixed as mentioned earlier. Alcian blue (AB) stain was added and removed after 10 minutes. Excess stain was washed with PBS and De-stained by 7% Glacial acetic acid. The detained supernatant was used to measure the optical density at 405 nm in Thermo Scientific spectrophotometry.

5.4.3 ALPase Assay

Alkaline phosphatase is an enzyme characteristic of osteoblast cells, the presence of which shows the ability of the cells to break down phosphate groups from their substrates. ALPase acts on 5-Bromo-4-chloro-3-indolyl phosphate/Nitro blue tenzolium (BCIP/NBT) substrate to give a purple stain. The cells were fixed by the method

mentioned above and the dye was added for 15 minutes. The supernatant was quantified through measurement of its optical density at 405 nm in Thermo Scientific spectrophotometer.

5.4.4 Alizarin Red Stain

This stain is used to detect the calcium present in the wells. The pre osteoblasts cells with the four groups of CPCs was stained with alizarin red stain (Alizarin monosodium sulfonate from Matheson Coleman & Bill Manufacturing Chemists, Norwood, Ohio). The cells were fixed by the method mentioned before and washed 3 times with water and images was taken under Fluorescence microscope in bright image every seven days for four weeks.

5.5 Drug Loading

Drugs were loaded in the HNTs, SrHNTs and HNTSr by vacuum method, washed with water after loading to remove externally attached Gentamicin as seen in **Figure 5-2**.

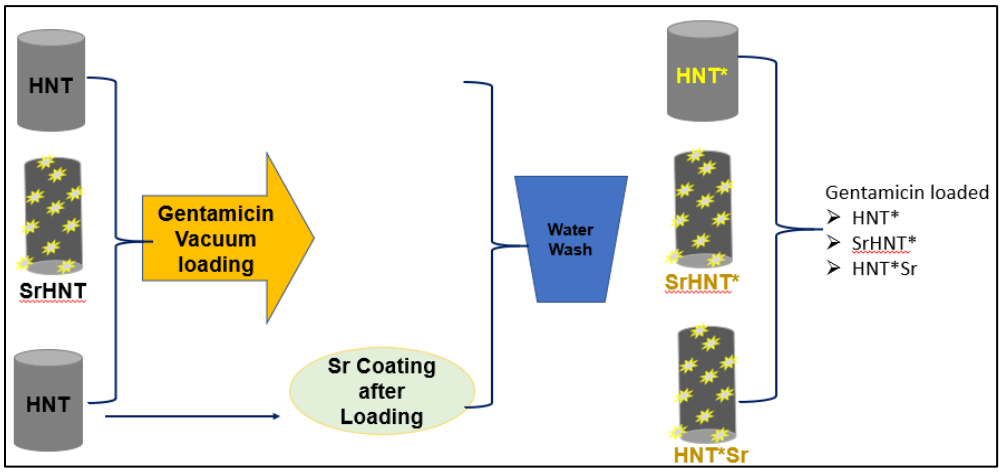

Figure 5-2: Process of loading gentamicin in HNT, SrHNT and HNTSr. HNTSr was HNTs loaded with gentamicin and then located with Sr.

5.6 Bacterial Growth Rate Study

The antibacterial properties of HNT, SrHNT and gentamicin loaded HNTs, SrHNTS and HNTSr (These HNTs were loaded with the drug and then coated with Sr) on *Escherichia coli* (ATCC 35218) and *Staphylococcus aureus* (ATCC BAA-1026) was evaluated.

5.6.1 Micro Titration Method

The effect of HNT, SrHNT and gentamicin loaded HNTs, SrHNTS and HNTSr was evaluated for their effect on bacterial growth rate and drug release using the micro-titration method since they were in powder form. The starting concentration of the sample was 10 μg/ml. It was serially diluted in 4 consecutive wells. Three colony cultures of bacterial was chosen to get 3 repetitions of the tests. Bacteria was grown on Luria-Bertani (LB) broth. The test was conducted in Miller Hilton broth.

5.6.2 Kirby Bauer Disk Susceptibility Test

In this method HNT, SrHNT and gentamicin (concentration 1g/10ml) loaded HNT, SrHNT, and HNTSr in CPC samples was made. The paste was then made into discs 6 mm in diameter, same as the size of the standard gentamicin discs. The discs were impregnated on a Mueller-Hilton agar plate which had the lawn of *E. coli* and *S. aureus* bacteria individually. The inoculation of the bacteria was done when the culture showed an absorbance of 0.08-0.1 at 630 nm which corresponds to 1 to 2 x 10^8 CFU/ml. The plates were then incubated at 37°C for 18 hours. The standards of testing of antibiotics affects are an accepted method by the U.S. Food and Drug Administration and was followed accordingly. The zone of inhibition around the disk was measured and noted. The method was done using cultures from 3 different colonies.

5.6.3 Drug Release Testing

5.6.3.1 *Pre-osteoblast Cells and E. coli*

To test the effectiveness of drug release in a cellular environment infected with E. coli, this test was performed. A 48 well plate was first seeded with pre-osteoblast cells (3.14×10^5/ml) for two days. After which the media was changed and fresh media was added. The media had 2% Trptic soy broth/nutrient media for bacterial growth. The gentamicin loaded HNT, SrHNT, and HNTSr was added to the wells in 3 different concentrations 1, 0.1, and 0.01 mg/ml. The bacterial culture was added in accordance with the standards. The bacterial culture had an absorbance of 0.08 at 630 nm. The plates were incubated at 37°C for 24 hours after which the absorbance. Live/dead assay, and proliferation assay was done to measure the effects of drug release on bacterial growth in pre-osteoblast cells.

5.6.3.2 Mammalian Osteosarcoma Cells

The drug release was also tested on CRL 2836 mouse osteosarcoma cells. The cells (2.76×10^5/ml) were plated in a 48 well plate and incubated for two days. The media was changed and methotrexate loaded HNT, SrHNT, and HNTSr was added to the wells in 3 different concentrations 1, 0.1, and 0.01 mg/ml. The plates were incubated at 37°C for 3 days after which the Live/dead assay and proliferation assay was done to measure the effects of drug release on bacterial growth in cancer cells.

5.7 Statistical Analysis

Statistical analysis was performed using Microsoft Excel Analysis ToolPak plugin and Origin 9.6. All experiments were done in triplicate, and one-way analysis of variance

(ANOVA) with $p < 0.05$ as the significance level was utilized for statistical analysis. Statistically significant data was reported ($p < 0.05$), and all the results were reported as mean ± standard deviation ($p < 0.05$, n=3) unless otherwise specified.

CHAPTER 6

RESULTS AND DISCUSSION

6.1 Project 1: Coating HNTs with Strontium

6.1.1 Surface Topography

The coating of Sr on HNT was done at three different temperatures. The SEM images were taken to confirm the coatings and also confirm the best temperature for coatings of the HNTs. The images of the HNTs coated by Sr at room temperature, 60°C, and microwaved were analyzed for successful coating and can be seen in **Figure 6-1**.

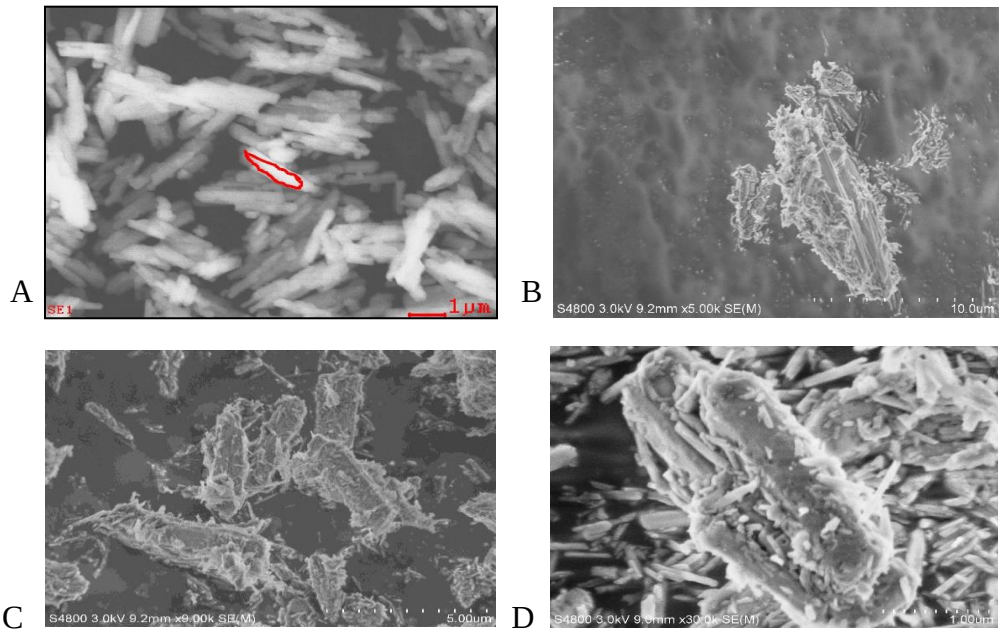

Figure 6-1: SEM images of A) HNT and Sr coated HNTs B) At oven C) Microwaved D) At room temperature.

As the SEM images show the coating of Sr was successful in all the three exposures. Since the coatings were observed at room temperature the experiment was conducted three more times to observe the consistency of the method. There is an irregular but complete coating of Sr on the HNTs as seen in **Figure 6-2**. HNTs by default have a smooth exterior. The $SrCO_3$ hydrolyze into Sr^{2+} and CO_3^{2-} ions when water is added to the salt. Since HNT has a negative exterior surface due to the presence of OH^-, it attracts the positively charges ions to form a bond which can be either a Vander Waal's bond or a weak ionic bond. In both cases the Sr^{2+} gets attached to the surface of the HNTs.

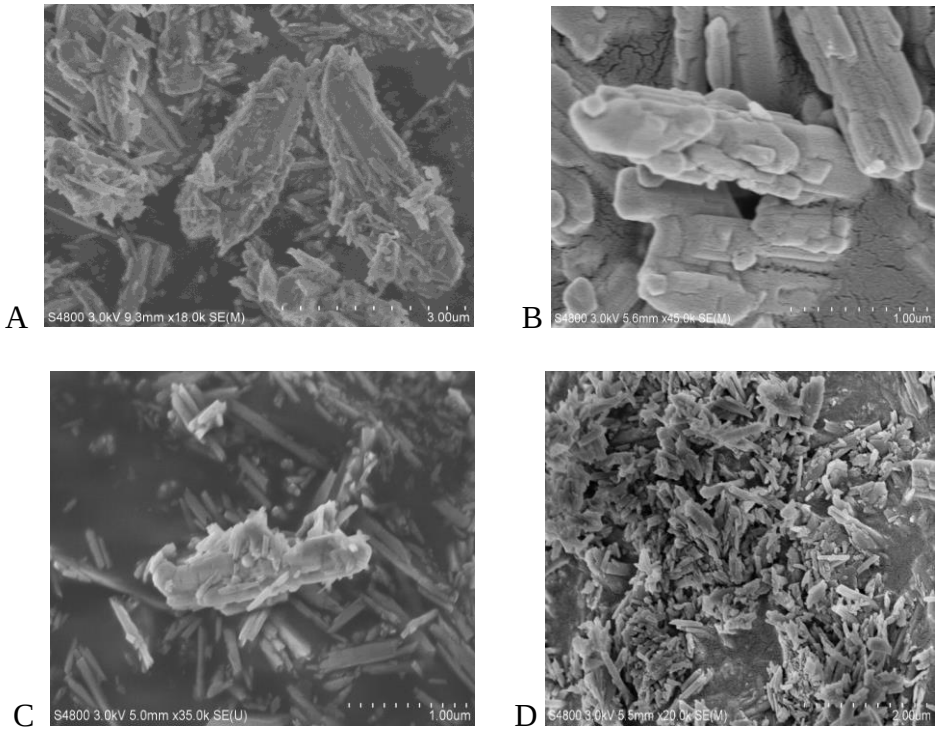

Figure 6-2: SEM images of SrHNTs of multiple attempts (A-D) showing sediment like formation on the surface of HNT.

The bond between Sr^{2+} and HNT surface was not weak since citric acid (pH=4) was used as a wash to remove excess of CO_3^{2-} ions and the remaining of $SrCO_3$ salt. The images were taken after the citric acid was washed away with water. Citric acid was used as a substitute for lemon juice (pH=2.5) to maintain consistency of the pH level during the washes. Different lemons possess slightly different properties which causes procedural variations each time they are used. At lower pH, citric acid is a harmless and non-toxic chemical which provides an environmentally safe option to remove the excess unwanted ions introduced during the formation of SrHNTs. SEM images showed that there was a successful layering of Sr on HNTs which formed a bond strong enough to remain stable even after exposure to acid with pH of 4.

6.1.2 EDS Report

To ensure the presence of Sr on the HNTs EDS was performed which is a quantitative analysis of the chemical elements present in a selected region. As seen in **Figure 6.3**. The EDS -SEM analyzed the chemical characterization of the region selected on HNTs and SrHNTs as seen in red outline in **Figure 6-3 A and B** respectively.

A 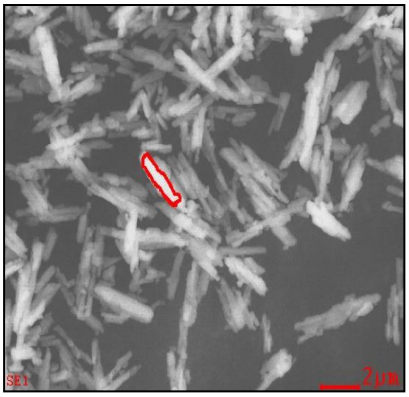

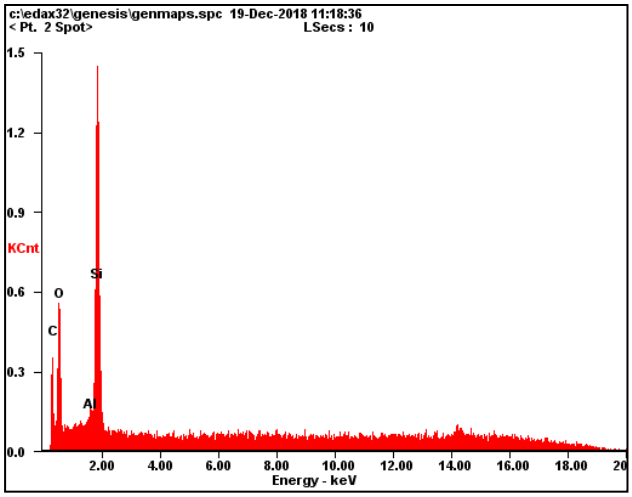

Figure 6-3 A: The quantitative elemental analysis of the area selected on (A) HNT and (C) SrHNT show the wt% of carbon [C], aluminum [Al], silicon [Si], oxygen [O] of HNT. The peak of Si is clearly seen

B 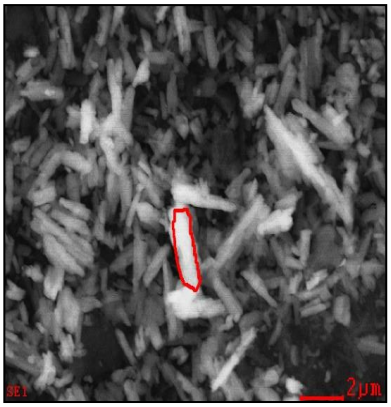

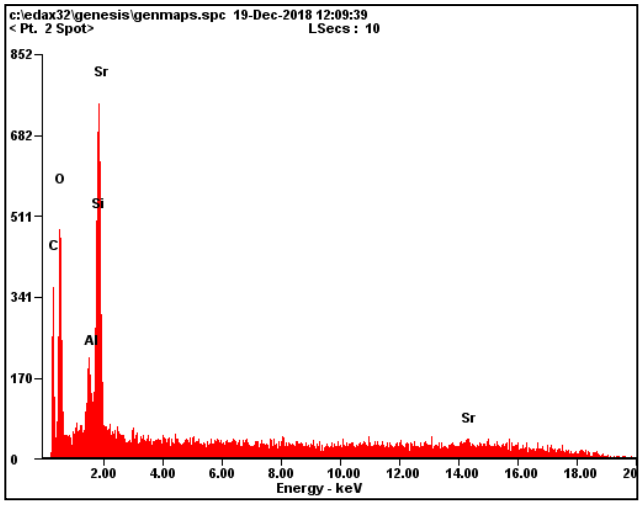

Figure 6-3 B: The quantitative elemental analysis of the area selected on (A) HNT and (C) SrHNT show the wt% of carbon [C], aluminum [Al], silicon [Si], oxygen [O] and Strontium [Sr] of SrHNT. The two peaks of Sr are the two peaks are the two shells K and L of Sr.

The quantitative analysis of the different elements present on HNT and SrHNT elemental report clearly show the presence of Sr on Sr coated HNTs. The same peak of Si is not visible in the reports of SrHNT and the value is 0 as the K shell peak of Si overlaps

the L shell peak of Sr. All the samples of HNTs and the average of the qualitative compositional information of HNTs and SrHNT was put in **Figure 6-4**.

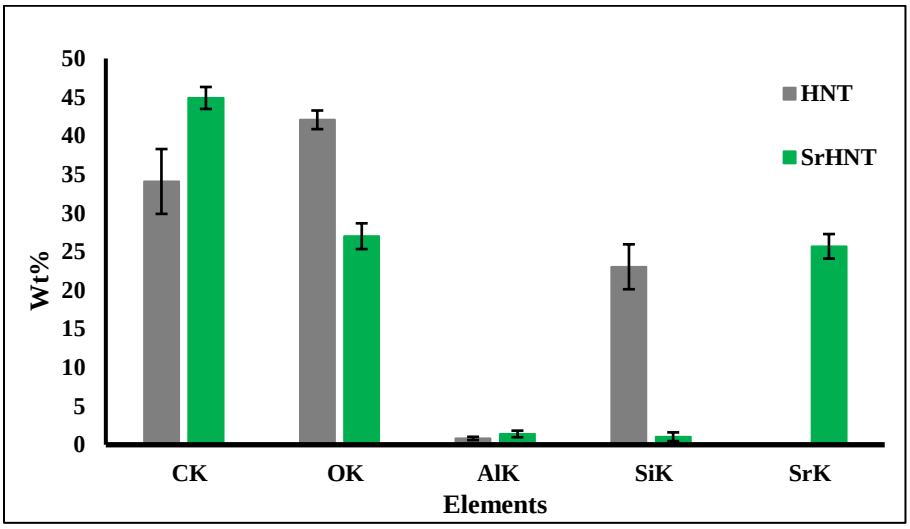

Figure 6-4: The graph of quantitative wt% of the elements present in HNT and SrHNT namely K shell of C, Al, Si, O, and Sr where n=5. The error bars are the standard deviation of the samples.

As seen in the graph the presence of the element Sr was confirmed by EDS giving value to the method of coating SrHNT. The method of EDS can be used to determine the presence of chemical element and it also gives an estimate of their abundance, the accuracy of this method can be affected by various other factors such as overlapping peaks. For more accurate estimation of the sample composition further tests were done.

6.1.3 FTIR -ATR

To confirm the presence of Sr on HNTs FTIR-ATR was conducted on the HNT samples, $SrCO_3$ and SrHNT which provided the molecular fingerprint to compare the samples. The high spectral resolution data of the three samples can be seen in **Figure 6-5**. Light in the infra-red region was absorbed corresponding to specific bonds present in the

samples. The absorption peaks on the inverted y-axis depicts the percent of transmittance of radiation of the particular sample.

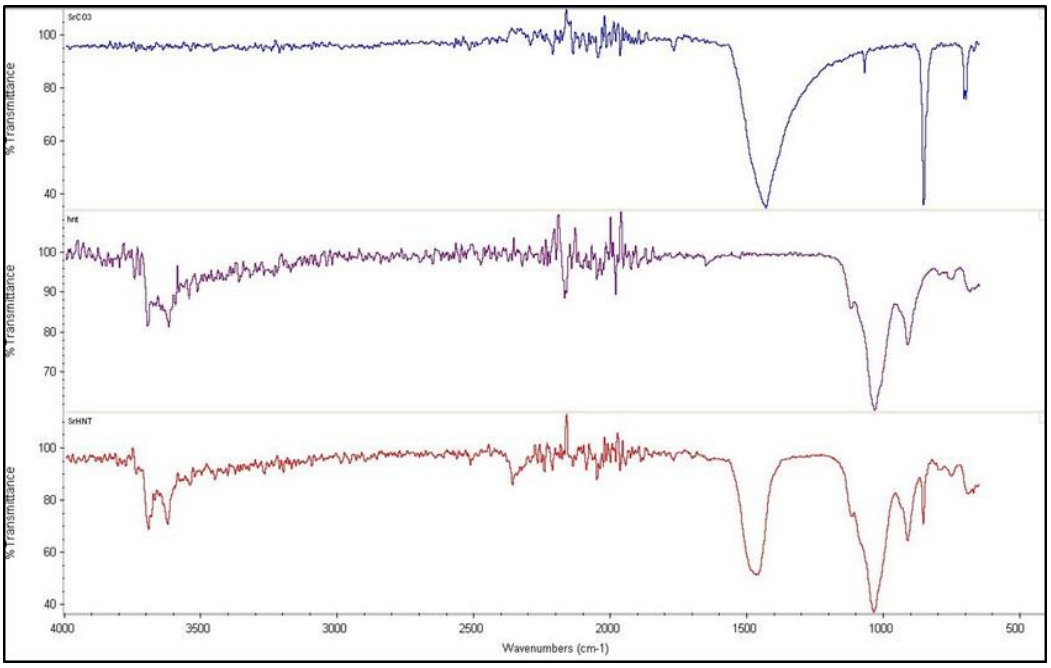

Figure 6-5: FTIR-ATR analysis of (-----) $SrCO_3$ (-----) HNT and (-----) SrHNT (n=3)

$SrCO_3$ has a strong peak at 1400 and 800 cm^{-1} depicting the -CO group. The position of carbonyl group depends on the function of the molecule. The position of carbonyl group here is characteristic to $SrCO_3$. For HNT there is a distinct peak at 1040 cm^{-1} showing the -SiO group. There is the peak at 900 cm^{-1} showing the presence of AlOH bond. Band peaks at 3100-3700 cm^{-1} are caused by -OH groups. The OH bond usually appears These peaks are distinctive factors of recognizing HNTs. For SrHNT there are combination of peaks at 3100-3700 cm^{-1}, 1400-800 cm^{-1}, and 3600-400 cm^{-1}. IR radiation effect in such a way that higher the frequency higher the wavelength. SrHNT showed a distinct presence of Sr on HNT in the sample. FTIR results also showed that the coating could be a combination of Sr^{2+} ions and $SrCO_3$. Since there are peaks showing

the CO bond along with the presence of HNT absorption peaks. The validity of $SrCO_3$ FTIR results were confirmed based of previously published data. Stronger the peaks on SrHNT more confirmed is the presence of the HNT and $SrCO_3$.

6.1.4 XRD

To further confirm the presence of Sr on HNT XRD was used as some bonds that are not visible through FTIR. Since the wavelength of X-rays is on atomic scale, this was the final tool to measure the accuracy of composition of SrHNTs. XRD was done to compare the diffractions of HNT, $SrCO_3$, and SrHNT as seen in **Figure 6-6**. The XRD peaks seen in the **Figure 6-6** were produced by the interference of a monochromatic beam of X-ray scattered at specific angle from each set of lattice plane in the sample measured.

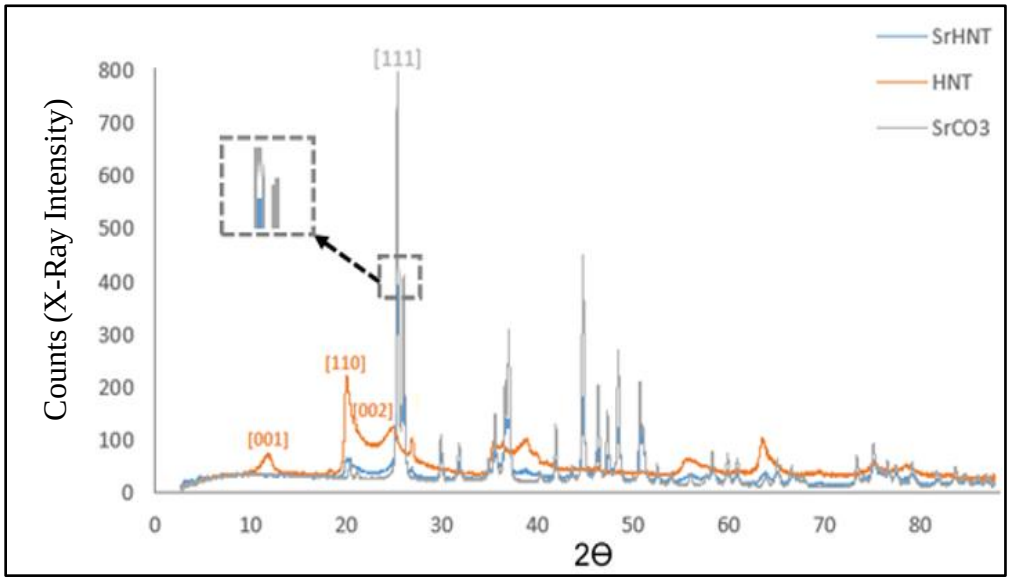

Figure 6-6: XRD graph image of HNT, $SrCO_3$ and SrHNT.

As seen in the **Figure 6-6** HNT has distinctive peaks at lattice structure 001, 110, and 002. There is a distinct peak of $SrCO_3$ at 111. Since the HNT is covered by Sr^{2-} The

crystal structure of SrHNT shows reduced peaks of HNT but the distinctive characteristic peak of $SrCO_3$. This showed that SrHNT did have Sr present either in ionic form to form bond with the free hydroxyl group and through the attachment of $SrCO_3$ to the surface of HNTs.

6.1.5 Cytotoxicity Test for SrHNTs

Having confirmed the presence of Sr on HNTs it was important understand the cytotoxic effect of Sr on biological cells. Literature shows that Sr in moderate mounts can be beneficial to the physiological systems. Live dead assay was performed to confirm the quantity of SrHNT that would allow the cells to grow unhindered. Two different concentration was tested on pre-osteoblast cells and the results are seen in **Figure 6-7**.

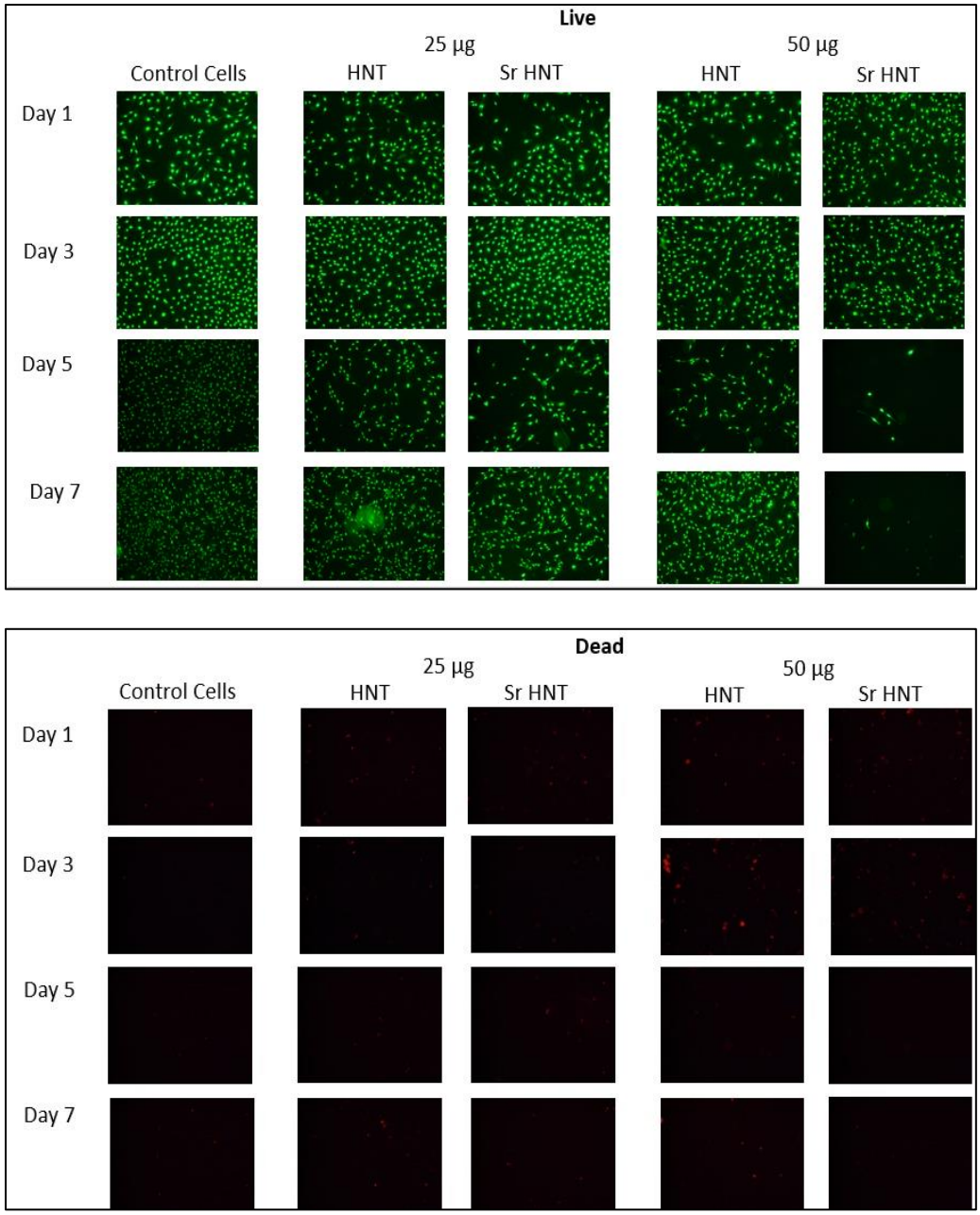

Figure 6-7: Live dead assay of two concentrations, 25 and 50 µg/ml of HNT and SrHNT showing the live cells in green on top image and dead cells in red on the image below for day 1, 3, 5, and 7.

As seen **Figure 6-7** HNTs showed a good viability of day 1 (95%), 3 (95.6%), 5 (95.67%), and 7 (95.9%) at lower and 1 (88.8%), 3 (88.9%), 5 (84.8%), and 7 (97.1%) at higher concentrations. Although the number of cells on day was affected by high

concentrations of HNT. SrHNTs show a good cell viability on day 1 (88.2%), 3 (91.47%), 5 (92.5%) and 7 (97.135) at lower concentration whereas at high concentration the affect was derogatory by day 5 (55.3%) and almost no live cells are seen by day 7. To get a quantitative analysis of the live-dead assay ImageJ app was used to count the cells and the graph was plotted using those numbers as seen in **Figure 6-8**. Data is missing for Day 7 for high concentration of SrHNT as the cells were visibly absent in the fluorescence image but the ImageJ app calculated the viability at 90%.

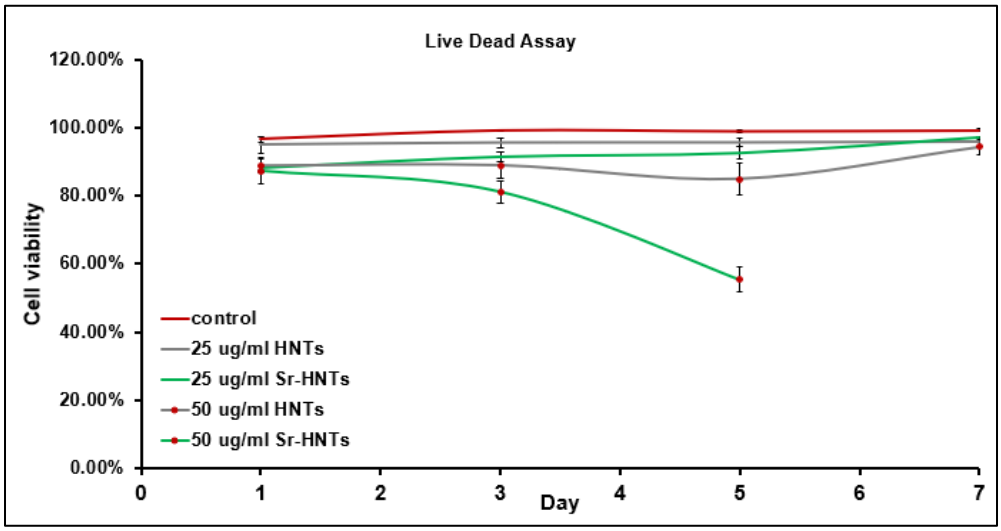

Figure 6-8: Graph showing the quantitive values of cell count calculated (live cell/total cell count). Grey and green lines depict HNT and SrHNT respectively. High concentration lines are depicted by marked lines. Error bars are standard deviation where n=3.

As seen in the **Figure 6-8**, high concentrations of SrHNT were not conducive for cell growth implying SrHNT did not favor cell growth at 50 µg/ml. Although no research has been published to show the absence of any toxic effect by Sr but for the use of SrHNT in biological systems it was necessary to predict the concentration that could be used without hindering cell growth. This test showed that the use of Sr should be limited

to 25 µg/ml. In order to ensure the cytocompatibility of the right amount of SrHNT, this information was important, also for further testing where SrHNTs was imbedded in CPCs and will be useful for further use in other biomedical applications.

6.1.6 Proliferation Assay

Since biological systems are a moving system due to blood flow, this test was conducted to see the effect of exposure of pre-osteoblast cells to different concentrations of HNTs and SrHNTs for a period of seven days and the values was plotted in a graph as seen in **Figure 6-9**. The cells were exposed to the different concentrations of the two samples for 48 hours. On y-axis the absorbance of the cells is seen at 630 nm. Higher cell count showed higher absorbance.

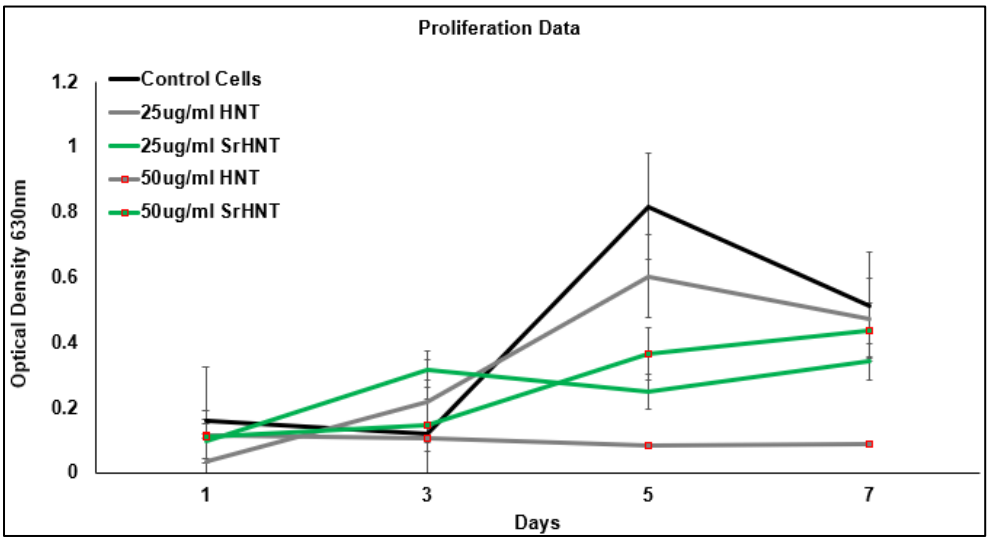

Figure 6-9: Graph showing proliferation of pre-osteoblast cells after exposed to two different concentrations 25 and 50 µg/ml of HNT and SrHNT for day 1, 3, 5, and 7. Grey and green lines depict HNT and SrHNT respectively. High concentration lines are depicted by marked lines. Error bars are standard deviation where n=3.

As the graph shows that exposure to low (0.341 Å) and high (0.439 Å) concentrations of SrHNTs did not affect the cell proliferation. But exposure to high

concentration (0.09 Å) of HNTs had a derogatory effect on proliferation when compared to low concentration (0.472 Å). As seen in **Figure 6-9** there was no emerging damage was seen by exposure of cells to high concentration of SrHNTs. The rate of proliferation was higher in case of SrHNTs. Cells after being exposed to SrHNTs proliferated, whereas the cells exposed high concentrations of HNTs showed a decline in proliferation. It is not completely understood at this point about the behavior of the cells in such a manner. Further tests must be conducted to determine the effect of exposure on cells and for a long period of time. The assay however proved that in presence of SrHNTs the cells did not alter their proliferation rate by a large number and could reach the rate of proliferation almost as the control cells over time.

6.1.7 Bacterial Growth Rate

The effect of HNT, SrHNT and gentamicin loaded HNT, SrHNT, HNTSr was tested for a period of 48 hours on the growth rate of three nosocomial bacteria *Escherichia coli* (**Figure 6-10**), *Staphylococcus aureus* (**Figure 6-11**), and *Staphylococcus epidermis* (**Figure 6-12**) separately. SrHNT lowered the growth rate in the case of all three bacteria when compared to HNT at a low concentration of 5 μg/ml. This showed that HNT had an inherent property has some bactericidal or bacteriostatic effect on nosocomial bacteria which was enhanced when HNT was coated with Sr. When HNTs was loaded with gentamicin it was released efficiently to inhibit the growth of bacteria. When SrHNT was loaded with HNT the cap of the cylindrical HNT was not closed with Sr covering and the antibiotics was released and hence there is no bacterial growth seen. When HNT was loaded and then coated with gentamicin, the graphs show no bacterial growth showing the effective release of antibiotics.

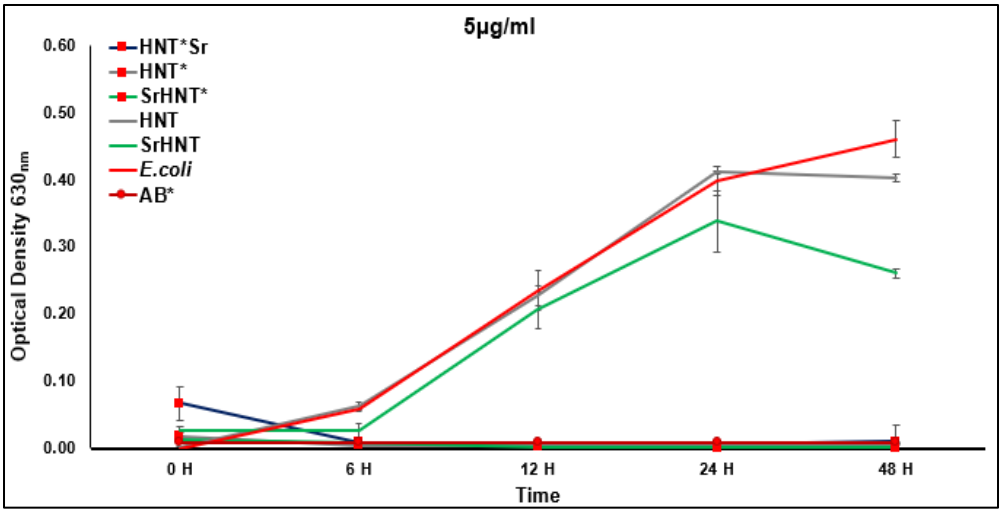

Figure 6-10: This graph shows the growth rate of *E. coli* over 24 hours. Bacterial growth was tested based on CSLI microtitration method. The data is average of 3 different colonies. In this graph the concentration of sample of HNT, SrHNT, Gentamicin loaded HNT*, SrHNT*, and HNTSr* was 5µg. Total reaction mixture was 100 µl. Error bars are standard error of the mean.

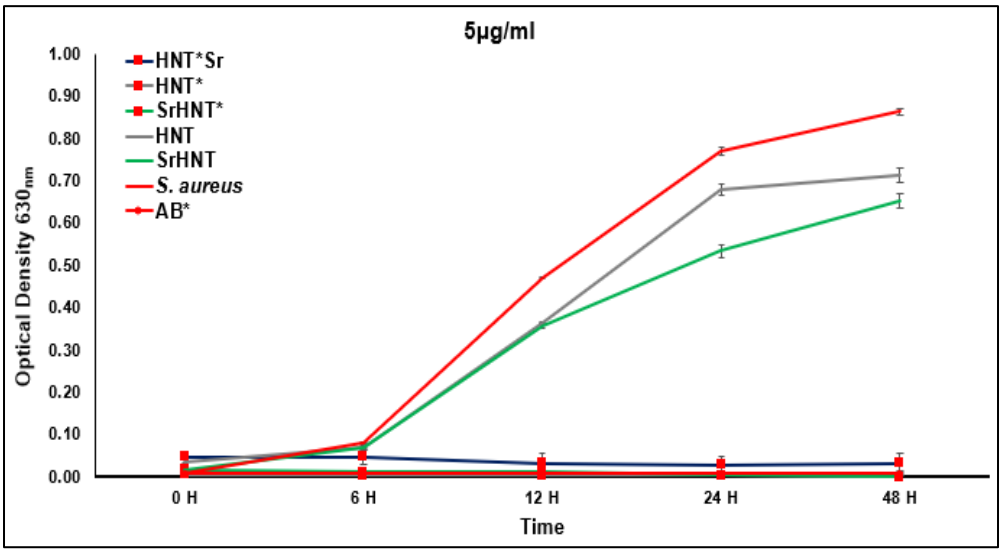

Figure 6-11: This graph shows the growth rate of *S. aureus* over 24 hours. Bacterial growth was tested based on CSLI microtitration method. The data is average of 3 different colonies. In this graph the concentration of sample of HNT, SrHNT, Gentamicin loaded HNT*, SrHNT*, and HNTSr* was 5µg. Total reaction mixture was 100 µl. Error bars are standard error of the mean.

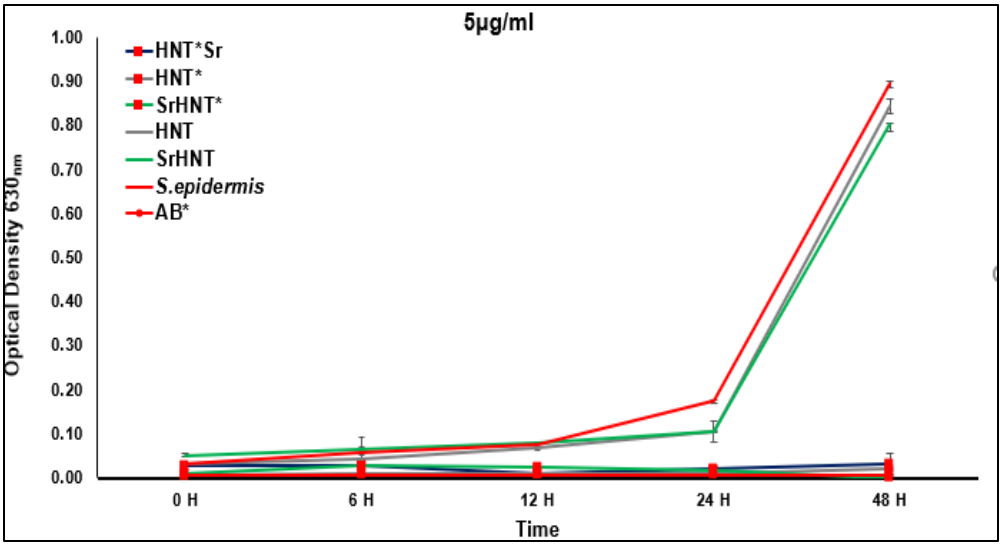

Figure 6-12: This graph shows the growth rate of *S. aureus* over 24 hours. Bacterial growth was tested based on CSLI microtitration method. The data is average of 3 different colonies. In this graph the concentration of sample of HNT, SrHNT, Gentamicin loaded HNT*, SrHNT*, and HNTSr* was 5µg. Total reaction mixture was 100 µl. Error bars are standard error of the mean.

SrHNT has some inherent quality that lowers the bacterial growth rate. Coating HNTs with Sr before or after loading with drugs does not hinder its drug release capacity making then good carriers. The SrHNTs can serve as carriers for many drugs and when embedded in biomaterials such as CPC or hydrogels, this will be a better way to release the drugs in the implant as research shows that loading drugs in carriers slows the rate of release and for prolonged duration of time. Since SrHNT itself lowers bacterial growth rate, it will help reduce the chance of infection on the implant site.

6.2 Project 2: Embedding SrHNT in CPC for Bone Regeneration

6.2.1 FTIR-ATR

The setting product of all the four groups was chitosan. To evaluate the detection of HNT and SrHNT FTIR was used. **Figure 6-13** compares the IR spectra of CPC with 10% HNT, $SrCO_3$, and SrHNT each. Three samples from each group was analyzed and

the average was plotted. Peaks seen at 900-1200 cm^{-1} is due to PO_4^{3-} groups. Peak at 1400-1300 cm^{-1} are characteristics of CO_3^{2-} groups in hydroxyapatite. Peaks around 3000 cm^{-1} are characteristics of -OH groups. In case of SrHNTs the peaks of -OH group is smaller it is theorized that the free Sr ions are attaching to the -OH groups.

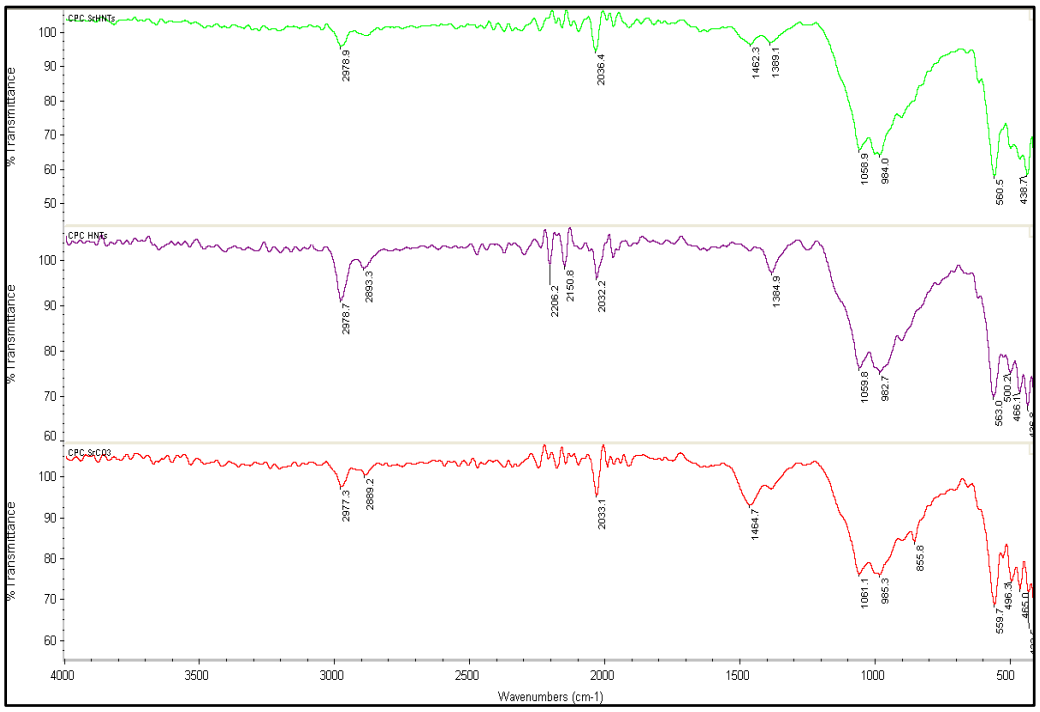

Figure 6-13: FTIR spectra of (-----) CPC HNT (-----) CPC SrHNT and (-----) CPC $SrCO_3$, n=3.

6.2.2 Cytotoxicity Test

This test was done to evaluate if there was any cytotoxic effect of SrHNT and CPC combination for all the different percentages. For Group 2 (**Figure 6-14 A** and **B** showed the live and dead cell images respectively. **Figure 6-14 C** showed the cell viability calculated for the images via ImageJ), Group 3 (**Figure 6-15 A** and **B** showed the live and dead cell images respectively. **Figure 6-15 C** showed the cell viability

calculated for the images via ImageJ), and Group 4 (**Figure 6-16 A** and **B** showed the live and dead cell images respectively. **Figure 6-16 C** showed the cell viability calculated for the images via ImageJ). The cell viability after 7 days increased to match the population of control cells as seen in the figures of images given below. There is increase in cell viability from day 1, 3, 5 to day 7 with all the groups as seen in green. The dead cells are seen in red. The sample also took up the color of the reagent and appear red and green in the live dead images. 1%, 5%, and 10% HNT, $SrCO_3$, and SrHNT in CPC was not cytotoxic to pre-osteoblast cell line and did not reduce the cell viability. The graphs for cell viability was plotted for all the groups, **Figure 6-14 C**, **Figure 6-15 C**, and **Figure 6-16 C** for 1%, 5%, and 10% respectively. Higher cell viability meant higher ratio of live cells over the total number of live and cell count. One-way Anova was calculated for all the groups and there was no significant difference between the groups where value of p was 0.05.

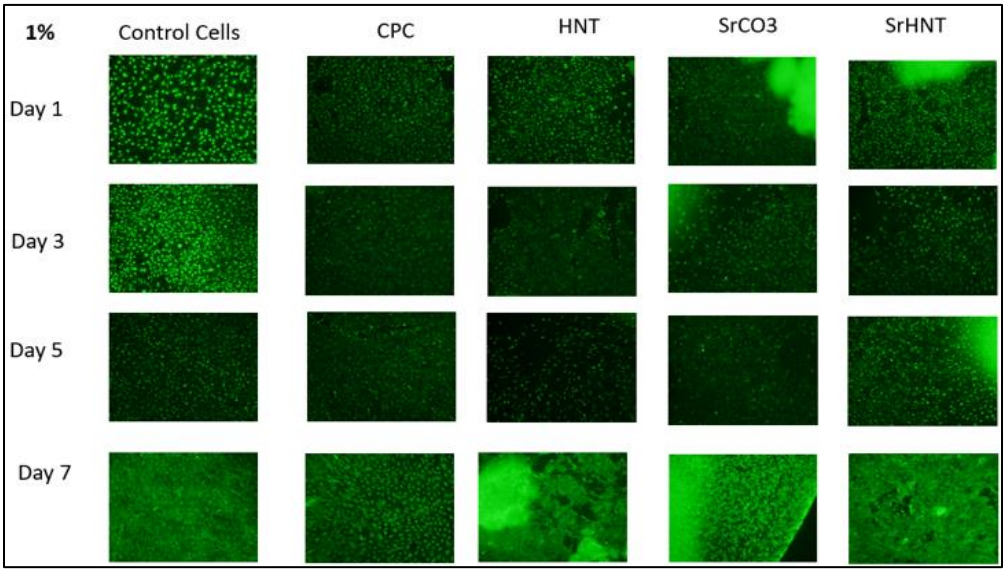

Figure 6-14 A: Live pre-osteoblast cells seen in green over a period of 1 week with 40 mg of 1% HNT, $SrCO_3$, and SrHNT in CPC respectively.

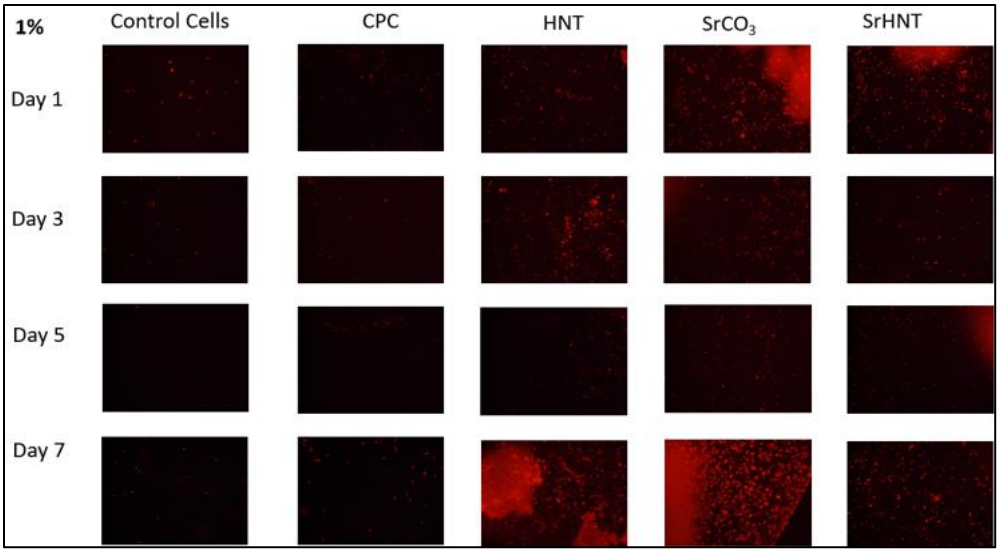

Figure 6-14 B: Dead pre-osteoblast cells seen in red over a period of 1 week with 40 mg of 1% HNT, $SrCO_3$, and SrHNT in CPC respectively.

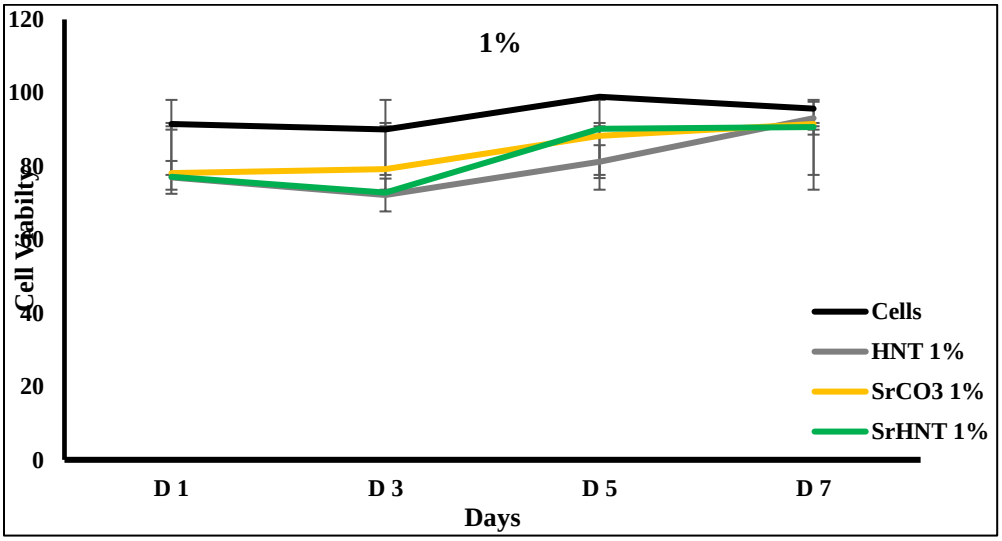

Figure 6-14 C: Cell viability graph for CPC and CPC with 1% HNT, $SrCO_3$, and SrHNT. Error bars show the standard deviation. n=3.

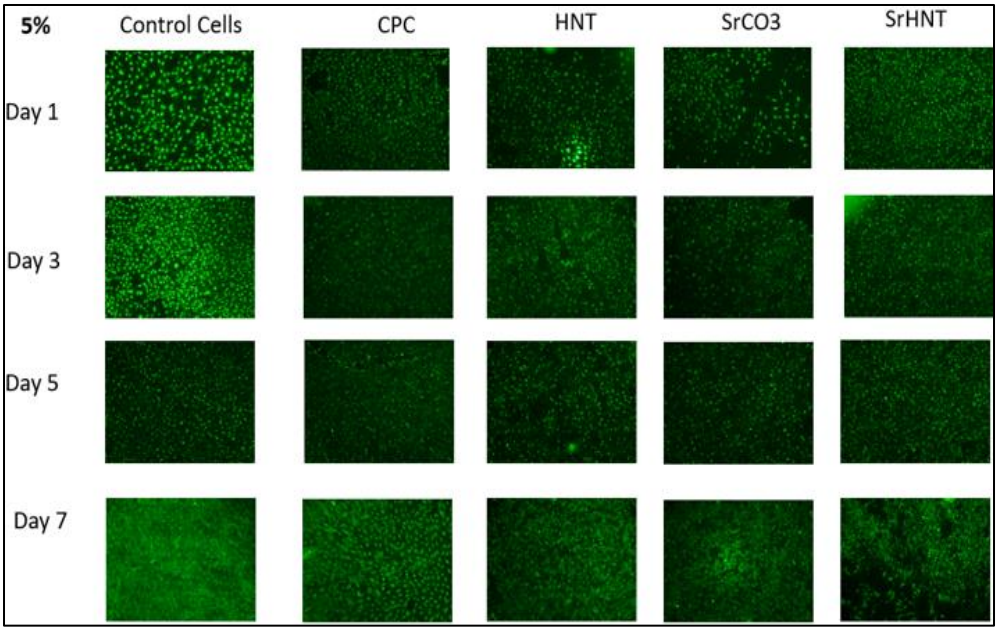

Figure 6-15 A: Live pre-osteoblast cells seen in green over a period of 1 week with 40 mg of 5% HNT, $SrCO_3$, and SrHNT in CPC respectively.

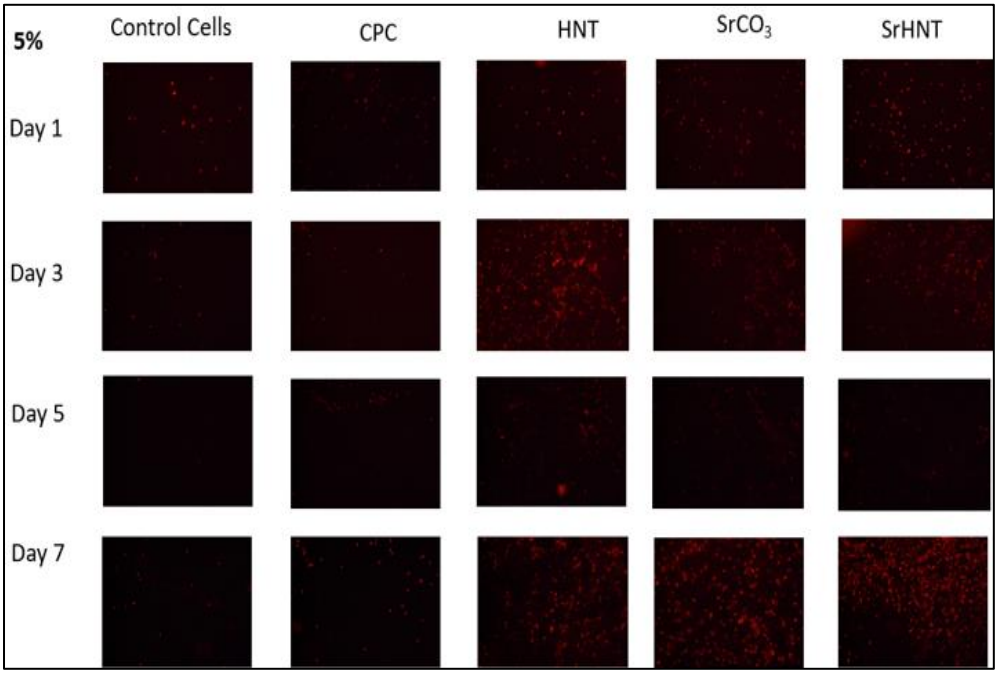

Figure 6-15 B: Dead pre-osteoblast cells seen in red over a period of 1 week with 40 mg of 5% HNT, $SrCO_3$, and SrHNT in CPC respectively.

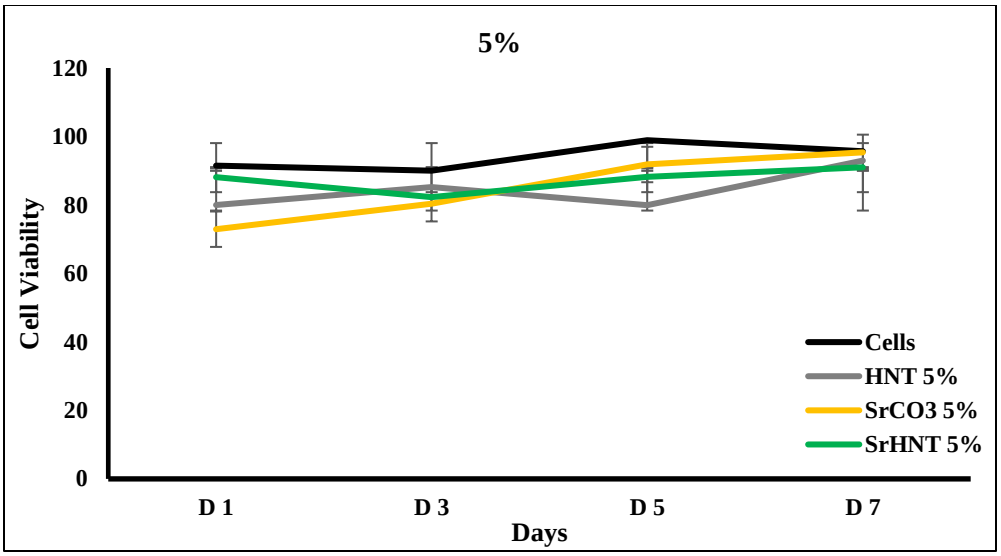

Figure 6-15 C: Cell viability graph for CPC and CPC with 5% HNT, $SrCO_3$, and SrHNT. Error bars show the standard deviation. n=3.

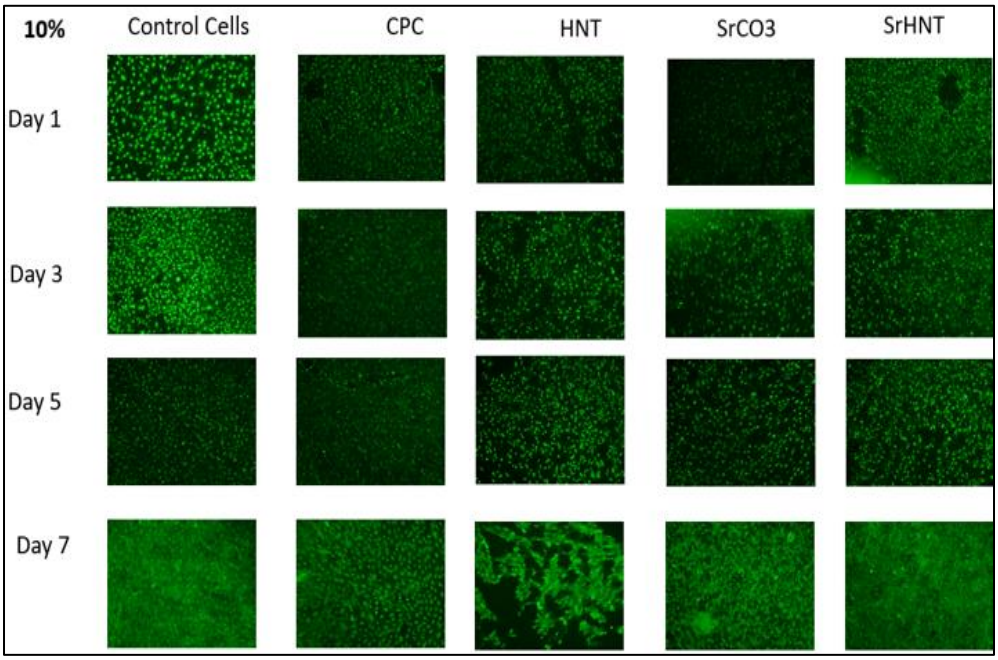

Figure 6-16 A: Live pre-osteoblast cells seen in green over a period of 1 week with 40 mg of 10% HNT, $SrCO_3$, and SrHNT in CPC respectively.

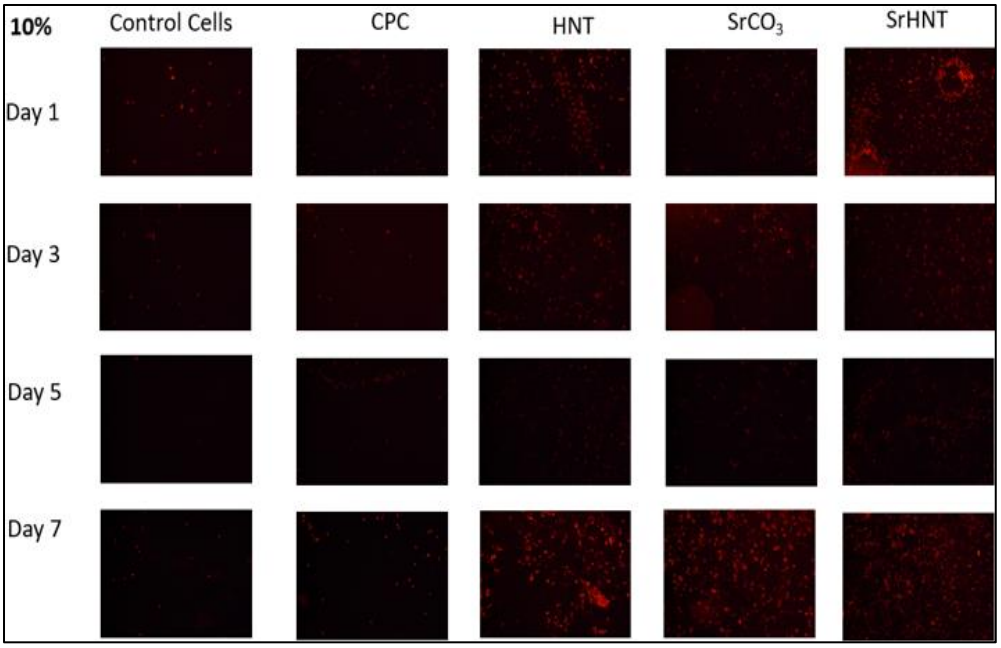

Figure 6-16 B: Dead pre-osteoblast cells seen in red over a period of 1 week with 40 mg of 10% HNT, $SrCO_3$, and SrHNT in CPC respectively.

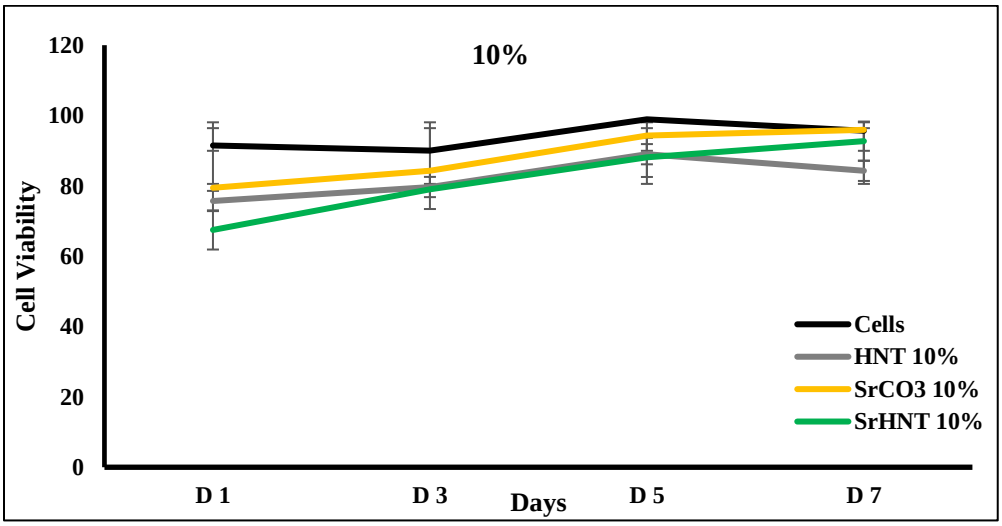

Figure 6-16 C: Cell viability graph for CPC and CPC with 10% HNT, $SrCO_3$, and SrHNT. Error bars show the standard deviation. n=3

6.2.3 Proliferation Assay

After testing for cytotoxicity, it was important to confirm that the presence of CPC with SrHNT will not hinder or inhibit cell proliferation. This test was conducted for a period of one month as usually the implants starts to biodegrade by that duration and the wound starts to heal. Adding SrHNTs in CPC was not cytotoxic and did not prevent cell proliferation as seen in graphical representation in **Figures 6-17 A**, **B**, and **C** show SrHNTs in 1%, 5%, and 10% wt in CPC respectively. Higher absorbance showed higher cell number. There is trend for all the groups where the cell counts show and increase from day 1 to 3 and there is a decrease on Day 5. This may be due to cell saturation. There is an increase on day 7 after which there is a decline during day 14 and 21. This may be due to increase in space after day 5 when the cells reached saturation and maturation creating more space which led to cell count increase on day 7 after which there was little probability since the cell proliferation had crossed the threshold saturation. Although the cell number did not match the control cells, this can be attributed to lack of space for cells to adhere in presence of CPC crystals which protruding arears which would make cell adherence difficult. After a period of 28 days there is a decline in cell number in control cells also and can be explained due to lack of space in the 48 well plates after cells grew to the point of space saturation. One-way Anova calculated for all the groups showed no significant difference between the groups. The highest mean calculated was for control cells. This test showed that embedding CPC with HNT, $SrCO_3$, and SrHNT did not prevent cell proliferation. SrHNT 10% in CPC showed better proliferation than just control cells. Graphs show that HNT and $SrCO_3$ individually add to the properties of SrHNT when they are tested in moderate amounts.

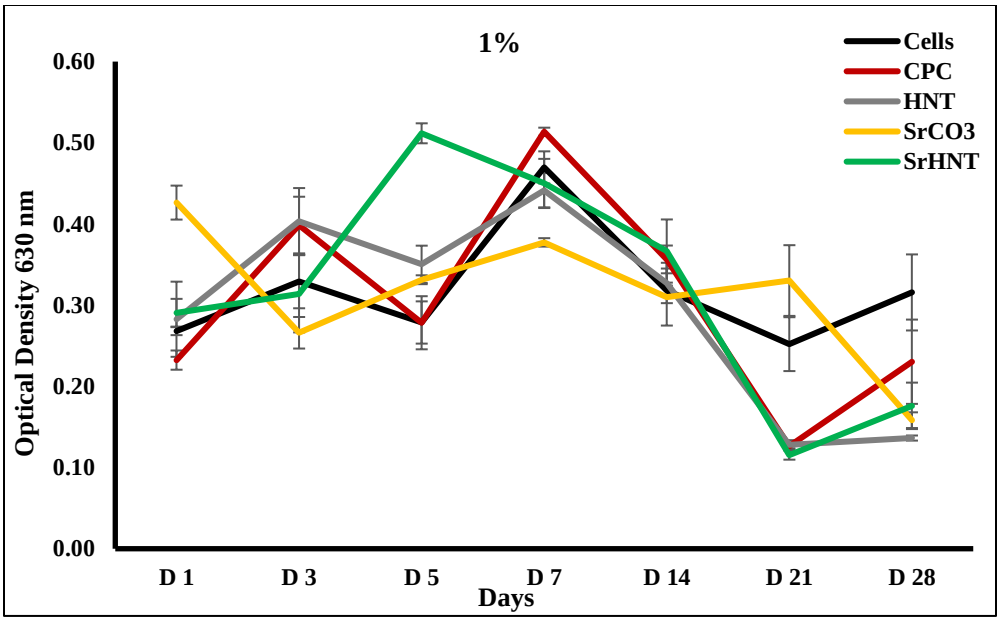

Figure 6-17 A: Cell proliferation measured as absorbance at 630 nm for control cells, CPC, and CPC with 1% HNT, $SrCO_3$, and SrHNT individually. n=3

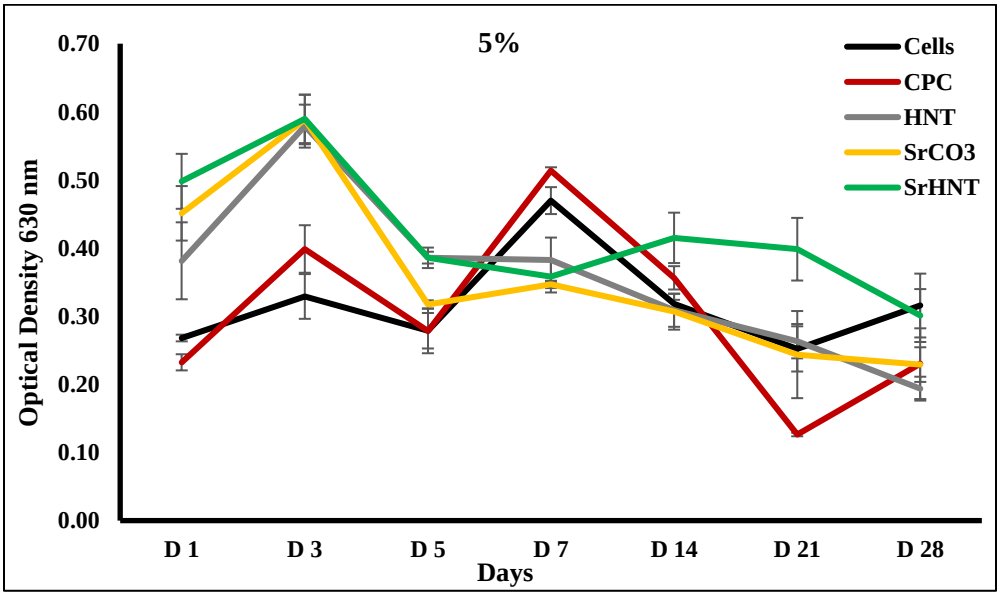

Figure 6-17 B: Cell proliferation measured as absorbance at 630 nm for control cells, CPC, and CPC with 5% HNT, $SrCO_3$, and SrHNT individually. n=3

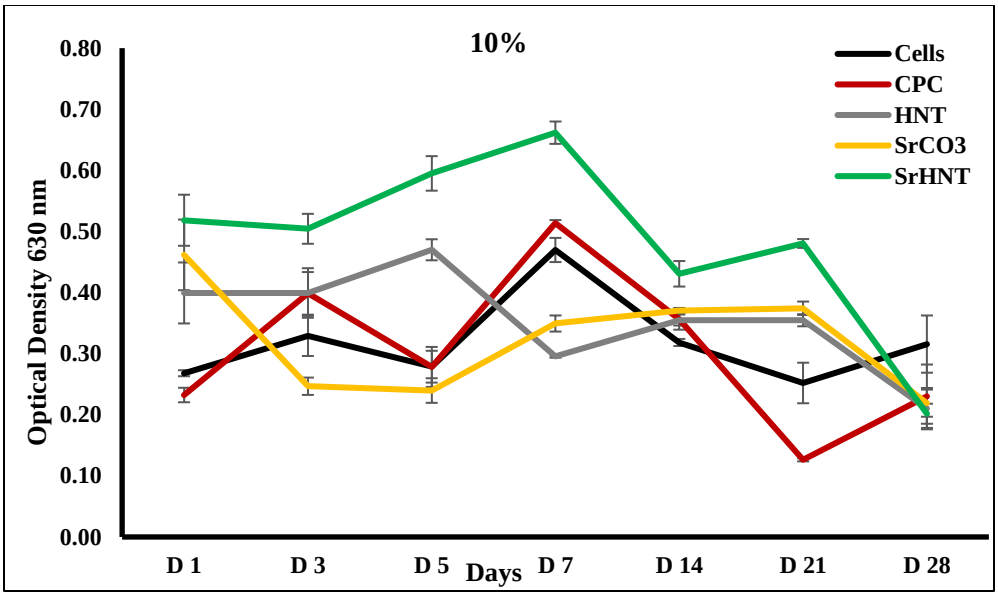

Figure 6-17 C: Cell proliferation measured as absorbance at 630 nm for control cells, CPC, and CPC with 10% HNT, $SrCO_3$, and SrHNT individually.

6.2.4 Alcian Blue Stain

To evaluate the synthesis of ECM molecules other than collagen, this staining procedure was used to identify acidic mucopolysaccharides. **Figure 6-18 A** (Mouse stromal cells and **Figure 6-18 B** (pre-osteoblast cells) show the graphical representation of alcian blue staining for a period of 28 and 21 days respectively. Higher absorbance showed higher synthesis of acidic mucopolysaccharides. For stromal cells there was an overall increase till day 14 and then there is a gradual reduction on day 21 and 28. This may be due the fact the cells further differentiated, developed further or broke down to simpler compounds. The peak of mucopolysaccharides was reached in two weeks. 10% SrHNT in CPC showed the maximum absorbance over the period of 28 days. Adding SrHNT to CPC added it value to help stromal cells to differentiate in mucopolysaccharide cells. One-way Anova showed no significant difference with highest average in 5% and 10% SrHNT in CPC. For pre-osteoblast cells adding HNTs and SrHNTs to CPC help

formation of acidic mucopolysaccharides. There was an overall increase for a period of 7 days and then 10% HNT and SrHNT in CPC showed the maximum absorbance on Day 21. One-way Anova showed no significance difference between the groups. Adding SrHNT provided the signal generation to the cells to produce more acidic mucopolysaccharides. Formation of acidic mucopolysaccharide is very essential for bone implants as it serves as a lubricant and increase elasticity to connective tissue. It is an essential part of ligament and cartilage. It plays an important role in motor functions, reduction of inflammation, and helps support the bone growth. It is also essential for the breakdown of excessive mucopolysaccharides as it can result in medical condition called mucopolysaccharidoses which can affect the cartilage and bones. The decline seen in the amount after 14 days is beneficial for break down or removal.

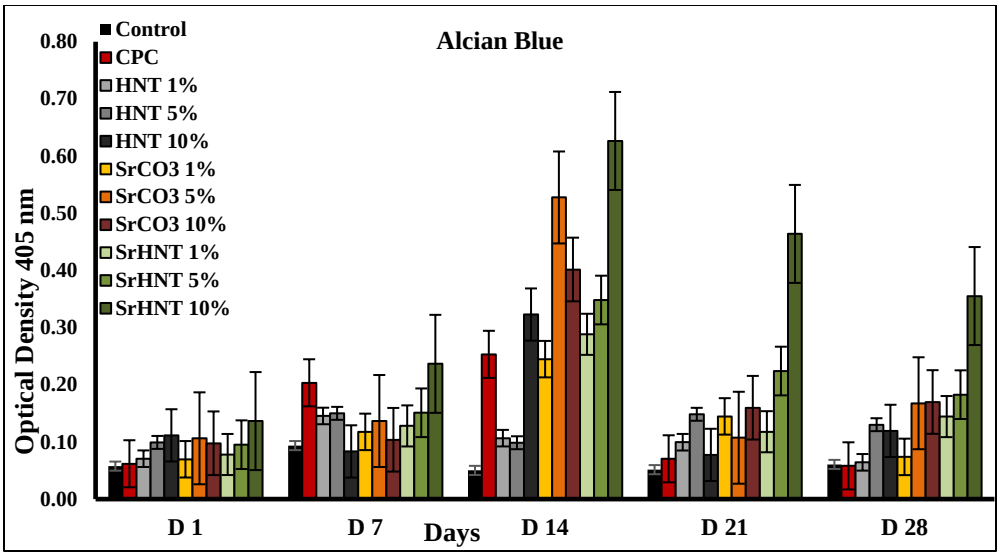

Figure 6-18 A: Alcian blue staining of mouse stromal cells for a period of 28 days with all the four groups (40 mg). n=5, Error bars=Standard Deviation

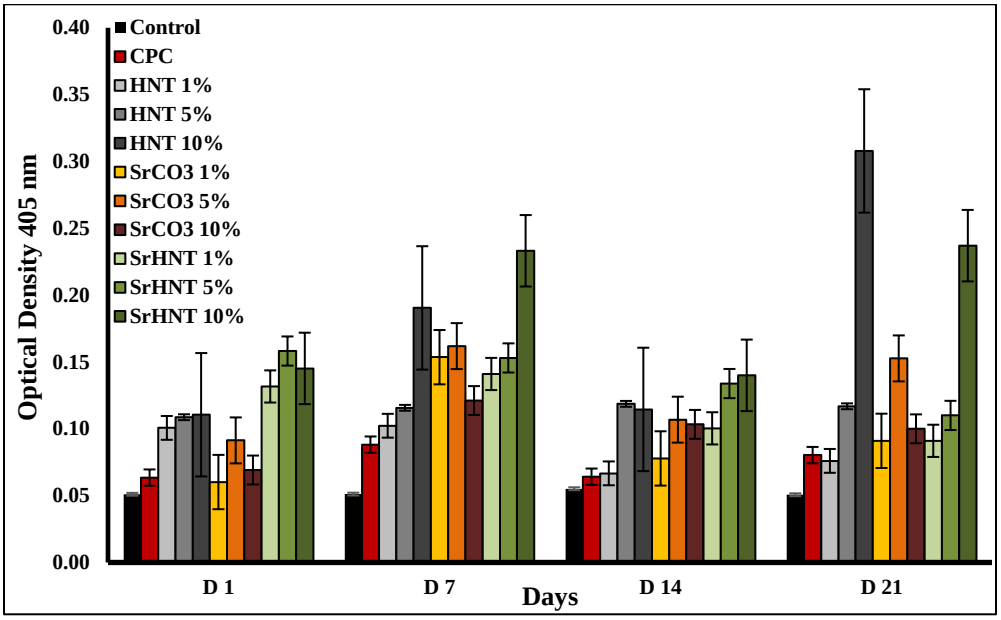

Figure 6-18 B: Alcian blue staining of pre-osteoblast cells for a period of 21 days with all the four groups (40 mg). n=5, Error bars=Standard Deviation

6.2.5 ALPase Assay

This test was conducted to evaluate the osteogenic lineage of stromal stem cells and pre-osteoblast cells when SrHNT was added to them. Addition of an external sample should not change the lineage or signal the cells towards other differentiation which is not bone or bone related. **Figure 6-19 A** (mouse stromal cells) and **Figure 6-19 B** (pre-osteoblast cells) show the graphical representation of ALPase assay where higher absorbance meant presence of more cells showing osteogenic lineage. For the stromal cells there is a general increase over 14 days and then there is a gradual decrease in absorbance. This can be due to the further differentiation of cells to osteoblast cells. One-way Anova showed a significant difference of 5% HNT and SrHNT in CPC, and 10% SrHNT in CPC. In **Figure 6-19 B** the graph of pre-osteoblast cell showed that pre-osteoblast cells by default had the osteogenic lineage. Adding CPC and CPC embedded with HNT and SrHNT added to their lineage potential. Although there was a clear trend of increase in 7 days and then a decrease for SrHNT embedded CPC. Adding HNTs showed a higher absorbance in 7 and 14 days. One-way Anova showed no significant difference among the groups. Adding HNTs, $SrCO_3$, and SrHNTs increased the mechanical stimulation required for the cells so they could experience the change in their architecture to promote their differentiation towards osteoblast cells. As the bone implant degrades, it is important for cells to differentiate into bone cells so they can replace the biodegradable implants.

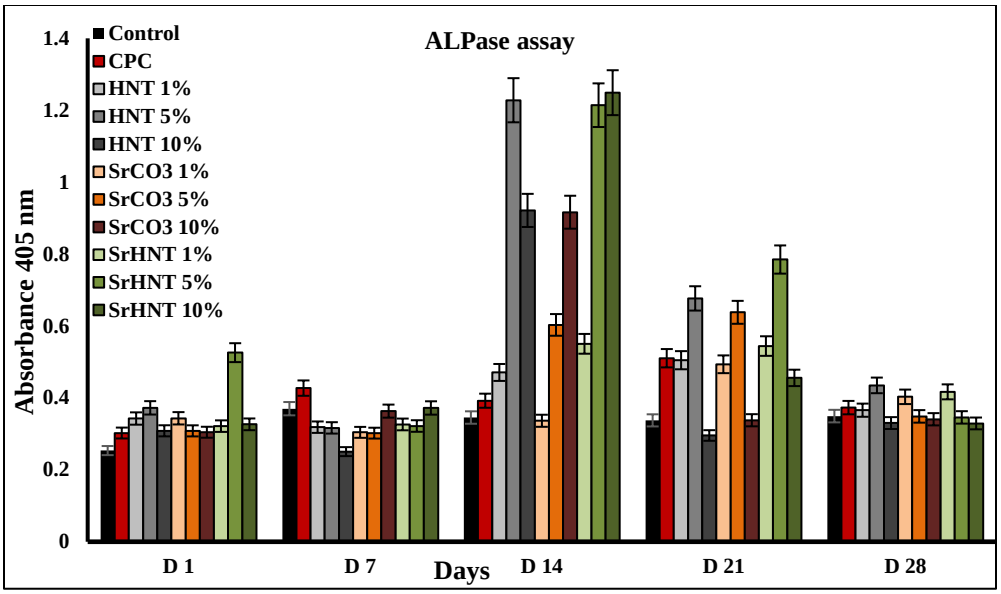

Figure 6-19 A: ALPase assay of mouse stromal cells for a period of 28 days with all the four groups (40 mg). n=5, Error bars=Standard Deviation

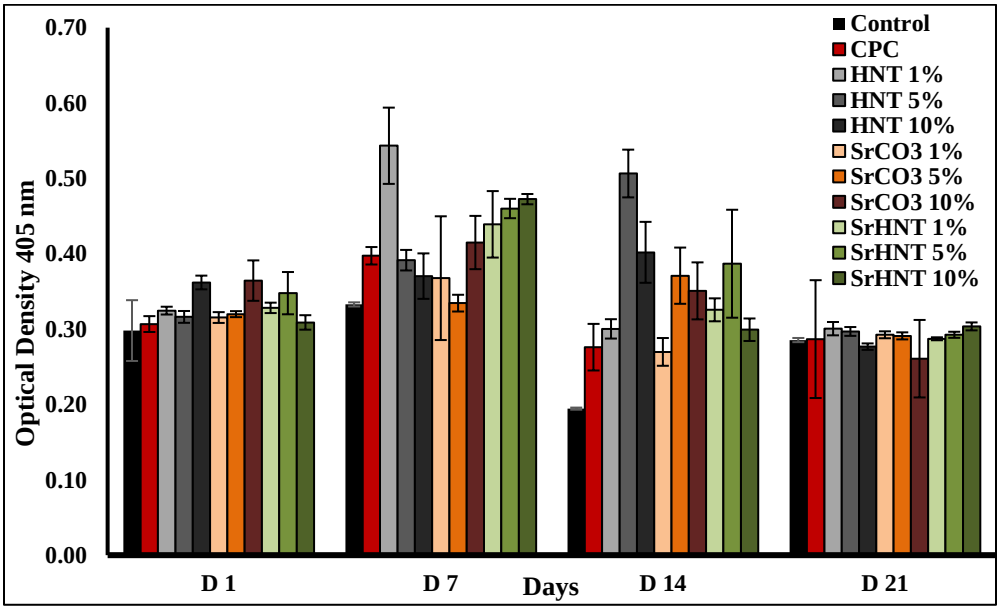

Figure 6-19 B: ALPase assay of pre-osteoblast cells for a period of 21 days with all the four groups (40 mg). n=5, Error bars=Standard Deviation

6.2.6 Picosirus Stain

PSR stain was used to evaluate the collagen content of the well after the addition of the four groups and compare the difference among them. Under *in-vitro* condition growth factors can stimulate the differentiation of stromal stem cells to type 1 collagen and osteogenic marker genes. Collagen provides structure and strength to the bones. **Figure 6-20 A** (mouse stromal cells) and **Figure 6-20 B** (pre-osteoblast cells) show the graphical representation of PSR stain where higher absorbance meant presence of more collagen. Collagen content was an overall high on day 7. For stromal cell the wells having 5% SrHNT in CPC showed the highest collagen content on day 7 and was significantly different from other groups when one-way Anova was calculated. For pre-osteoblast cells 1% SrHNT in CPC showed the highest collagen content on day 7 and overall. There was no significant difference among the groups and samples. Addition of SrHNT in CPC increased the formation of collagen over 21 days. High collagen content is important as it prevents bone loss and relieve pain in the joints.

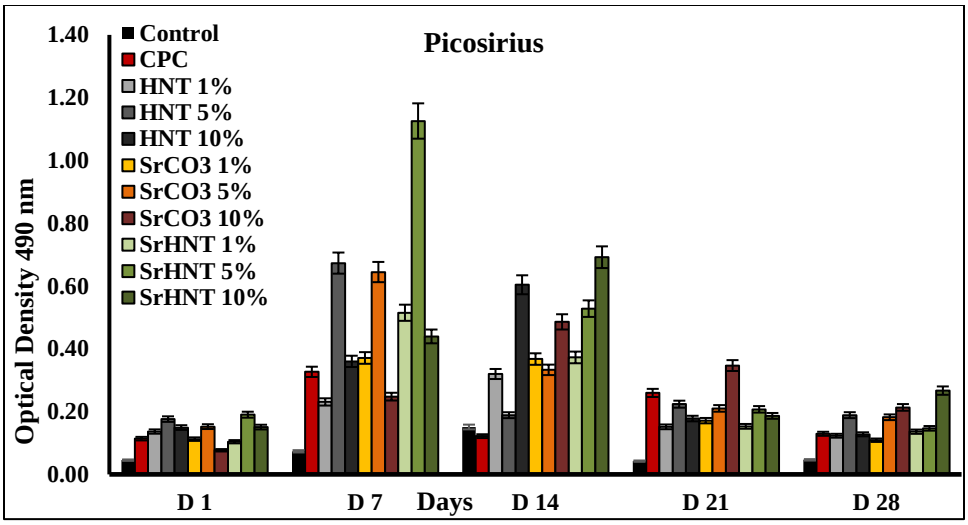

Figure 6-20 A: PSR stain of mouse stromal cells for a period of 28 days with all the four groups (40 mg). n=5, Error bars=Standard Deviation

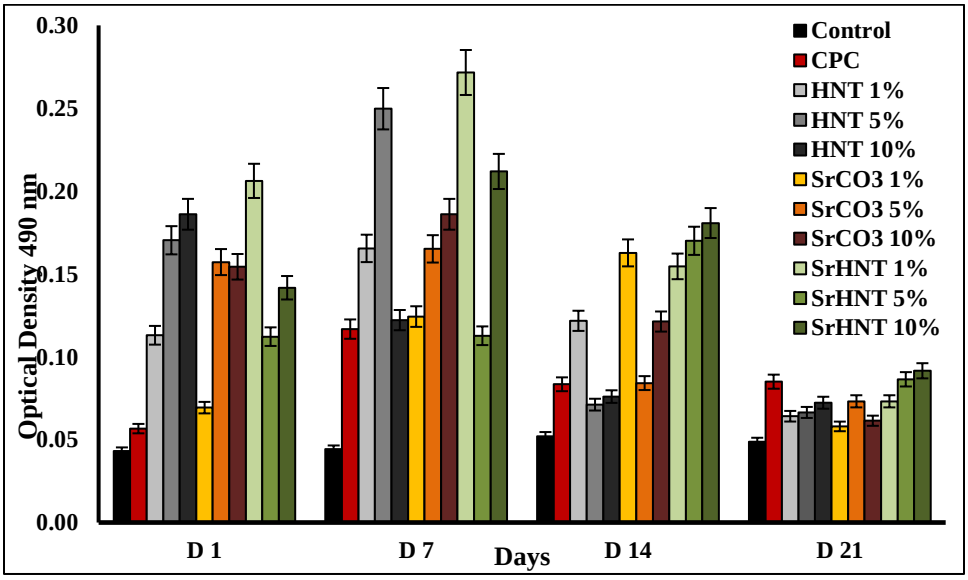

Figure 6-20 B: PSR stain of pre-osteoblast cells for a period of 21 days with all the four groups (40 mg). n=5, Error bars=Standard Deviation.

6.2.7 Alizarin Red Stain

This stain was done on pre-osteoblast cells with the four groups of samples for a period of 28 days and compared to a commercially available product. This stain was done

to evaluate the impact of Sr in production of Ca by pre-osteoblast cells. The images taken through a fluorescence microscope is observed in **Figures 6-21 A** (day 7), **B** (day 14), **C** (day 21), and D (day 28) respectively. Alizarin red highlights the calcium deposits in red. There is overall increase in calcium deposit by day 21. The commercial product is seen to have less calcium compared to SrHNT 1% in CPC on day 7. Alizarin red deposits are not seen in abundance on day 28. This can be due to high acidic nature of the stain which tends to remove the cells and contents of the well during the washes. On day 28 HNT 1% and 5% in CPC showed a lot of red staining showing a high calcium content 1% SrHNT showed purple color stain showing calcium compounds. Since these images could not be diagnosed through ImageJ, no numerical value could be added to the content of Ca.

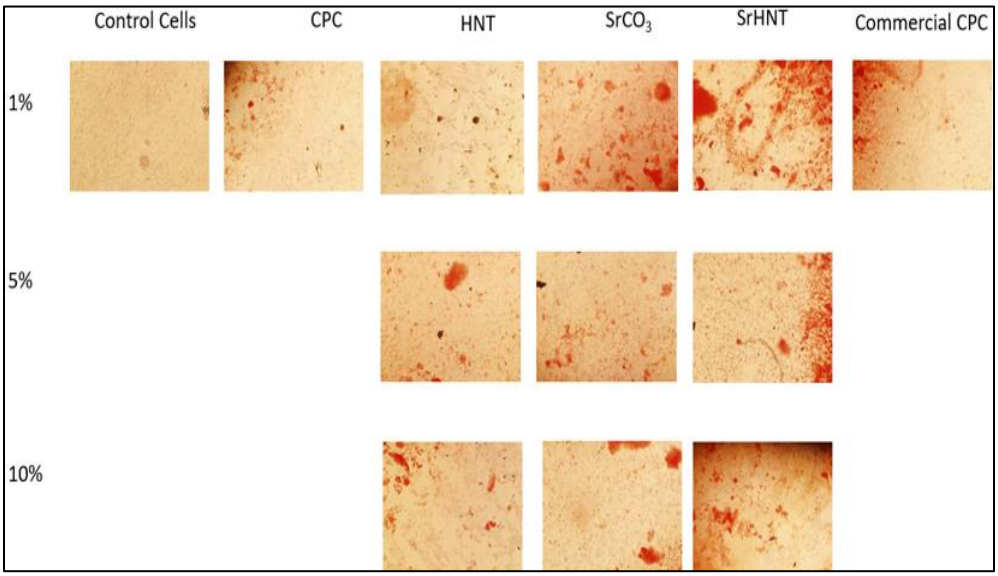

Figure 6-21 A: Alizarin red stain of pre-osteoblast cells for day 7 with all the four groups and a commercially available CPC (40 mg).

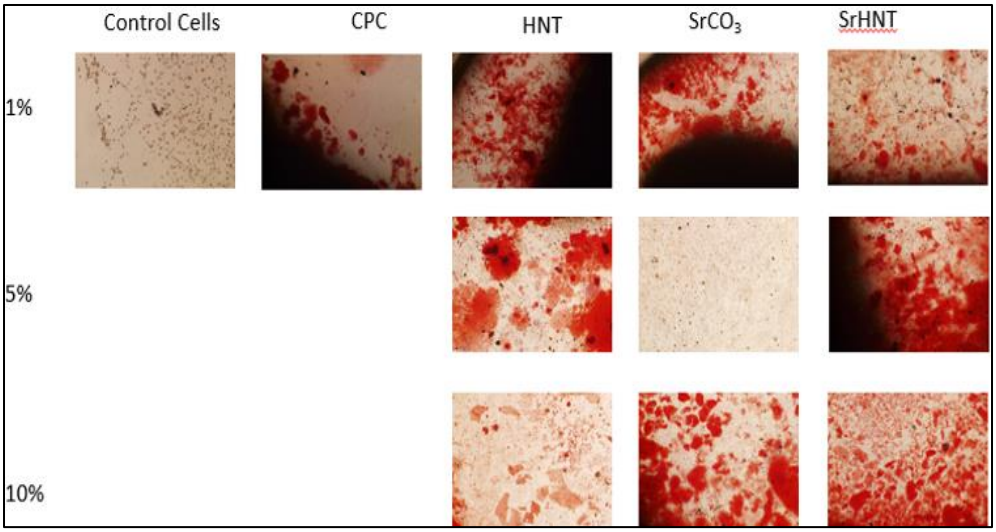

Figure 6-21 B: Alizarin red stain of pre-osteoblast cells for day 14 with all the four groups (40 mg).

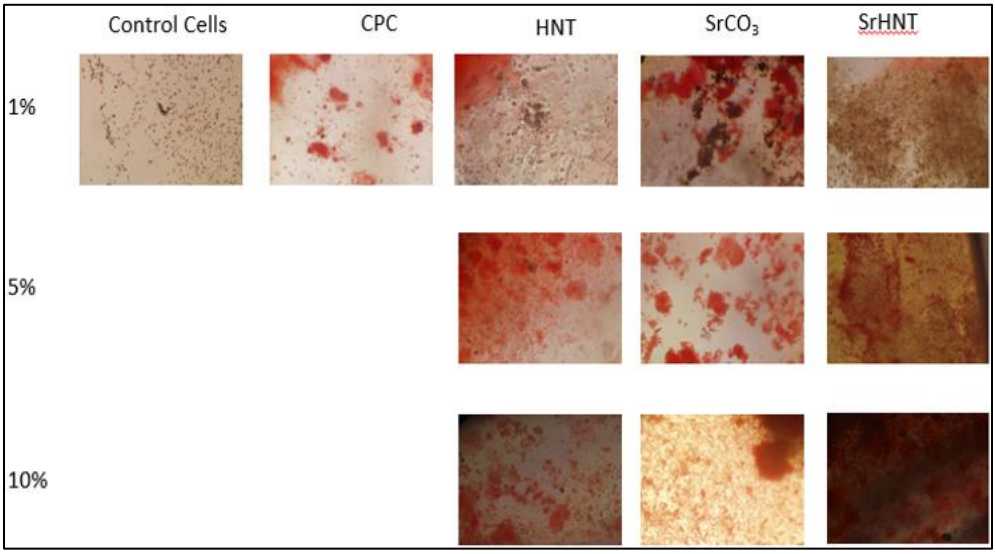

Figure 6-21 C: Alizarin red stain of pre-osteoblast cells for day 21 with all the four groups (40 mg).

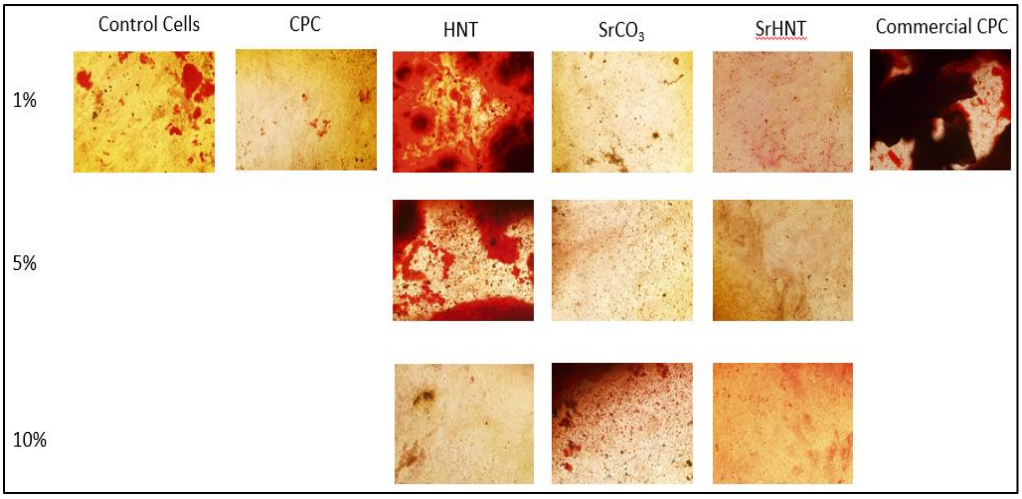

Figure 6-21 D: Alizarin red stain of pre-osteoblast cells for day 14 with all the four groups and a commercially available CPC (40 mg).

6.2.8 Surface Topography

SEM images were taken to analyze the surface topography of all the groups of CPC. Since cell viability and proliferation mainly depend on the surface of the substrate. Rougher the surface higher the probability for cell attachment and cell viability **Figures 6-22 A** (CPC and Group 2), **B** (CPC and Group 3), and **C** (CPC and Group 4) show the SEM images. As seen in the images CPC has comparatively very smooth surface. Adding HNTs, $SrCO_3$, and SrHNT introduced a more granular and porous surface. Higher the pore density higher the surface available for cell attachment. This distribution of HNTs and SrHNTs as seen in all the images can help in increasing the mechanical strength and prevent crack propagation in implants or filling when CPC is used.

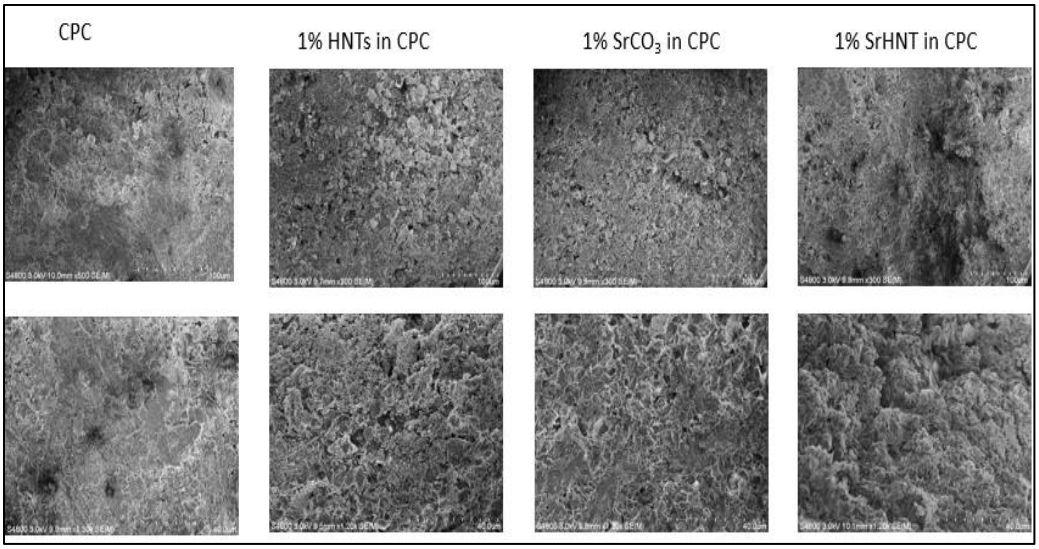

Figure 6-22 A: SEM images of CPC and Group 2 samples with 1% HNT, $SrCO_3$, and SrHNT in CPC. The top and bottom layer images were taken at 100 µm and 40 µm respectively.

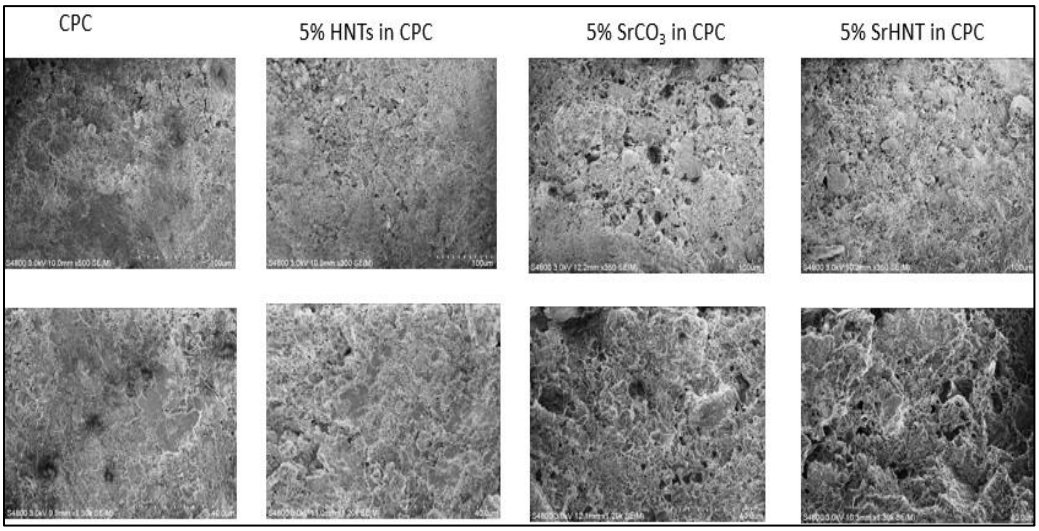

Figure 6-22 B: SEM images of CPC and Group 3 samples with 5% HNT, $SrCO_3$, and SrHNT in CPC. The top and bottom layer images were taken at 100 µm and 40 µm respectively.

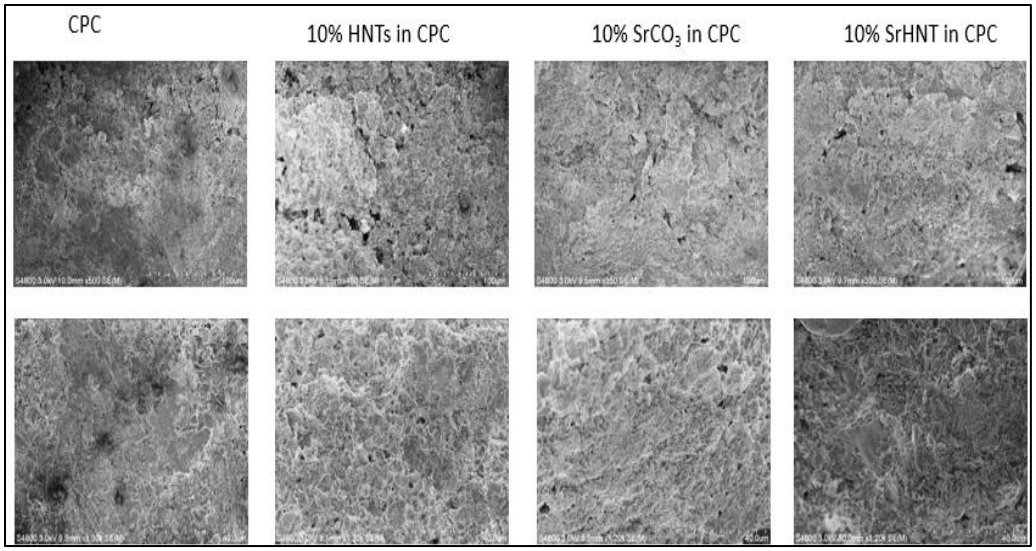

Figure 6-22 C: SEM images of CPC and Group 4 samples with 10% HNT, $SrCO_3$, and SrHNT in CPC. The top and bottom layer images were taken at 100 µm and 40 µm respectively.

6.2.9 Multi BET

BET pore size was done with helium adsorption-desorption method. This evaluation helped asses the differences in pore size after the addition of HNTs and SrHNT. **Figure 6-23** shows the graph of pore size based on the average of 1gm of 2 different samples size. The third data was taken for 200 mg and was considered too small an amount to give accurate results and hence was not used for graphical representation. As seen in the graph addition of 10% of HNT and SrHNT showed an increase in pore radius compared to plain CPC. Larger the pore sizes more surface is available for cell to adhere.

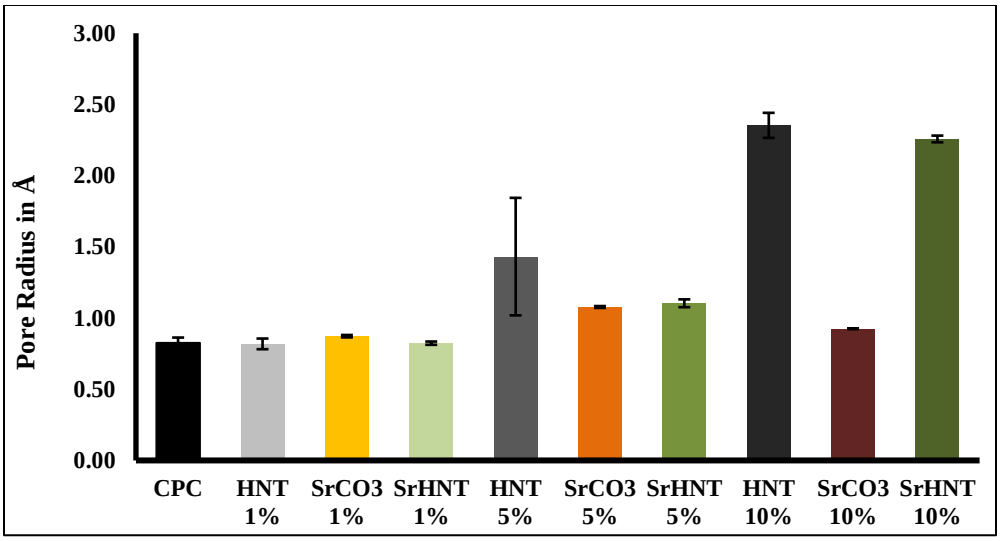

Figure 6-23: Shows the average pore radius of all the groups measured by NOVA e2000 surface are and pore analyzer. N=2 and error bars are Standard deviation.

6.2.10 Compression Strength

Compression test was done to analyze the maximum compressive strength and the peak load taken by the materials from all the 4 groups before they fractured. **Figure 6-24** shows the graphical representation of the peak load taken by the samples. Samples with 5% HNT and SrHNT in CPC showed high compression strength, highest in CPCs with 5% SrHNT. CPCs with 10% $SrCO_3$ also showed high compression strength. SrHNT 5% in CPC shows the combined properties of HNT and $SrCO_3$ and hence has a strong peak at 100 Mpa. Over all the addition of HNTs, $SrCO_3$, and SrHNT improved the load bearing strength of CPC. Human bones have a high compression strength of 180 -150 Mpa based on the nature of their formations which slowly decreases with age. This result showed that of all the compositions tested, 5% SrHNT in CPC showed a much higher improvement especially compared to plain CPC. One-way Anova calculated showed significant differences among all the groups with highest value of difference in 5%

SrHNT in CPC. Further testing needs to be conducted to find the right ration of SrHNT in CPC to reach the strength of human bones.

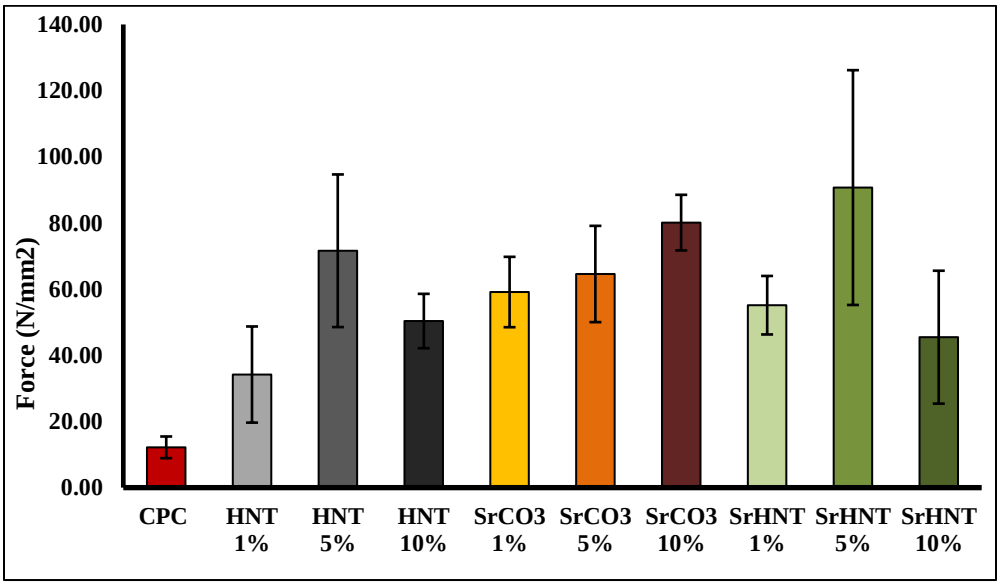

Figure 6-24: Peak compression strength of all the groups. The error bars are standard deviation where n=5, Error bars=Standard Deviation.

6.2.11 Flexural Strength

A three-point bend test was performed to get the estimate of the flexural strength of all the groups. This test evaluates the maximum force to bend the materials before it breaks. **Figure 6-25** shows the graphical representation of the peak flexural strength of all the samples in the four groups. Human bones have a fracture toughness of 4 MPa. Overall samples showed a high flexural strength After the addition of HNT 10% and SrHNT 1% to the CPCs, it showed the highest flexural strength of 13.1 and 13.3 MPa respectively. This may be due to the binding of CPC with chitosan was affected by SrHNT. Higher the SrHNT in the sample less binding of the particles on a larger surface area resulting in low bending threshold. One-way Anova showed a significant difference

for all the groups with highest difference of 1% SrHNT in CPC. Adding HNTs and SrHNTs improved the flexural strength of the cement and hence increasing the fracture toughness of the samples.

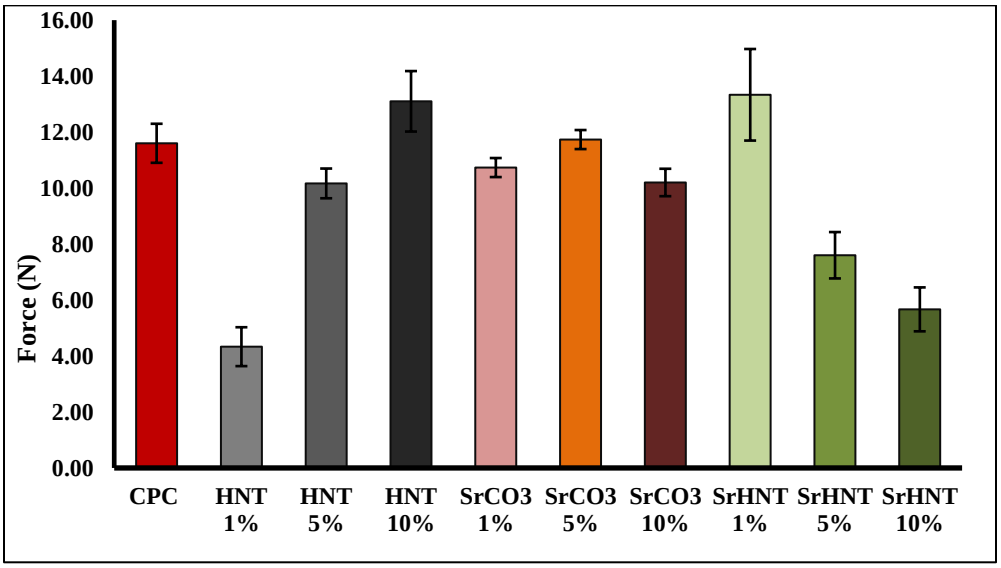

Figure 6-25: graphical representation of the peak flexural strength of all the groups. Error bars are the standard deviation where n=3, Error bars=Standard Deviation.

6.2.12 Anti-Bacterial Property

To measure the bactericidal properties of all the groups, 5mm x 2mm discs for all the groups were made and place on the petri dish with Mueller Hilton agar and two separate lawns of *E. coli* (**Figure 6-26 A**) and *S. aureus* (**Figure 6-26 B**) representing a gram-negative and a gram-positive bacterium respectively. Zones of inhibition were measured for all the samples and graph was made based on the area of inhibition for all the groups as seen in **Figure 6-27 A** for *E. coli* and **Figure 6-27 B** for *S. aureus*. CPC by nature did not show any bactericidal properties. Although the zones of inhibition of gentamicin discs were the maximum, all the groups showed anti-bacterial property

inhibiting the growth of both gram positive and negative bacteria. One-way Anova showed np significant difference among the groups. SrHNT in CPC discs showed the highest zone of inhibitions. Sr by inherent nature has antibacterial properties which showed effect in these discs. Implants with SrHNT will have lower the infections around the implants.

A 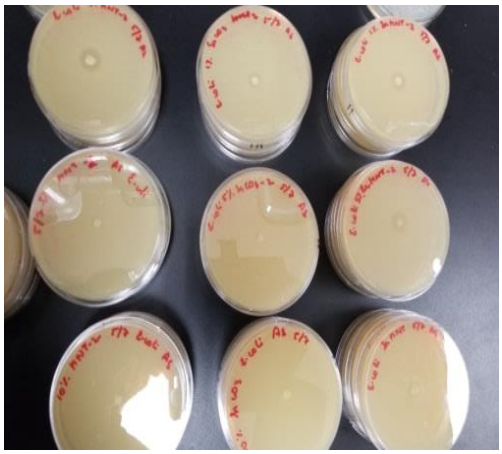 B 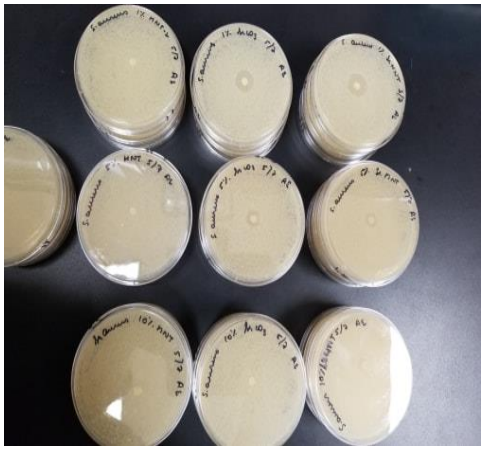

Figure 6-26: Image showing the petri dishes with the discs over lawns of A) *E. coli* and B) *S. aureus*. The experiment was done in triplicate from cultures of 3 different colonies of bacteria.

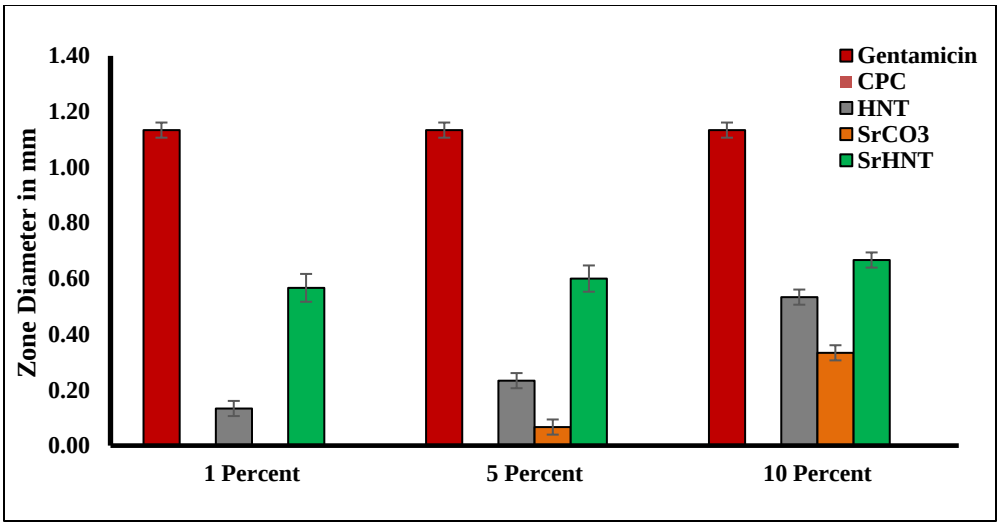

Figure 6-27 A: Graphical representation of the zones of inhibition measured in mm for all the groups for *E. coli*. Error bars are standard deviation where n=3.

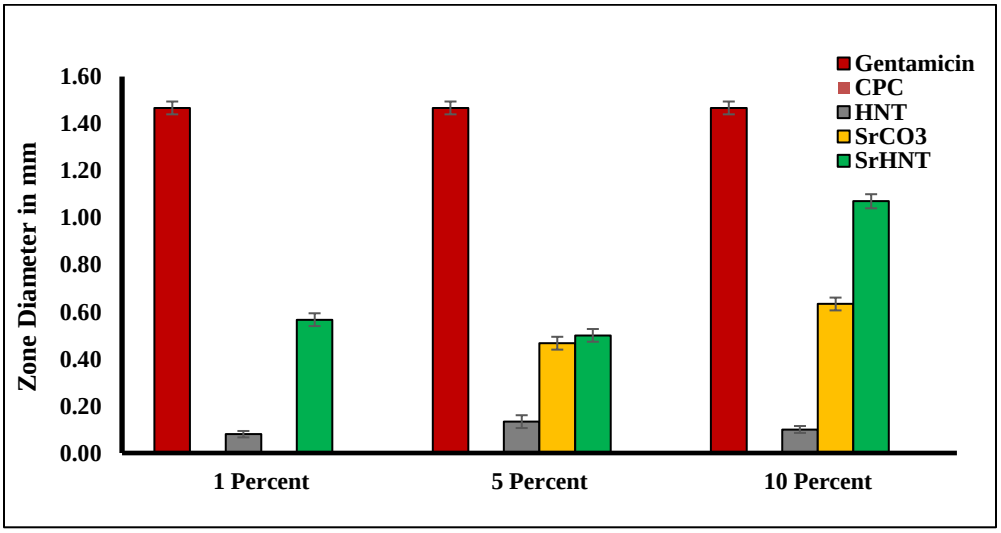

Figure 6-27 B: Graphical representation of the zones of inhibition measured in mm for all the groups for *S. aureus*. Error bars are standard deviation where n=3.

6.2.13 Biodegradability

It is an important property of CPC implants to dissolve slowly after a period of time an allow for the bones cells to grow the affected part again. To evaluate the degradability of the all the 4 groups 5 mm in diameter x 2mm in thickness discs were

place in 1 ml of SBF for six weeks till when the weight of the samples started to lower and the samples started to disintegrate. The weight of the samples was taken as dry weight and dipped in SBF and measured for wet weight on day zero. After which the samples were taken and blotted off the excess water and measured every seven days. The values of triplicate of triplicate samples was plotted in the graphs as seen in **Figures 6.28 A** (CPC and Group 2), **B** (CPC and Group 3), and **C** (CPC and Group 4). The weights of the discs increased over a period of 1 week and stayed around at that weight till week 4 before it started to decrease in weight and started to disintegrate. This test was done in SBF which had a pH of 7.4 matching the body fluid pH and ion concentration of a normal healthy human body. The pH of different systems is different and pH near the injury or cancerous region in the body is acidic. Further testing needs to be done to test for the biodegradability in different acidic and basic pH fluids.

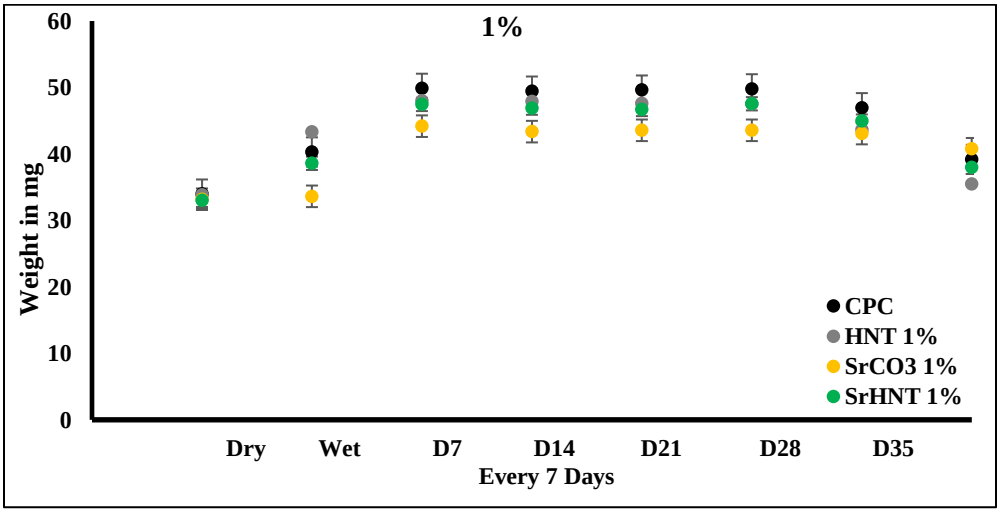

Figure 6-28 A: Graphical representation of degradability of CPC and group 2 over 6 weeks. Error bars are standard deviation where n=3x3.

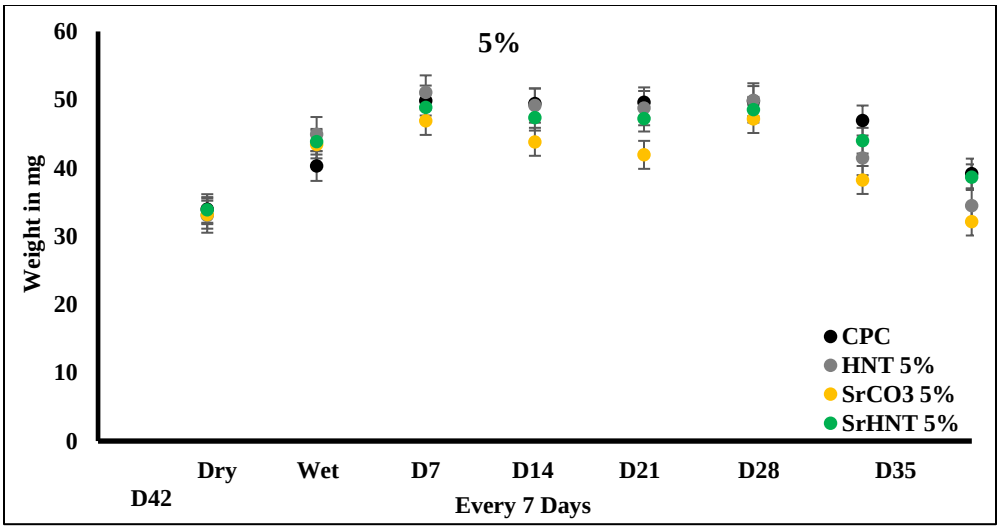

Figure 6-28 B: Graphical representation of degradability of CPC and group 3 over 6 weeks. Error bars are standard deviation where n=3x3.

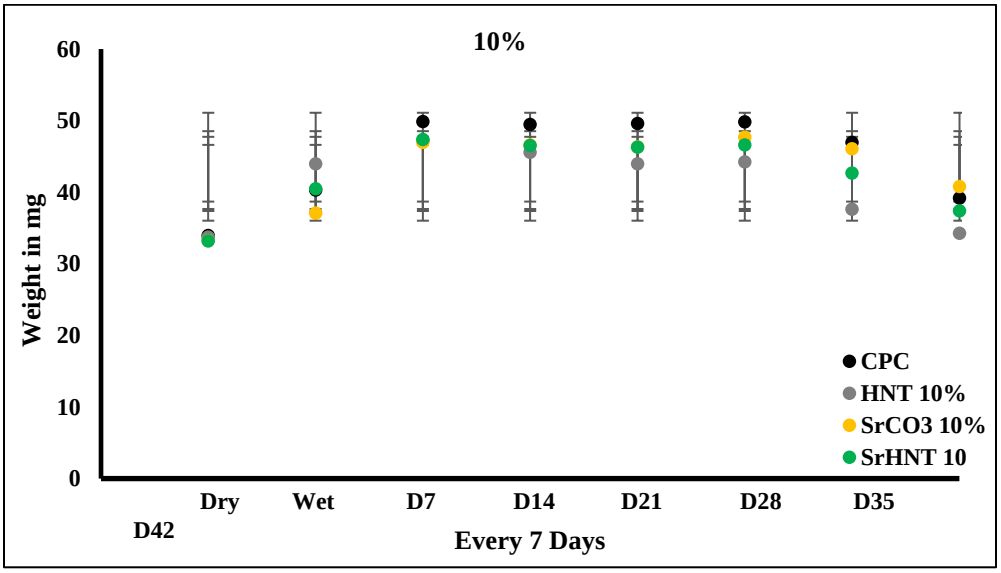

Figure 6-28 C: Graphical representation of degradability of CPC and group 4 over 6 weeks. Error bars are standard deviation where n=3x3.

6.3 Project 3: Using SrHNT as a Drug Carrier

6.3.1 SEM

The method of coating SrHNT involved hydrolysis of Sr^{2+} ions in water and then forming a bond with the hydroxyl ion on the surface of HNT. it was important to evaluate the retainment of Sr coating on HNTs after they were immersed in liquid phase of drugs used for vacuum loading. SEM images were taken of SrHNT after drug loading as seen in **Figure 6-29**. The images showed that the SrHNT retained the coating after drug loading also. HNTSr were samples where the loading was followed by coating of Sr. As seen in the SEM images the Sr coating was successful after loading the HNTs with drugs.

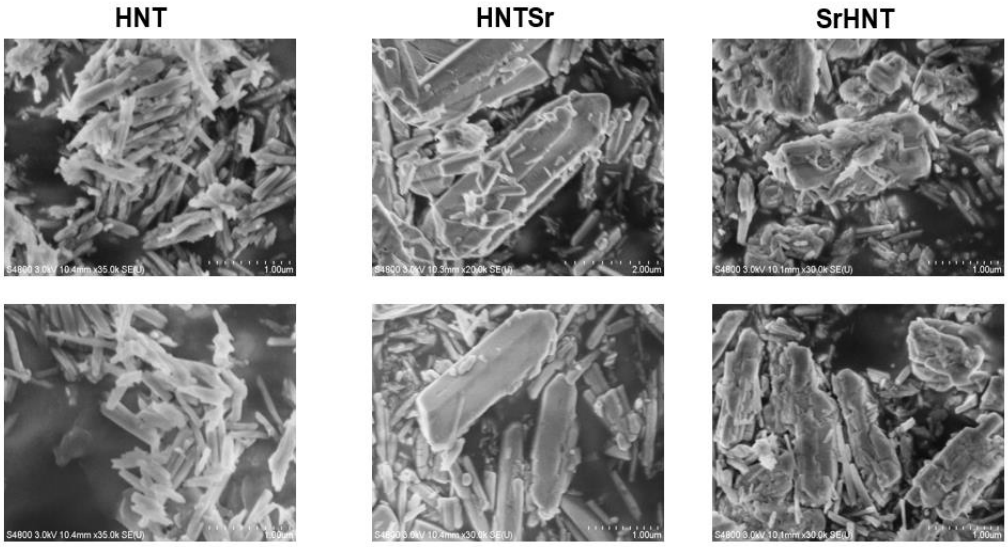

Figure 6-29: SEM images of gentamicin loaded HNT, HNTSr, and SrHNTs.

6.3.2 Gentamicin

6.3.2.1 *Live Dead Assay*

The HNTs SrHNTs and HNTSr is loaded with any drug, it is important to evaluate the right concentration of the particular antibiotic and loaded nanoparticle

combination which will not affect the cell viability. Cells used for this test was pre-osteoblast cells. A live dead assay was conducted for three different concentrations of 1 mg/ml, 0.1 mg/ml, and 0.01 mg/ml for day 1 (**Figure 6-30 A** and **B** for live and dead), day 3 (**Figure 6-31 A** and **B** for live and dead), and day 7 (**Figure 6-32 A** and **B** for live and dead) to narrow down the right concentration for suitable cell viability. As seen in the image high concentrations of all the three nanoparticles were not conducive for cell viability. Even on day 1 there is a low concentration of green cells for 1 mg/ml and 0.1 mg/ml. Although they did not appear to have a toxic effect as the red dead cells are very few. By day seven the live green cells for both the higher concentrations is very low but the cells thrived in 0.01 mg/ml with loaded nanoparticles. This experiment showed that the drug loaded HNTs, SrHNTs, and HNTSr would not have a negative impact of cell viability in low concentrations.

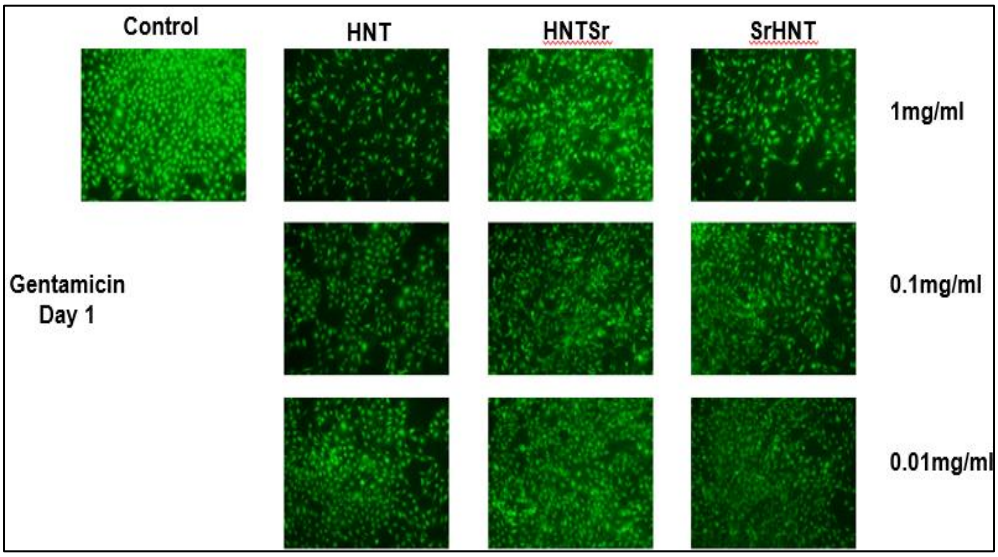

Figure 6-30 A: Live dead cell assay where the live cells are seen in green for 3 different concentrations of HNT, HNTSr, and SrHNT for day 1.

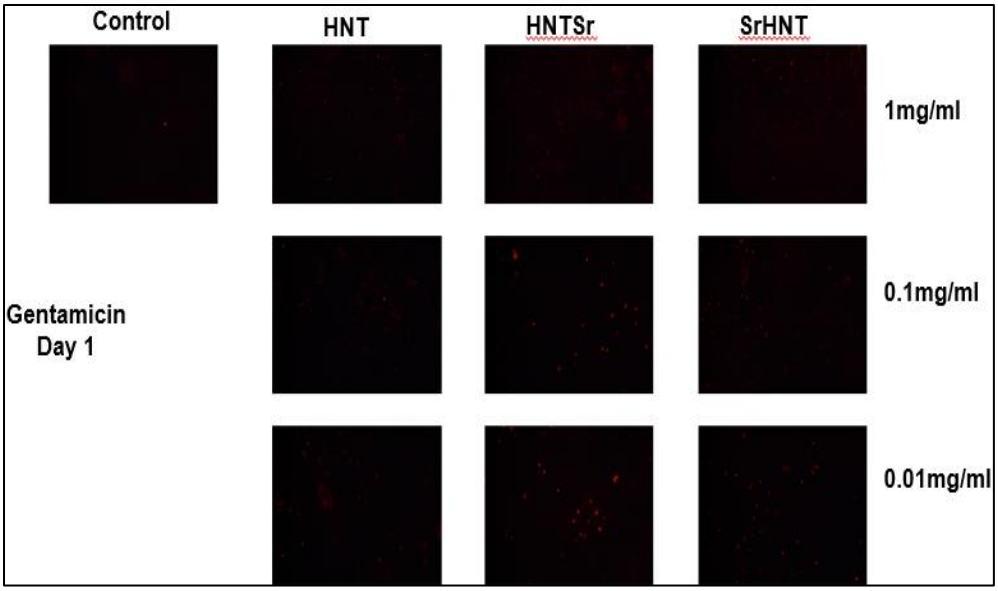

Figure 6-30 B: Live dead cell assay where the dead cells are seen in red for 3 different concentrations of HNT, HNTSr, and SrHNT for day 1.

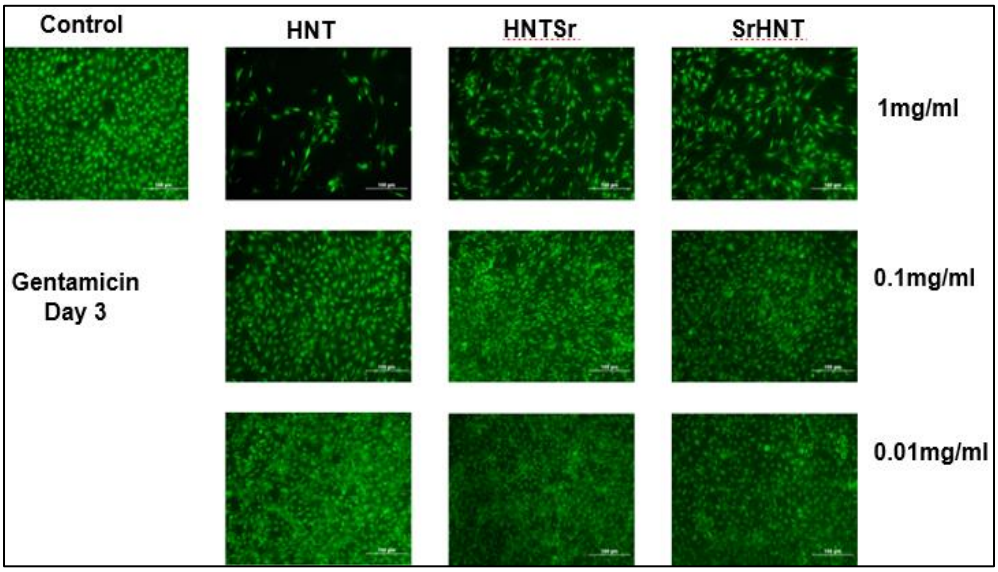

Figure 6-31 A: Live dead cell assay where the live cells are seen in green for 3 different concentrations of HNT, HNTSr, and SrHNT for day 3.

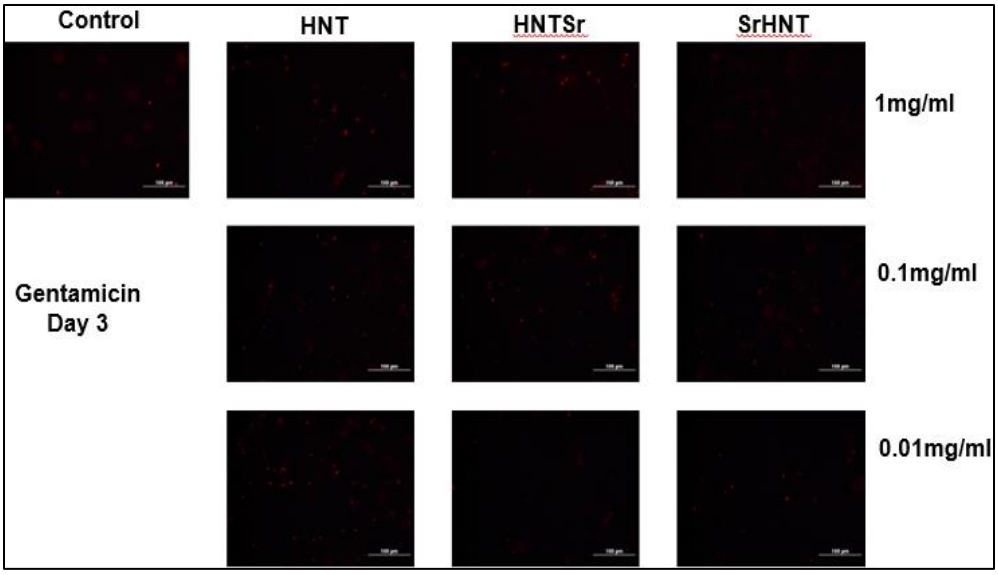

Figure 6-31 B: Live dead cell assay where the dead cells are seen in red for 3 different concentrations of HNT, HNTSr, and SrHNT for day 3.

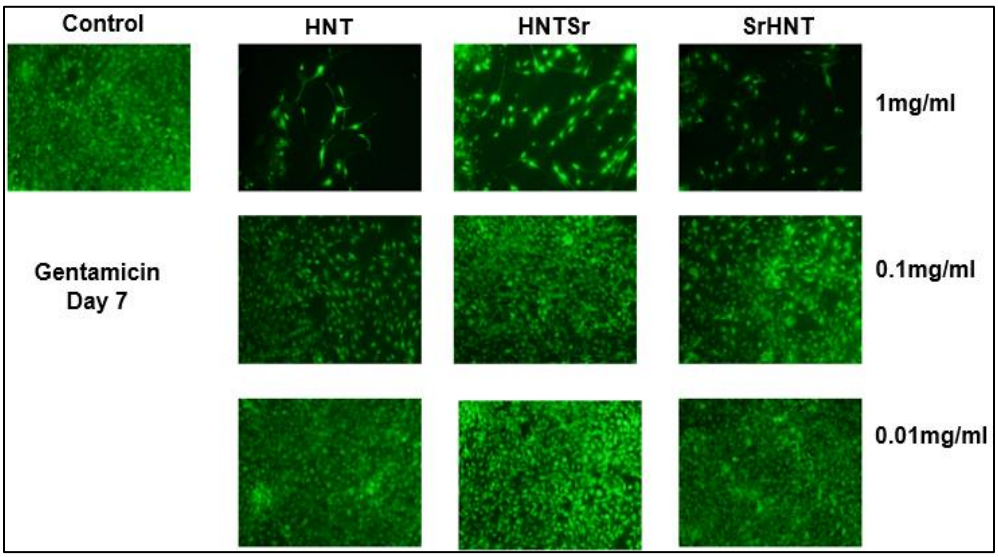

Figure 6-32 A: Live dead cell assay where the live cells are seen in green for 3 different concentrations of HNT, HNTSr, and SrHNT for day 7.

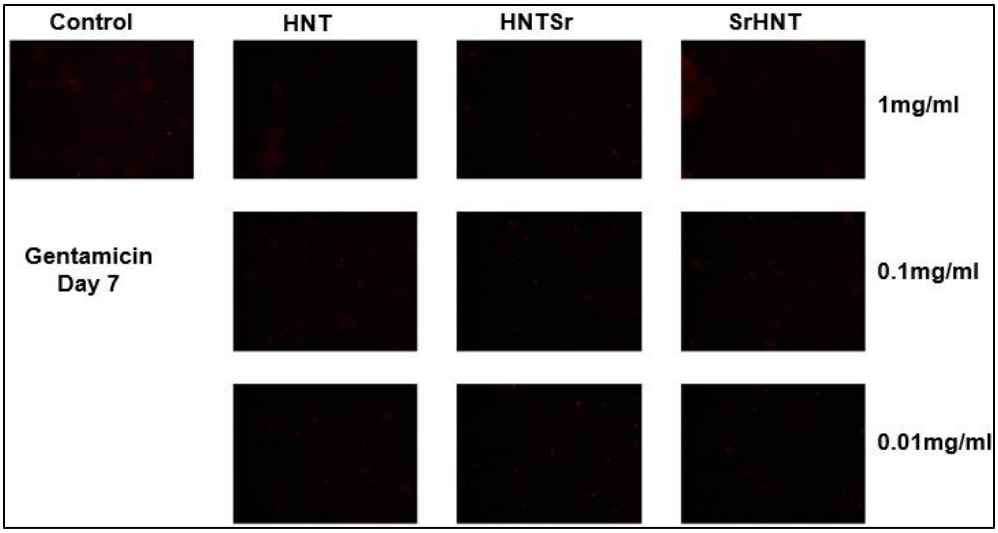

Figure 6-32 B: Live dead cell assay where the dead cells are seen in red for 3 different concentrations of HNT, HNTSr, and SrHNT for day 7.

Image J was used to quantitatively analyze the live dead assay and was graphically represent in **Figures 6-33 A** (1 mg/ml), **B** (0.1 mg/ml), and **C** (0.01 mg/ml). As the graphs show the cell viability count on day seven was highest for 0.01 mg/ml. Overall SrHNT showed better cell viability in all the concentration. Coating HNTs with Sr may provide a layer that effects the cells in a positive manner. One-way Anova showed no significant difference between the samples in same concentrations.

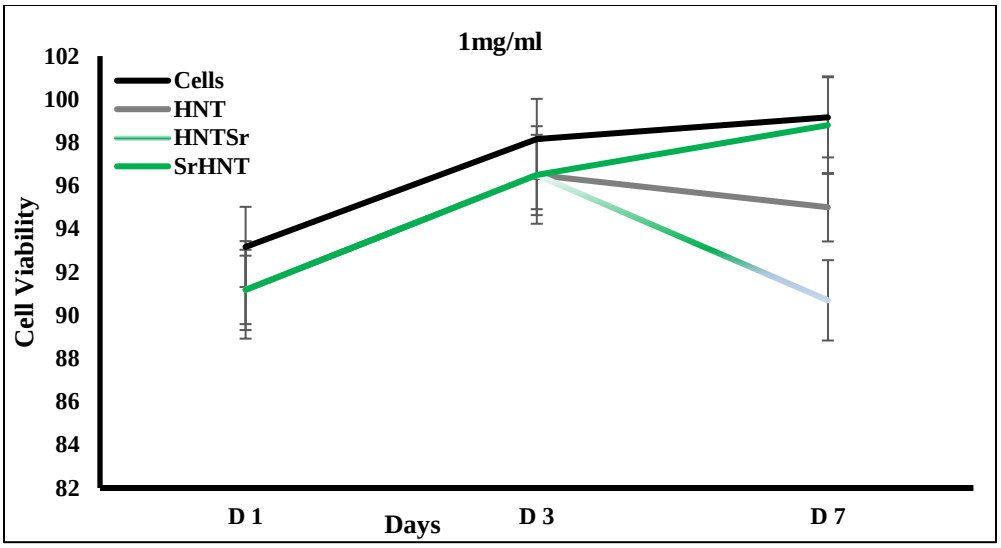

Figure 6-33 A: Graphical representation of Live dead cell assay of HNT, HNTSr, and SrHNT for 1 mg/ml for day 1, 3, and 7 where n=3, error bars are Standard deviation.

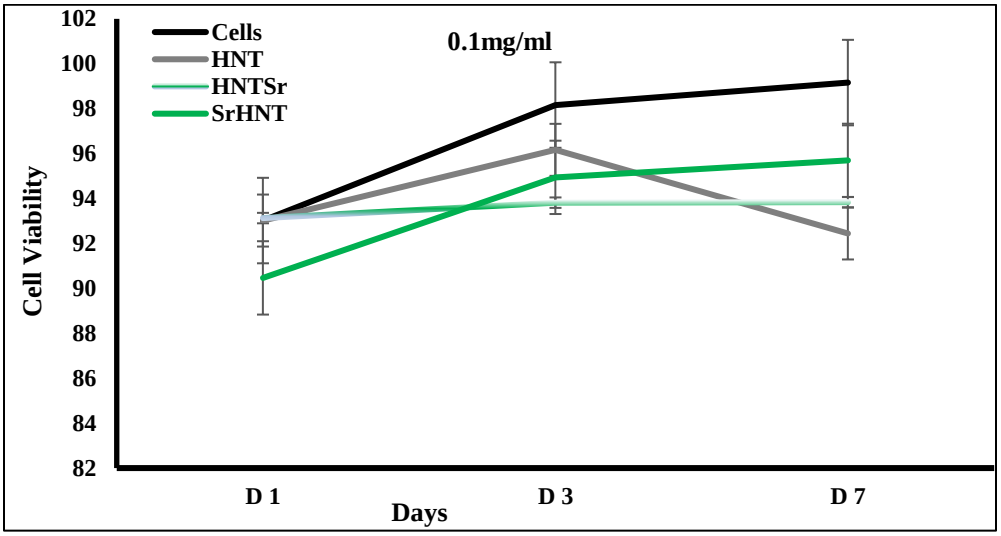

Figure 6-33 B: Graphical representation of Live dead cell assay of HNT, HNTSr, and SrHNT for 0.1 mg/ml for day 1, 3, and 7 where n=3, error bars are Standard deviation.

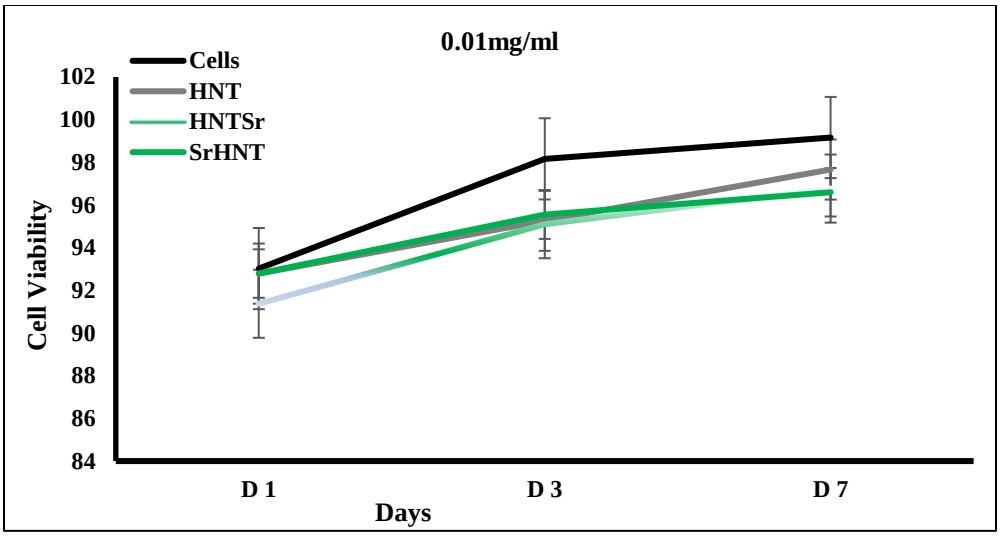

Figure 6-33 C: Graphical representation of Live dead cell assay of HNT, HNTSr, and SrHNT for 0.01 mg/ml for day 1, 3, and 7 where n=3, error bars are Standard deviation.

6.3.2.2 *Disk Diffusion Method for CPC*

This test was done to evaluate the successful release of drugs from drug loaded SrHNT and HNTSr when they are embedded in CPC in different percentages by weight. The same percentages were used as in project 2. The discs of CPC were made as 6mm diameter x 2mm thickness and place in lawns of *E. coli* and *S. aureus* in Mueller Hilton plates as seen in **Figure 6-34 A** and the control was the ready gentamicin discs and to test for the viability of the bacteria plates with just the lawn of the bacteria was made as seen in **Figure 6-34 B**. The bactericidal effect of the drugs released through these discs was measured by the diameter of zone of inhibition. A clear are around the disks showed that gentamicin was released to kill the bacteria around the discs containing gentamicin loaded HNT, SrHNT, and HNTSr, in different percentages. The graphical representation of the zones of inhibition created by drug loaded HNT, SrHNT, and HNTSr was plated as seen in **Figure 6-35 A** (*E. coli*) and **B** (*S. aureus*). One-way Anova shows no significant different among the samples and gentamicin discs. The graphs show that the drug was

effectively release through the nanoparticles and CPC. The overall zone of inhibitions was slightly more that caused by standard gentamicin discs. This can be explained as the SrHNTs and HNTSr have inherent antibiotic properties. This test showed that drug loaded SrHNTs can be embedded in CPC implants.

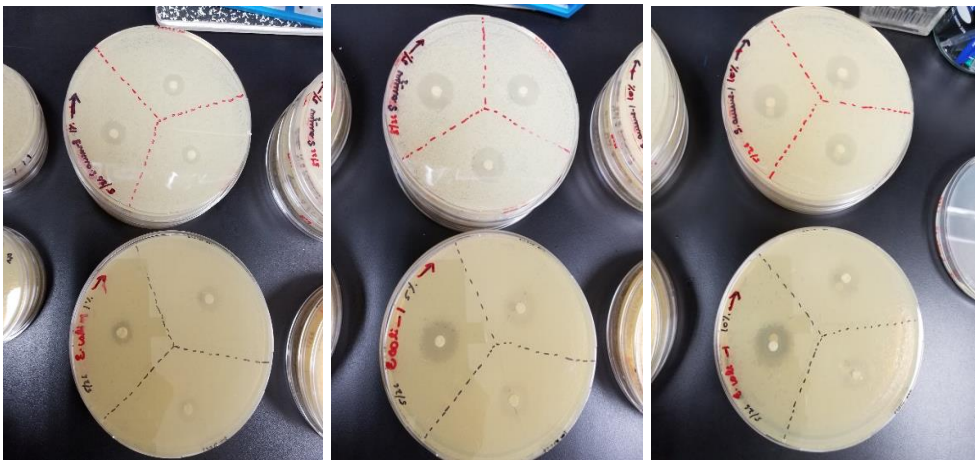

Figure 6-34 A: Disk diffusion plates with discs of 1%, 5%, and 10% HNT, SrHNT, and HNTSr individually in CPC for *E. coli* and *S. aureus*.

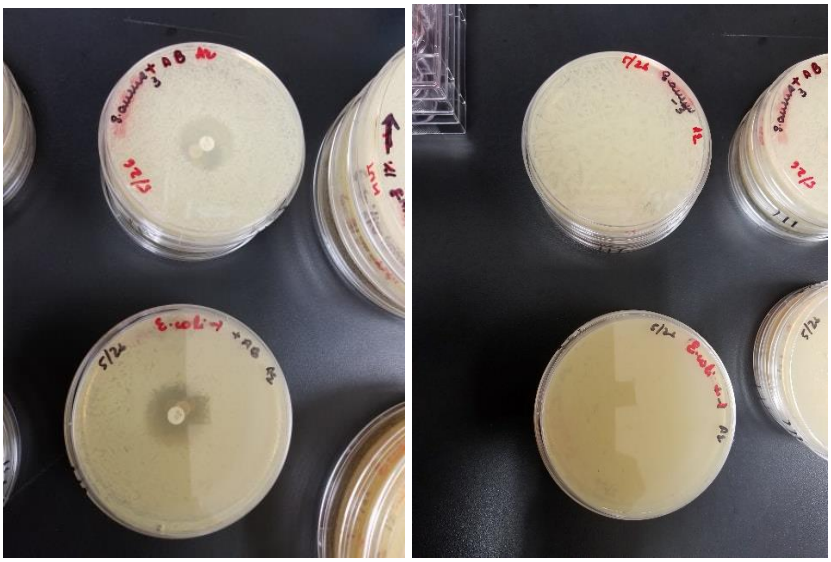

Figure 6-34 B: Disk diffusion plates with and without gentamicin disc in *E. coli* and *S. aureus* lawn.

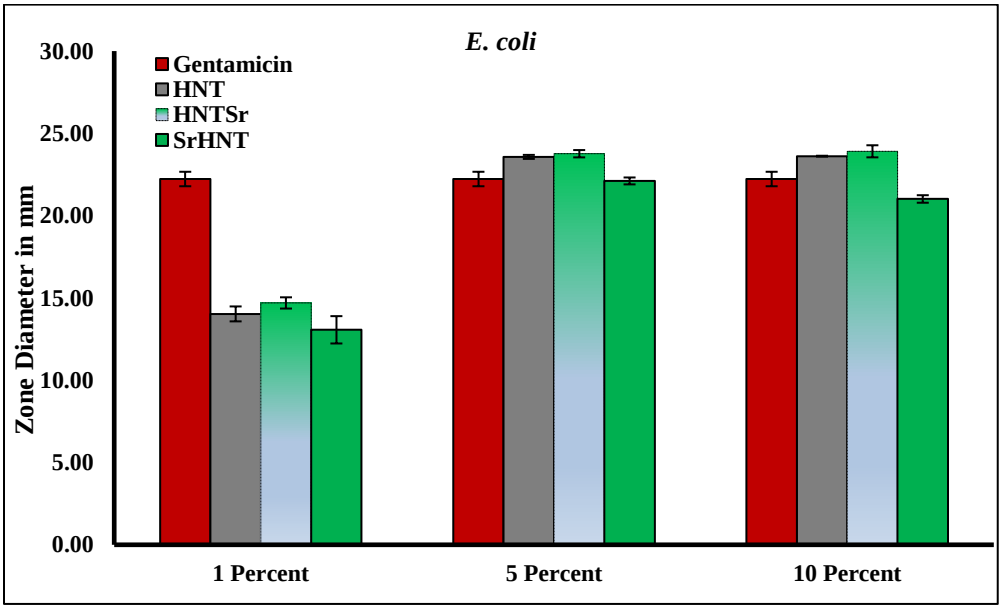

Figure 6-35 A: Graphical representation of zone of inhibition of gentamicin discs, and CPC discs with 1%, 5%, and 10% of HNT, SrHNT, and HNTSr individually in lawns of *E. coli*. The error bars are standard deviations where n=3.

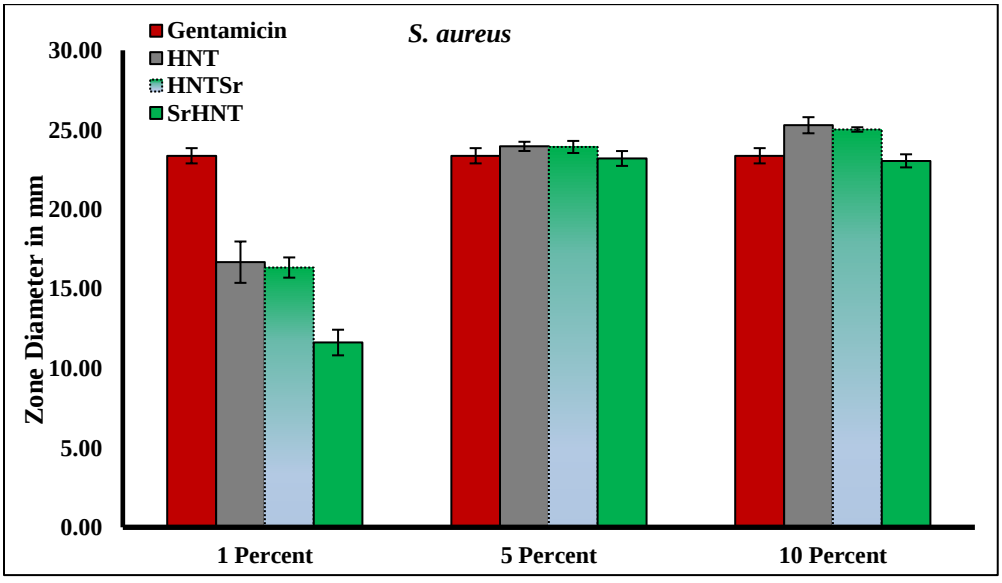

Figure 6-35 B: Graphical representation of zone of inhibition of gentamicin discs, and CPC discs with 1%, 5%, and 10% of HNT, SrHNT, and HNTSr individually in lawns of *S. aureus*. The error bars are standard deviations where n=3.

6.3.2.3 *Drug Loaded Nanoparticles in a Contaminated Cell Environment*

The release and effectiveness of gentamicin loaded SrHNT and HNTSr was tested in a cell environment using pre-osteoblast cells with the addition of *E. coli* bacteria. After inoculating the cells with the bacteria live dead assay was performed after 24 hours to visualize the health of the pre-osteoblast cells. The images were taken as seen in **Figures 6-36 A** (live cells) and **B** (dead cells), for pre-osteoblast cells (POB), POB with gentamicin (AB), POB with AB and *E. coli*, just *E. coli*, POB with *E. coli* and the three loaded HNTs, SrHNT, and HNTSr individually. As seen in the images, POB are able to survive even after the contamination with bacteria and addition of AB reduces the blurriness of the images caused by bacterial growth. Clear cells are seen in the images of HNT, SrHNT, and HNTSr indicating the release of gentamicin which was bactericidal. The presence of *E. coli* caused a higher cell death seen in red in the images of dead cells after 24 hours.

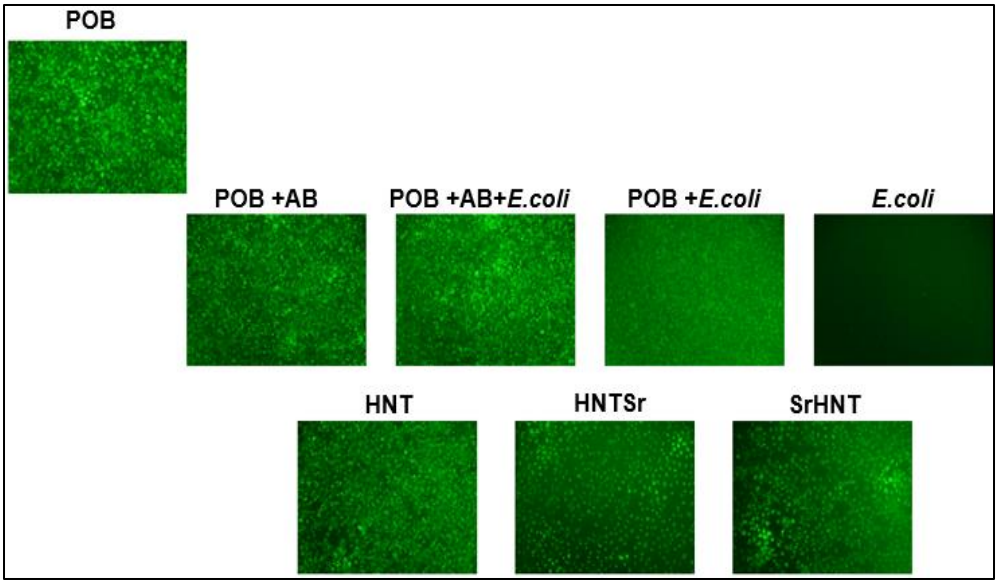

Figure 6-36 A: Images from Live and dead assay where live cells are seen in green. The images show pre-osteoblast cells (POB), POB with gentamicin (AB), POB with AB and *E. coli*, just *E. coli*, POB with *E. coli* and the three loaded HNTs, SrHNT, and HNTSr individually after 24 hours.

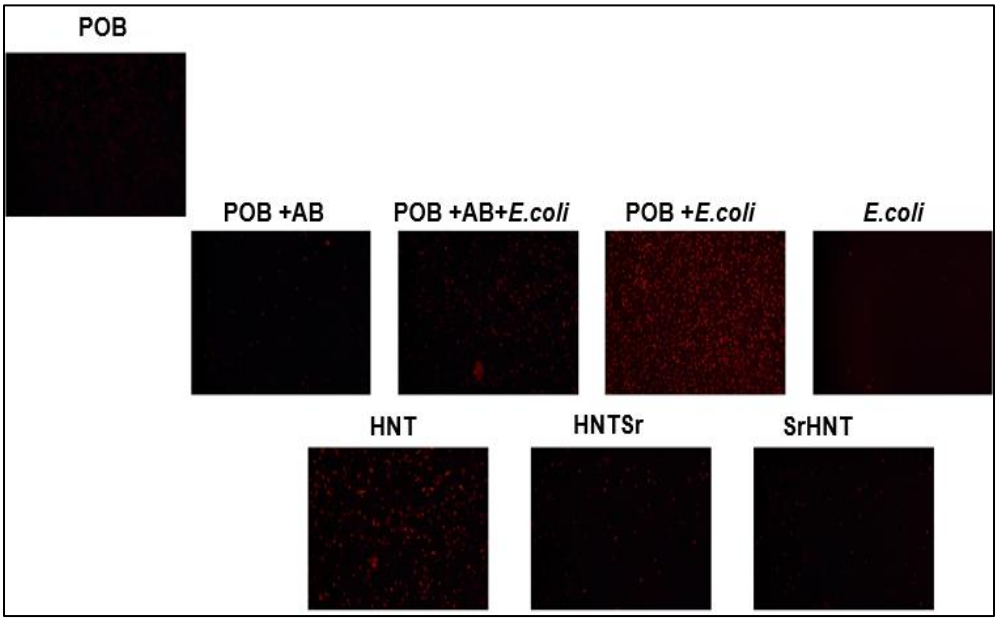

Figure 6-36 B: Images from Live and dead assay where dead cells are seen in red. The images show pre-osteoblast cells (POB), POB with gentamicin (AB), POB with AB and *E. coli*, just *E. coli*, POB with *E. coli* and the three loaded HNTs, SrHNT, and HNTSr individually after 24 hours.

6.3.2.4 *Bacterial Growth*

To access the rate of bacterial growth, optical density was measured for the multiple 48 well plates with the samples before addition of bacteria, after addition of samples as Time 0, and after 24 hours from the time bacteria was inoculated as T 24 and plotted in a graph as seen in **Figure 6-37**. As the graph shows the bacterial growth was unhindered and showed highest absorbance in the wells containing just the bacteria and POB with bacteria. The bacterial growth rate was stopped by gentamicin release in the well having 0.01 mg/ml of HNTs, SrHNT, and HNTSr. This graph showed that AB loaded SrHNT and HNTSr released the drugs effectively and the caps of the halloysites was not closed due to Sr coatings. This also went on to show that SrHNTs and HNTSr can be effectively loaded with this AB and be embedded in these particular cells at a concentration of 0.01 mg/ml and be effective. Further tests have to be conducted to ensure that Sr coated HNTs will be effective with multiple drugs and various cell lines.

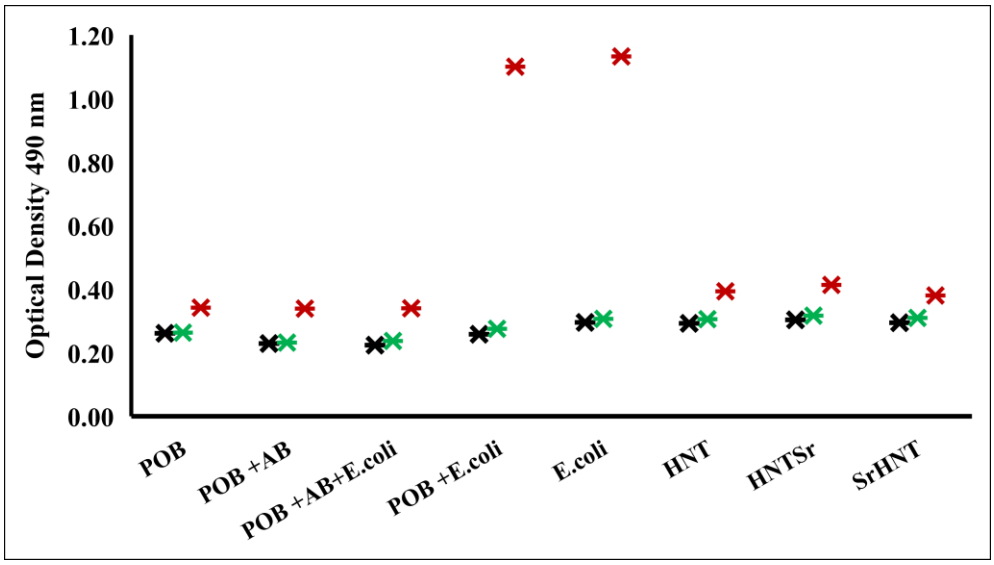

Figure 6-37: Graphical representation of pre-osteoblast cells (POB), POB with gentamicin (AB), POB with AB and *E. coli*, just *E. coli*, POB with *E. coli* and he three loaded HNTs, SrHNT, and HNTSr individually. ***** shows the reading before addition of Bacteria, * shows Time 0 after adding *E. coli*, and * shows the readings at time 24. n=6

6.3.2.5 *Proliferation Assay*

Proliferation assay was conducted to analyze if the POB proliferated with bacteria and AB and the drug loaded SrHNTs and HNTSr with the same rate as control cells. This test was to evaluate the effectiveness of drug release by the nanoparticles which was bactericidal, and at the same time would not impact the POB to proliferate. The proliferation rate was represented in a graph as seen in **Figure 6-38**. As seen in the graph the cells showed a higher absorbance when the bacteria were present in the wells which was due to the presence of bacteria. One -way Anova showed no significant difference between the wells. The cells with the nanoparticle showed normal proliferation rate but higher absorbance then just pre-osteoblast which may be due to the presence of the cell debris.

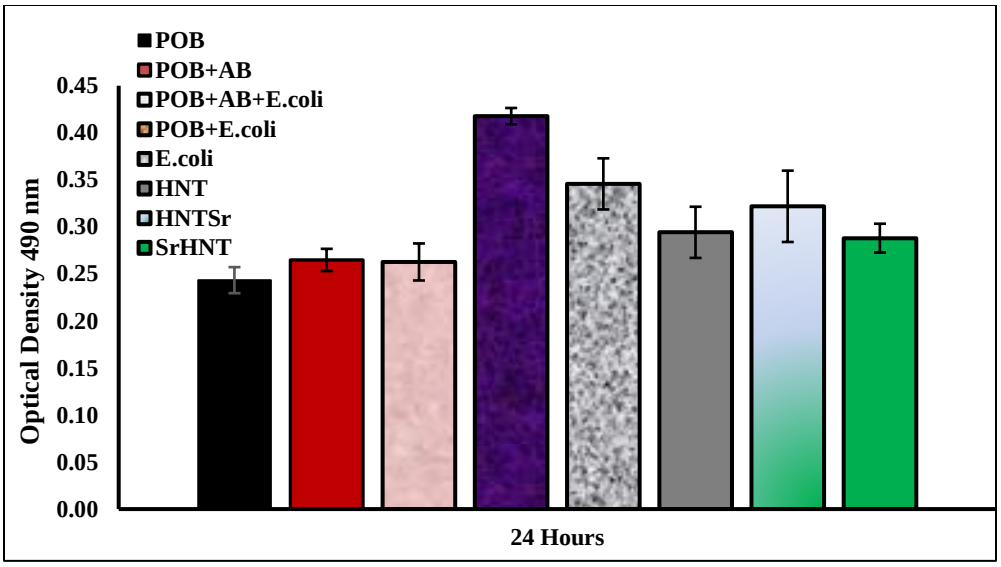

Figure 6-38: Graphical representation of the proliferation assay of pre-osteoblast cells (POB), POB with gentamicin (AB), POB with AB and *E. coli*, just *E. coli*, POB with *E. coli* and he three loaded HNTs, SrHNT, and HNTSr individually. n=6. Error bars are Standard deviation.

6.3.3 Methotrexate Loading

6.3.3.1 *Live Dead Assay*

Methotrexate is used as a chemotherepautic agent. The combination with SrHNT and HNTSr was studied to evaluate the right concentration which will not affect the cell viability. Cells used for this test pre-osteoblast cells. A live dead assay was conducted for three different concentration 1 mg/ml, 0.1 mg/ml, and 0.01 mg/ml for day 1 (**Figures 6-39 A** and **B** for live and dead), day 3 (**Figures 6-40 A** and **B** for live and dead), and day 7 (**Figure 6-41 A** and **B** for live and dead)to narrow down the right concentration for suitable cell viability. As seen in the image high concentrations of all the three nanoparticles reduced the live cells. Even on day 1 there is a low concentration of green cells for 1 mg/ml and 0.1 mg/ml. Although they did not appear to have a toxic effect as the red dead cells are very few. By day seven the live green cells for both the higher

concentrations is very low but the cells thrived in 0.01 mg/ml with loaded nanoparticles. This experiment showed that 0.01 mg/ml methotrexate loaded HNTs, SrHNTs, and HNTSr would not have a negative impact of cell viability in low concentrations.

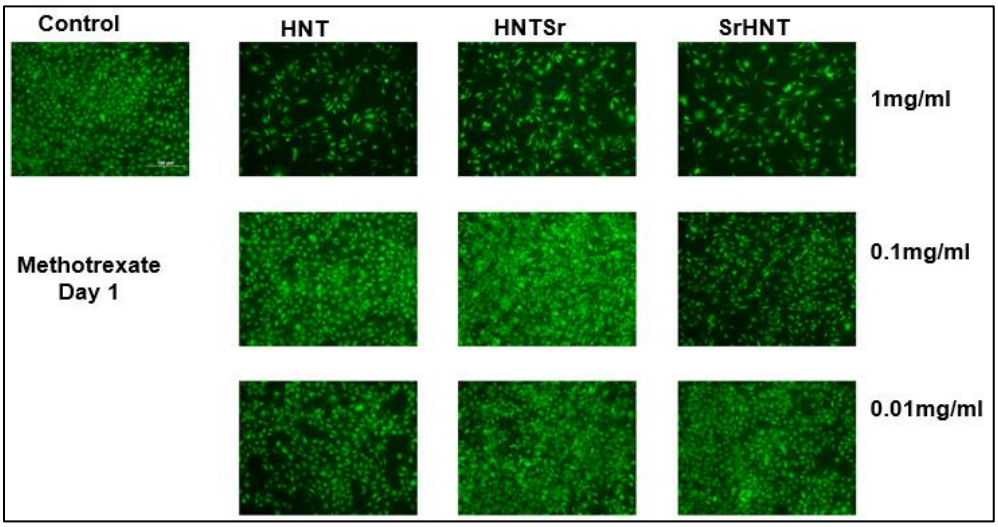

Figure 6-39 A: Live dead cell assay where the live cells are seen in green for 3 different concentrations of HNT, HNTSr, and SrHNT for day 1.

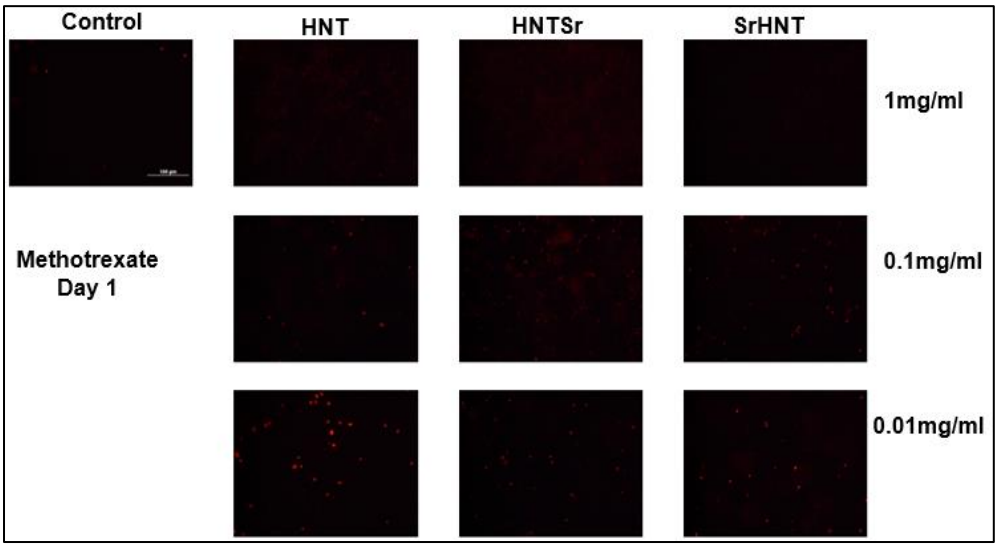

Figure 6-39 B: Live dead cell assay where the dead cells are seen in red for 3 different concentrations of HNT, HNTSr, and SrHNT for day 1.

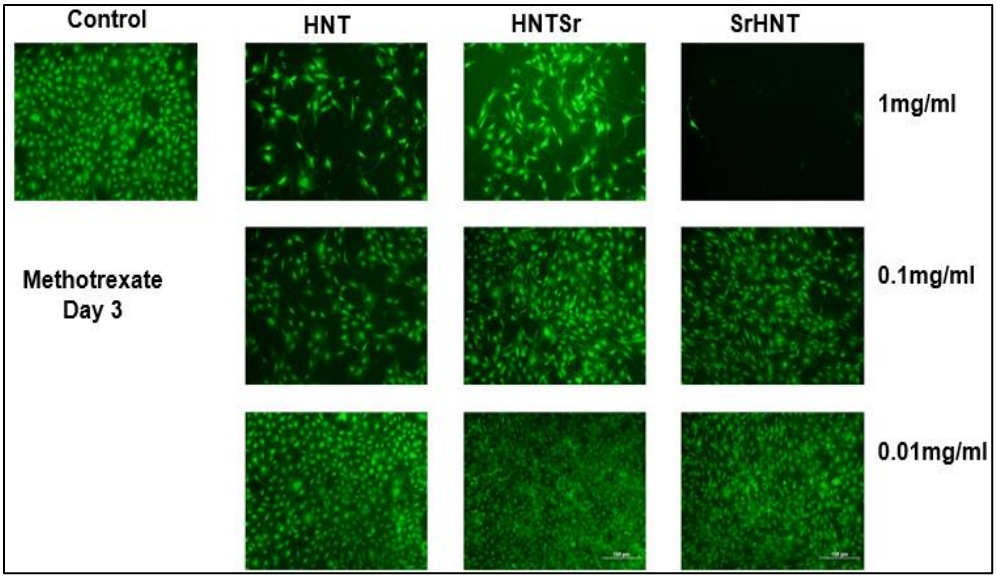

Figure 6-40 A: Live dead cell assay where the live cells are seen in green for 3 different concentrations of HNT, HNTSr, and SrHNT for day 3.

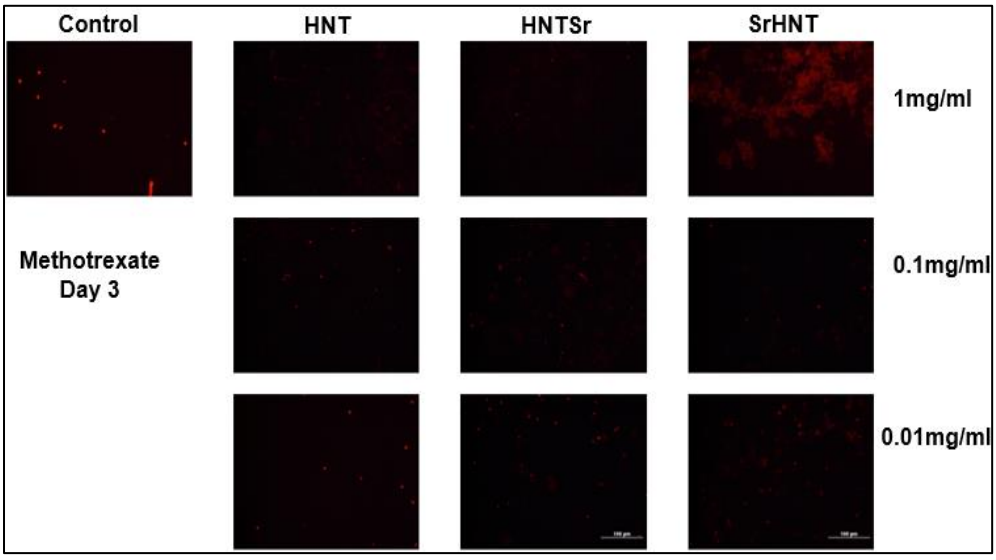

Figure 6-40 B: Live dead cell assay where the dead cells are seen in red for 3 different concentrations of HNT, HNTSr, and SrHNT for day 3.

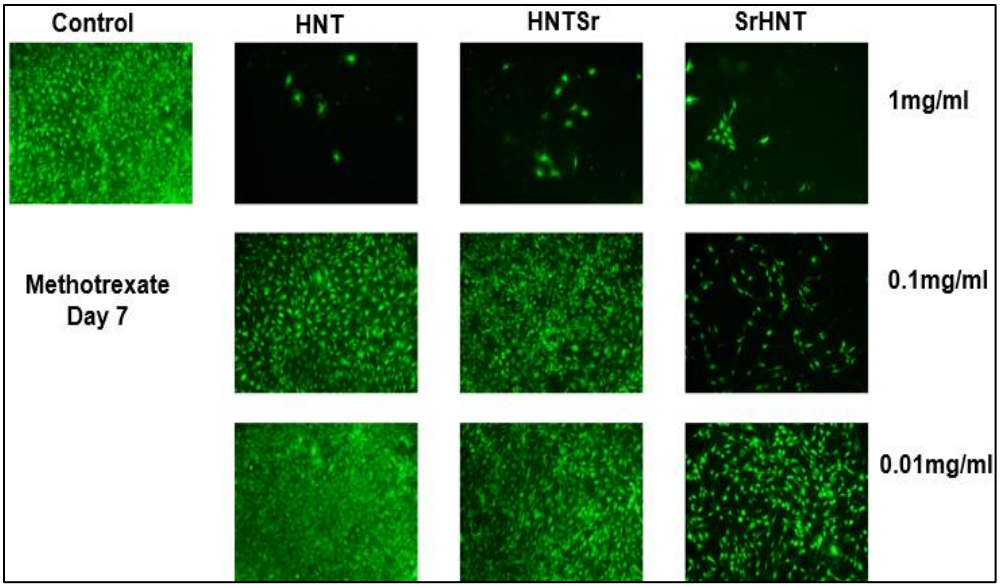

Figure 6-41 A: Live dead cell assay where the live cells are seen in green for 3 different concentrations of HNT, HNTSr, and SrHNT for day 7.

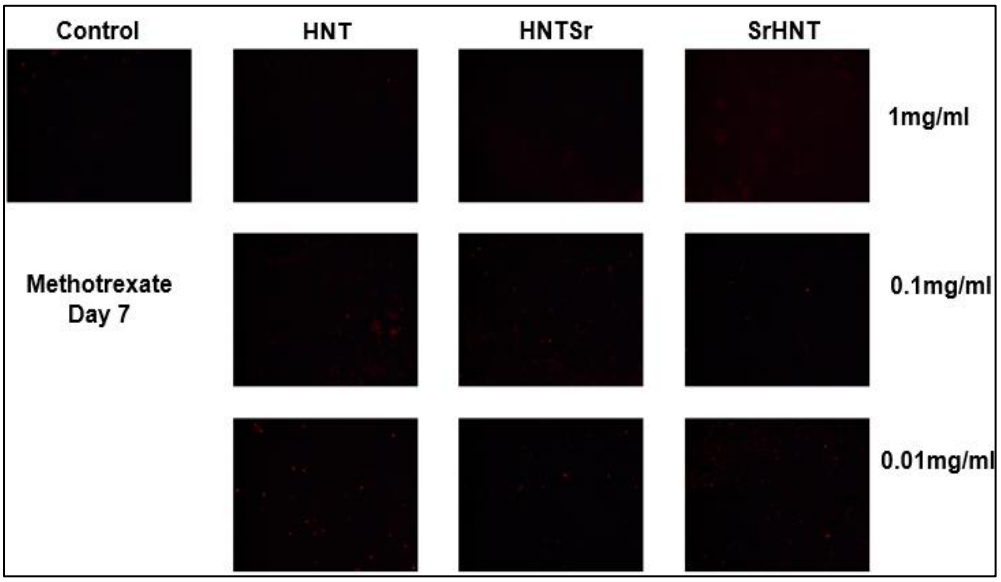

Figure 6-41 B: Live dead cell assay where the dead cells are seen in red for 3 different concentrations of HNT, HNTSr, and SrHNT for day 7.

Image J was used to quantitatively analyze the live dead assay and was graphically represent in **Figures 6-42 A** (1 mg/ml), **B** (0.1 mg/ml), and **C** (0.01 mg/ml).

As the graphs show the cell viability count on day three was highest for 0.01 mg/ml among all the concentrations. The control cells showed a decrease in growth by day 3 and then the cell showed increase in the live count by day 7. This can be explained that the drug methotrexate is light sensitive and hence the plates were wrapped in an aluminum foil when incubated. The cells may have taken a few days to get acclimatized to the environment. Overall SrHNT showed better cell viability in all the concentration. Coating HNTs with Sr may provide a layer that effects the cells in a positive manner. One-way Anova showed no significant difference between the samples.

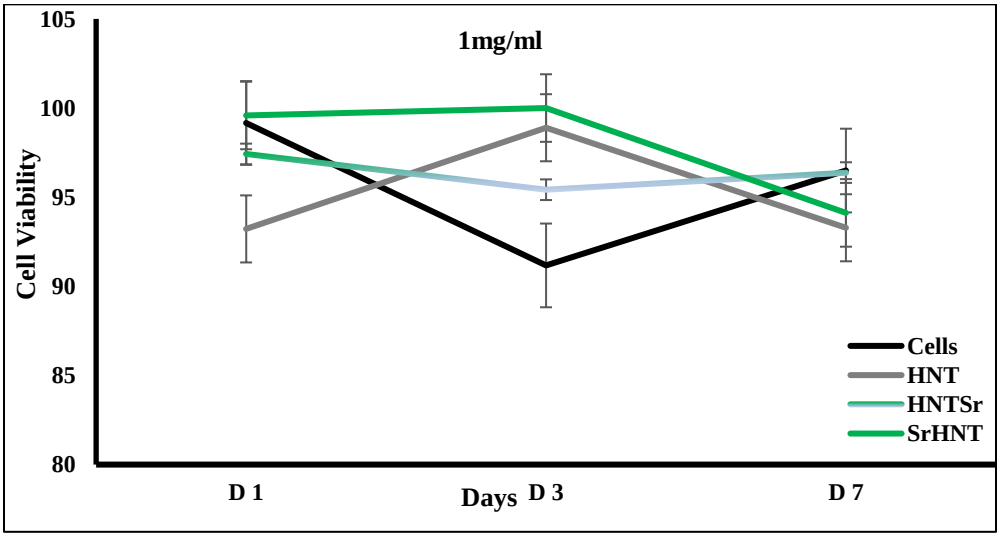

Figure 6-42 A: Graphical representation of Live dead cell assay of HNT, HNTSr, and SrHNT for 1 mg/ml for day 1, 3, and 7 where n=3 and error bars are Standard deviation.

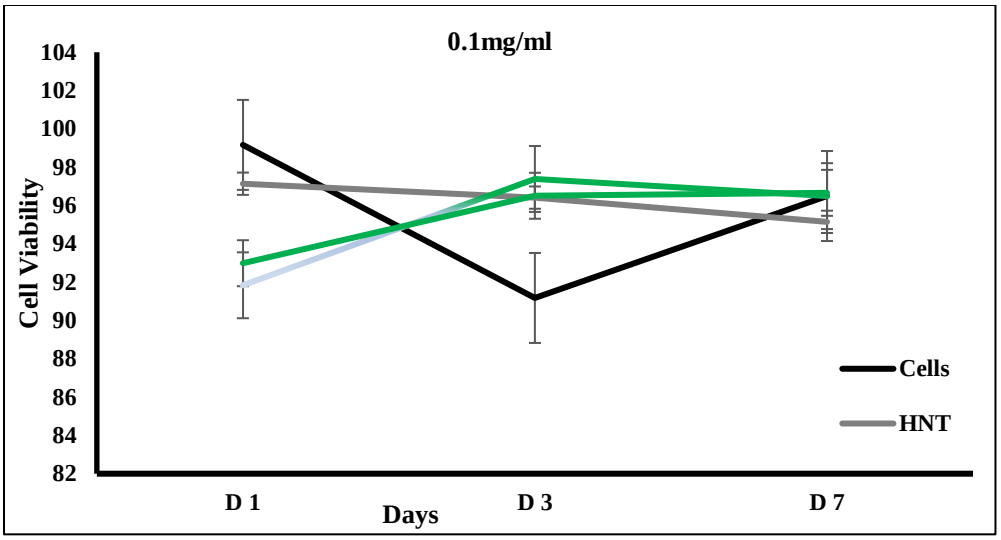

Figure 6-42 B: Graphical representation of Live dead cell assay of HNT, HNTSr, and SrHNT for 0.1 mg/ml for day 1, 3, and 7 where n=3 and error bars are Standard deviation.

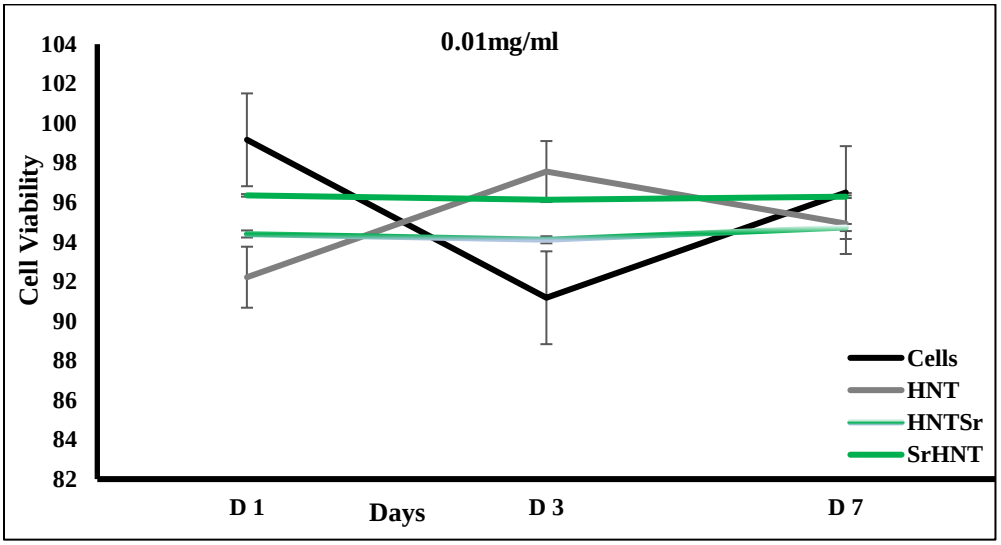

Figure 6-42 C: Graphical representation of Live dead cell assay of HNT, HNTSr, and SrHNT for 0.01 mg/ml for day 1, 3, and 7 where n=3 and error bars are Standard deviation.

6.3.3.2 *Drug Loaded Nanoparticles in CRL 2836 Cell*

The release and effectiveness of methotrexate loaded SrHNT and HNTSr was tests in a cell environment (mouse bone cancer cells). After inoculating the cells with the

bacteria live dead assay was performed on day 1 and day 3 to visualize the effectiveness of drug release and cell death. The images were taken as seen in **Figure 6-43 A** (live cells), and **B** (dead cells) with osteosarcoma cells, cells with methotrexate, and cells with the three loaded HNTs, SrHNT, and HNTSr individually. As seen in the images, cancer cells are only able to survive when there is no methotrexate or drug loaded nanoparticles. The presence of methotrexate loaded HNT, SrHNT, and HNTSr caused a higher cell death seen in red in the images of dead cells after 3 days. The live cells were also lower after day three.

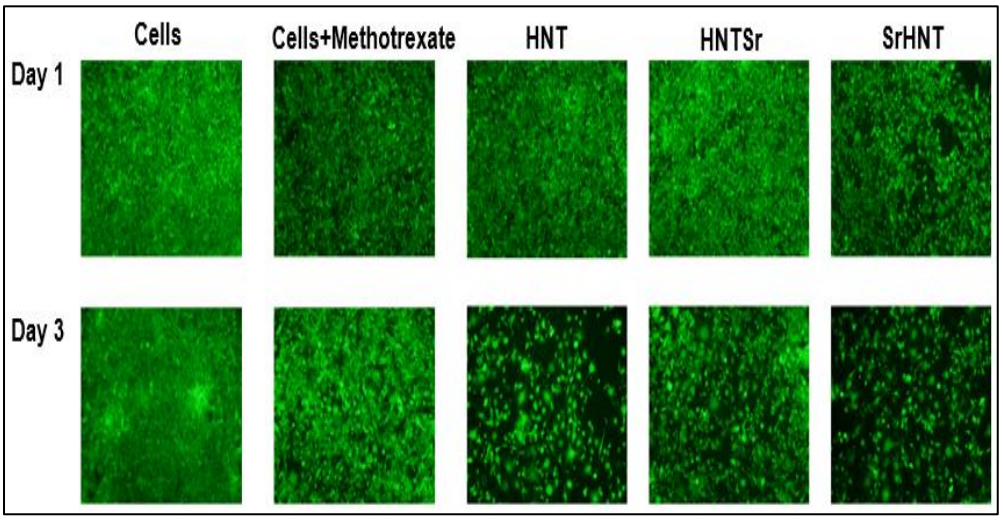

Figure 6-43 A: Live dead assay where the live osteosarcoma cells are seen in green for day 1 and 3.

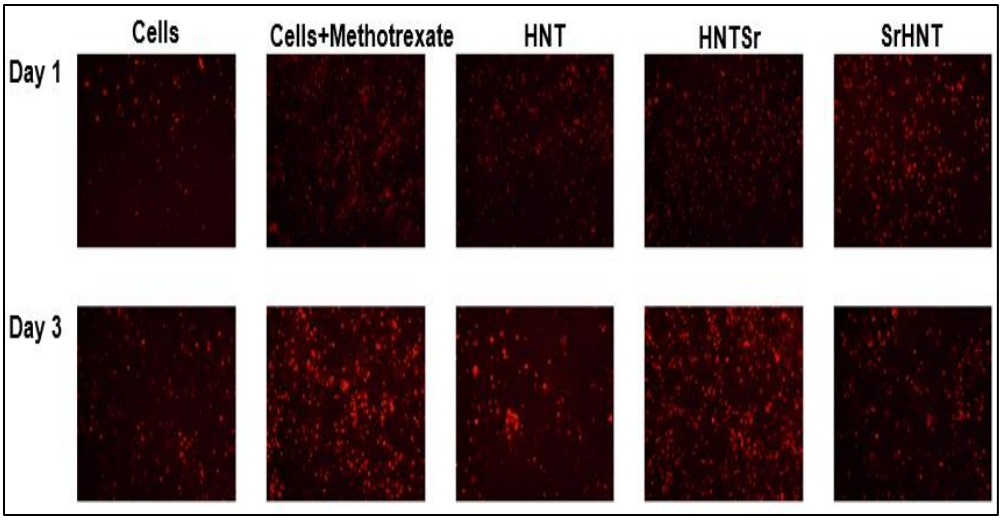

Figure 6-43 B: Live dead assay where the dead osteosarcoma cells are seen in red for day 1 and 3.

6.3.3.3 *Proliferation Assay for Osteosarcoma Cells*

To evaluate the effectiveness of drug release from the nanoparticle's proliferation assay was conducted. In case of osteosarcoma cells, where lower the cell proliferation higher the expectancy from the SrHNTs and HNTSr to be successful in releasing chemotherapeutic drugs on the cancerous sites. This drug loaded nanoparticles can also be embedded in bone implants where the bone is replaced due to cancer. The cell proliferation was plotted in a graph as seen in **Figure 6-44**. The proliferation assay shows that osteosarcoma cells have an increasing rate of proliferation on day and day 7.

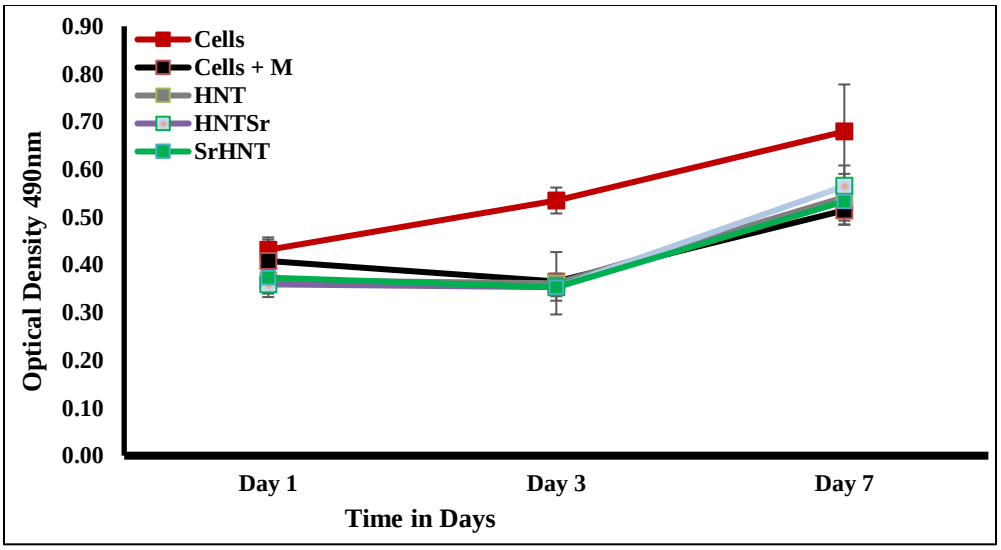

Figure 6-44: Graphical representation of the osteosarcoma cell proliferation assay for day 1, 3, and 7. Error bars are Standard deviation. n=5.

Adding methotrexate directly and through loaded HNTs, SrHNTs, and HNTSr reduced the rate of proliferation on day 3 and the rate was lower on day 7 when compared to just cells. This can be explained due to the media change every 2 days that can be the cause of removal of the drugs released and present in the wells. Overall methotrexate loaded SrHNT and HNTSr released the drug and resulted in osteosarcoma cell death.

CHAPTER 7

CONCLUSIONS AND FUTURE WORK

Projects 1, 2, and 3 discussed the tests and results of interrelated concepts and novel applications of green SrHNTs in CPC and as drug carriers. This chapter synthesizes the recorded observations and integrates them. Plan for future direction of this work is also provided.

7.1 Sr Coating on HNTs

Project 1 discussed in detail the successful coatings of HNT with Sr in testing of hypothesis that Sr can be coated on HNTs without the use of harsh chemical and producing any toxic waste. The observations from the results showed that the coating was successful. Live dead assay gave the appropriate quantities that could be applied to SrHNT to good cell viability. SrHNT was beneficial for cell proliferation in preosteoblast cells Micro-titration testing with nosocomial bacteria showed that and in limited quantities were beneficial for drug release and had inherent antibacterial properties. For future studies SrHNTs cell viability needs to tested in multiple cells lines. These studies will reveal the effectiveness of the SrHNT in various cell environments. The behavior of SrHNT and the pattern of proliferation can modify the utilization of SrHNTs in the body. This information can also provide information for further use of SrHNT in three dimensional constructs and implants.

7.2 Project 2: Embedding SrHNT in CPC for Bone Regeneration

Project 2 discussed in detail the tests conducted when SrHNT was embedded in different concentrations in CPC paste. The cell viability and proliferation tests showed that introducing SrHNT in CPC only enhanced the richness of cellular environment. Various histological staining for stromal cells and preosteoblast cells showed the addition of SrHNT increased Ca, acidic mucopolysaccharides production and the mechanical stress required for cells to increase the osteogenic lineage increased. Further tests have to be done to confirm the efficiency of SrHNTs in other cell lines. Disc diffusion analysis showed that CPCs with SrHNT had inherent antibacterial properties. The hypothesis that coating HNT with Sr will increase the compression and mechanical strength of CPC was accepted since the compression testing showed 5 times increase in mechanical strength when compared to plain CPC. Compression strength was maximum for 10% SrHNT in CPC and mechanical strength showed the maximum at 1% SrHNT in CPC. Further tests needs to be done to find the correct weight ratios of SrHNT and CPC so that the bone implant mimics the stress load it can take to that of natural human bones. SrHNTs in CPC caused prominent changes in the surface properties of CPC. Upon addition of SrHNT the surface was significantly modified which promotes better cell attachment and viability. Drug release from doped SrHNT and HNTSr was studied for 24 hours. Clear zones of inhibition were observed in *E. coli* and *S. aureus* cultures. Three-dimensional printed bone implants should have the capacity to encourage cell growth, increase the production of bone cells, have high compression strength to bear loads, and also prevent infection on the site of the implant. These implants should be biodegradable so that the bone cells can grow and overtake the implant material. Further tests need to be done to confirm the rate

of biodegradability in different Ph environment. Embedding drug loaded SrHNTs in the CPC paste used for printing the bone scaffolds is seen to have all those properties based on the results obtained so far.

7.3 Project 3: Using SrHNT as a Drug Carrier

Project 3 showed test and results in regards to the practical applications of drug loaded SrHNT and HNTSr in an infected cell environment and a cancerous cell environment. Two drugs gentamicin and methotrexate were loaded in SrHNT and HNTSr. The third hypothesis that the SrHNT will act a good drug carrier was accepted based on the results of tests done in this project. The drug release was tested in a cell environment contaminated with a nosocomial bacterial culture. SrHNT and HNTSr both effectively reduced the bacterial growth and showed no decrease in cell proliferation. The second test was done with a chemo drug loaded SrHNT and HNTSr and introduced to cancer cells. The test results showed that drug was effectively released and caused reduction in cell viability. Further tests have to be done with various other drugs. The drugs also should be tested in multiple cell environment.

Since new methods are needed for a more patient specific needs in the areas of bone grafts and drug delivery can use the product and concept from this research. SrHNTs can be used in 3D printed grafts and can be seeded with cells. These grafts can be used in patients to create a living graft. SrHNTs in various field has a great potential for bone and tissue engineering.

BIBLIOGRAPHY

1. X. Yuan, Y. Guo, and M. Rafailovich, "Flame Retardant Polymer Nanocomposites and Interfaces," *In Flame Retardants*, IntechOpen, 2019.

2. S. Crowe, F. John, P. S. Thomas, and B. Kahn, "Revision total hip arthroplasty: hospital cost and reimbursement analysis," *Clinical Orthopedics and Related Research®*, vol. 413, 175-182, 2003.

3. D. Nesteruk, K. Wertheim-Tysarowska, and J. Bal, "Cystic fibrosis emerging therapies," *Dev Period Med*, vol. 18, pp. 256-265, 2014.

4. M. Dobbelstein and U. Moll, "Targeting tumor-supportive cellular machineries in anticancer drug development," *Nat Rev Drug Discovery*, vol. 13, pp. 179-96, 2014.

5. F. Rowena, S. Gehlert, C. Jeanne, M. Edwina, S. Uehara, and J. H. Williams, "Reflections on the History of the Society for Social Work and Research, 2008–2018," *Journal of the Society for Social Work and Research* 10, no. 2, 189-211, 2019.

6. Y. Zhang, A. Tang, H.Yang, and J. Ouyang. "Applications and interfaces of halloysite nanocomposites," *Applied Clay Science*, 119: 8-17, 2016.

7. A. Glotov, A. Stavitskaya, A. Novikov, A. Semenov, E. Ivanov, P. Gushchin, Y. Darrat, V. Vinokurov, and Y. Lvov. "Halloysite Based Core-Shell Nanosystems: Synthesis and Application," *Nanomaterials from Clay Minerals*, pp. 203-256, Elsevier, 2019.

8. P. V. Strandmann, K. Philip, R. Hendry, J. Hatton, and L. Robinson, "The response of magnesium, silicon and calcium isotopes to rapidly uplifting and weathering terrains: South Island, New Zealand," *Frontiers in Earth Science*, 7: 240, 2019.

9. W. Ian, and J. Keeling, "Global occurrence, geology and characteristics of tubular halloysite deposits," *Clay Minerals*, vol 51, no. 3: 309-324, 2016.

10. M. Marina, C. G. Colletti, G. Lazzara, and S. Riela. "The use of some clay minerals as natural resources for drug carrier applications," *Journal of functional biomaterials*, vol 9, no. 4: 58, 2018.

11. A. Deniz, "Halloysite containing polyurethane foams as insulation materials with enhanced flame retardance," *PhD diss*, 2019.

12. K. Sandeep, M. Nehra, N. Dilbaghi, K. Tankeshwar, and K. H. Kim, "Recent advances and remaining challenges for polymeric nanocomposites in healthcare applications," *Progress in Polymer Science*, vol 80: 1-38, 2018.

13. M. Marina, F. Armetta, G. Cavallaro, D. F. C. Martino, M. Gruttadauria, G. Lazzara, S. Riela, and D. I. Marco, "Effect of halloysite nanotubes filler on polydopamine properties," *Journal of colloid and interface science*, vol 555: 394-402, 2019.

14. T. Karthik, U. M. Jammalamadaka, and D. K. Mills, "Formulation and evaluation of nanoenhanced anti-bacterial calcium phosphate bone cements," *Orthopedic Biomaterials*, pp 85-108, 2017.

15. U. M. Jammalamadaka, K. Tappa, J. A. Weisman, J. C. Nicholson, and D. K. Mills, "Effect of barium-coated halloysite nanotube addition on the cytocompatibility, mechanical and contrast properties of poly (methyl methacrylate) cement," *Nanotechnology, science and applications*, vol 10: 105, 2017.

16. K. Amelia, and M. Ahmad, "A review of cell adhesion studies for biomedical and biological applications," *International journal of molecular sciences*, vol 16, no 8: 18149-18184, 2015.

17. C. Hsin, and Y. Wang, "Cell responses to surface and architecture of tissue engineering scaffolds," *Regenerative medicine and tissue engineering-cells and biomaterials*, 2011.

18. F. Rawil, and Y. M. Lvov, "Halloysite clay nanotubes for tissue engineering," vol 2246, 2016.

19. S. C. Ana, C. Ferreira, F. Veiga, A. J. Ribeiro, A. Panchal, Y. Lvov, and A. Agarwal, "Halloysite clay nanotubes for life sciences applications: From drug encapsulation to bioscaffold," *Advances in colloid and interface science*, vol 257: 58-70, 2018.

20. N. T. Anh, and A. A. Assadi, "Smart Nanocontainers: Preparation, Loading/Release Processes and Applications." *Kenkyu Journal of Nanotechnology and Nanoscience*, vol 4: 1-6, 2018.

21. T. Evgenya, E. Naumenko, E, Rozhina, F. Akhatova, and R. Fakhrullin," Cytocompatibility and uptake of polycations-modified halloysite clay nanotubes," *Applied Clay Science*, vol 169: 21-30, 2019.

22. W. Y. Chun, J. Martinez, and C. R. Dass, "Oral delivery of insulin for treatment of diabetes: status quo, challenges and opportunities," *Journal of Pharmacy and Pharmacology*, vol 68, pp 9: 1093-1108, 2016.

23. K. Amelia, and M. Ahmad, "A review of cell adhesion studies for biomedical and biological applications," *International journal of molecular sciences*, vol 16, no. 8: 18149-18184, 2015.

24. C. Vinatier, and J. Guicheux, “Cartilage tissue engineering: From biomaterials and stem cells to osteoarthritis treatments,” *Annals of physical and rehabilitation medicine*, vol *59*(3), pp 139-144, 2015.

25. D. N. Elumalai, Y. Lvov, and P. Derosa. "Implementation of a simulation model of the controlled release of molecular species from halloysite nanotubes," *Journal of Encapsulation and Adsorption Sciences*, vol 5, pp 0: 74, 2015.

26. D. N. Elumalai, "Tunable controlled release of molecular species from Halloysite nanotubes," PhD Diss, 2016.

27. A. Lisa, C. Gallina, V. Turinetto, and C. Giachino, "Stem cell tracking with nanoparticles for regenerative medicine purposes: an overview," *Stem cells international*, 2016.

28. Y. Moran, R. Feiner, and T. Dvir, "Gold nanoparticle-integrated scaffolds for tissue engineering and regenerative medicine," *Nano letters*, vol 19, no 4: 2198-2206, 2019.

29. A. A. Dayem, H. Y. Choi, K. Kim, K. Saha, S. H. Kim, and S. G. Cho, “The potential of nanoparticles in stem cell differentiation and further therapeutic applications,” *Biotechnol Journal*, vol 11: 1550–1560, 2016.

30. Q. Wang, B. Chen, M. Cao, and J. Sun, “Response of MAPK pathway to iron oxide nanoparticles in vitro treatment promotes osteogenic differentiation of hBMSCs,” *Biomaterials*, vol 86: 11–20, 2016.

31. G. Franci, A. Falanga, M. Rai, G. G. Morelli, S. Galdiero, L. Palomba, G. Galdiero, “Silver nanoparticles as potential antibacterial agents,” *Molecules*, vol 20: 8856-8874, 2015. doi:10.3390/molecules20058856

32. R. Zhang, P. Lee, V. C. Lui, and Y. Chen, “Silver nanoparticles promote osteogenesis of mesenchymal stem cells and improve bone fracture healing in osteogenesis mechanism mouse model,” *Nanomed Nanotechnol Biol Med*, vol 11: 1949–1959, 2015.

33. H. Qin, C. Zhu, Z. An, Y. Jiang, J. Zhao, J. Wang, and Y. Wang, “Silver nanoparticles promote osteogenic differentiation of human urine-derived stem cells at noncytotoxic concentrations,” *International Journal of Nanomedicine*, vol 9: 2469–2478, 2016. http://doi.org/10.2147/IJN.S59753

34. H. W. Zhang, F. Meng F, J. Guo, D. Wang, S. Qian, X. Jiang, X. Liu, and P. K. Chu, “Osteogenesis catalyzed by titanium-supported silver nanoparticles,” *ACS Appl Mater Interfaces*, vol 9(6):5149-5157, 2017. doi: 10.1021/acsami.6b15448.

35. S. Val, R. L. Reid, and M. Oliveira, “Recent advances using gold nanoparticles as a promising multimodal tool for tissue engineering and regenerative medicine,” *Current Opinion in Solid State and Materials Science*, vol 21(2): 92-112, 2017.

36. D. Zhang, D. Liu, J. Zhang, C. Fong, and M. Yang, “Gold nanoparticles stimulate differentiation and mineralization of primary osteoblasts through the ERK/MAPK signaling pathway,” *Mater Sci Eng*, vol 42:70–77, 2014.

37. C. Yi, D. Liu, C. Fong, J. Zhang, and M. Yang, “Gold nanoparticles promote osteogenic differentiation of mesenchymal stem cells through p38 MAPK pathway,” *ACS Nano*, vol 4: 6439–6448, 2010.

38. R. Ravichandran, R. Sridhar, J. R. Venugopal, and S. Sundarrajan, “Gold nanoparticle loaded hybrid nanofibers for cardiogenic differentiation of stem cells for infarcted myocardium regeneration,” *Macromol Biosci*, vol 14: 515–525, 2014.

39. K. Baranes, M. Shevach, O. Shefi, and T. Dvir, “Gold nanoparticle-decorated scaffolds promote neuronal differentiation and maturation,” *Nano Letter*, vol 11;16(5):2916-2, 2016. doi: 10.1021/acs.nanolett.5b04033.

40. Z. Xiang, K. Wang, and W. Zhang, “Gold nanoparticles inducing osteogenic differentiation of stem cells: a review,” *J Cluster Sci*, vol 1: 29, 2018.

41. S. Narayanan, S. Park, and M. H. Lee, “Surface modification of magnesium and its alloys for biomedical applications: opportunities and challenges. Biological Interactions, Mechanical Properties and Testing,” *Elsevier*, 2015.

42. Q. Wang, L. Xie, Z. He, D. Di, and J. Liu, “Biodegradable magnesium nanoparticle-enhanced laser hyperthermia therapy,” *International Journal of Nanomedicine*, vol 7: 4715, 2012.

43. M. S. Fazliah, M. M. Yusuf, T. K. Abdullah, and H. Zuhailawati, “Human mesenchymal stem cells response to magnesium-based biomaterials,” *Procedia Chemistry*, vol 19: 75-82, 2016.

44. T. Y. Nguyen, S. Garcia, C. G. Liew, and H. Liu, “Effects of magnesium on growth and proliferation of human embryonic stem cells,” *Engineering in Medicine and Biology Society*, Annual International Conference of the IEEE, pp. 723-726, 2012.

45. J. M. Diaz-Tocados, C. Herencia, J. M. Martinez-Moreno, A. M. DeOca, M. E. Rodriguez-Ortiz, N. Vergara, and J. R. Munoz-Castaneda, “Magnesium Chloride promotes Osteogenesis through Notch signaling activation and expansion of Mesenchymal Stem Cells,” *Scientific reports*, vol 7(1): 7839, 2017.

46. T. G. Baboolal, C. Simon, C. Mastbergen, E. Jones, J. C. Stuart, P. J. Floris, K. Lafeber, and D. McGonagle, "Synovial fluid hyaluronan mediates MSC attachment to cartilage, a potential novel mechanism contributing to cartilage repair in osteoarthritis using knee joint distraction," *Annals of the rheumatic diseases*, vol 75, no. 5: 908-915, 2015.

47. X. Zhang, H. Zu, D. Zhao, K. Yang, S. Tian, X. Yu, and F. Lu, "Ion channel functional protein kinase TRPM7 regulates Mg ions to promote the osteoinduction of human osteoblast via PI3K pathway: In vitro simulation of the bone-repairing effect of Mg-based alloy implant," *Acta biomaterialia*, vol 63: 369-382, 2017.

48. J. Chou, J. Hao, H. Hatoyama, B. Ben-Nissan, B. Milthorpe, and M. Otsuka, "Effect of biomimetic zinc-containing tricalcium phosphate (Zn–TCP) on the growth and osteogenic differentiation of mesenchymal stem cells," *Journal of tissue engineering and regenerative medicine*, vol 9(7): 852-858, 2015.

49. Y. Qiao, W. Zhang, P. Tian, F. Meng, H. Zhu, X. Jiang, and P. K. Chu, "Stimulation of bone growth following zinc incorporation into biomaterials," *Biomaterials*, 35(25): 6882-6897, 2014.

50. H. J. Seo, Y. E. Cho, T. Kim, H. I. Shin, and I. S. Kwun, "Zinc may increase bone formation through stimulating cell proliferation, alkaline phosphatase activity and collagen synthesis in osteoblastic MC3T3-E1 cells," *Nutrition research and practice*, vol 4(5): 356-361, 2010.

51. J. Yu, L. Xu, K. Li, N. Xie, Y. Xi, Y. Wang, and X. Ye, "Zinc-modified calcium silicate coatings promote osteogenic differentiation through TGF-β/Smad pathway and osseointegration in osteopenic rabbits," *Scientific Reports*, vol 7(1): 3440, 2017.

52. M. Y. Moon, H. J. Kim, B. Y. Choi, M. Sohn, T. N. Chung, and S. W. Suh, "Zinc Promotes Adipose-Derived Mesenchymal Stem Cell Proliferation and Differentiation towards a Neuronal Fate," *Stem cells international*, 2018.

53. E. Fathi, R. Farahzadi, "Enhancement of osteogenic differentiation of rat adipose tissue-derived mesenchymal stem cells by zinc sulphate under electromagnetic field via the PKA, ERK1/2 and Wnt/β-catenin signaling pathways," *PloS one*, vol 12(3), e0173877, 2018.

54. T. Wang, J. C. Zhang, Y. Chen, P. G. Xiao, and M. S. Yang, "Effect of zinc ion on the osteogenic and adipogenic differentiation of mouse primary bone marrow stromal cells and the adipocytic trans-differentiation of mouse primary osteoblasts," *Journal of Trace Elements in Medicine and Biology*, vol 21(2): 84-91, 2007.

55. F. Yang, D. Yang, J. Tu, Q. Zheng, L. Cai, and L. Wang, "Strontium enhances osteogenic differentiation of mesenchymal stem cells and in vivo bone formation by activating Wnt/catenin signaling," *Stem cells*, vol 29(6): 981-991, 2011.

56. C. Clément, L. Xiao, W. R. Carl, F. Benoit, and K. Behnia. "Metallicity and superconductivity in doped strontium titanate." *Annual Review of Condensed Matter Physics*, vol 10: 25-44, 2019.

57. S. Takaoka, T. Yamaguchi, S. Yano, M. Yamauchi, and T. Sugimoto, “The Calcium-sensing Receptor (CaR) is involved in strontium ranelate-induced osteoblast differentiation and mineralization,” *Hormone and metabolic research*, vol 42(09): 627-63, 2010.

58. F. Louis, W. Bouleftour, A. Rattner, M. T. Linossier, L. Vico, and A. Guignandon, “RhoGTPase stimulation is associated with strontium chloride treatment to counter simulated microgravity-induced changes in multipotent cell commitment.,” *NPJ Microgravity*, vol 3(1): 7, 2017.

59. A. Aimaiti, A. Maimaitiyiming, X. Boyong, K. Aji, C. Li, and L. Cui, “Low-dose strontium stimulates osteogenesis but high-dose doses cause apoptosis in human adipose-derived stem cells via regulation of the ERK1/2 signaling pathway,” *Stem cell research & therapy*, vol 8(1): 282, 2017.

60. S. Peng, G. Zhou, K. D. Luk, K. M. Cheung, Z. Li, W. M. Lam, and W. W. Lu, “Strontium promotes osteogenic differentiation of mesenchymal stem cells through the Ras/MAPK signaling pathway,” *Cellular Physiology and Biochemistry*, vol 23(1-3): 165-174, 2009.

61. G. Colin, A. Gennady, and G. C. Dismukes, "The strontium inorganic mutant of the water oxidizing center (CaMn4O5) of PSII improves WOC efficiency but slows electron flux through the terminal acceptors," *Biochimica et Biophysica Acta (BBA)-Bioenergetics*, vol 1857, no. 9: 1550-1560, 2016.

62. G. Silva, A. Borges, B. M. Bertassoli, C. A. Sousa, J. D. Albergaria, R. S. Paula, and E. C. Jorge, "Effects of strontium ranelate treatment on osteoblasts cultivated onto scaffolds of trabeculae bovine bone," *Journal of bone and mineral metabolism*, vol 36, no. 1: 73-86, 2018.

63. A. Almeida, M. Marletti, E. P. Nani, L. N. Teixeira, D. C. Peruzzo, J. C. Joly, M. H. Napimoga, and E. F. Martinez. "Strontium ranelate increases osteoblast activity," *Tissue and Cell*, vol 48, no. 3: 183-188, 2016.

64. S. Agrawal, M. Kelkar, A. De, A. R. Kulkarni, and M. N. Gandhi, "Surfactant free novel one-minute microwave synthesis, characterization and cell toxicity study of mesoporous strontium hydroxyapatite nanorods," *RSC Advances*, vol 6, no. 97: 94921-94926, 2016.

65. R. Jah, C. Vana, N. N. Devi, N. Khongthaw, D. Syiem, and S. Majaw, "Evaluation of the antidiabetic property of aqueous leaves extract of Zanthoxylum armatum DC. using in vivo and in vitro approaches," *Journal of traditional and complementary medicine*, vol 8, no. 1: 134-140, 2018.

66. R. A. Field, M. L. Riley, F. C. Mello, J. H. Corbridge, and A. W. Kotula, "Bone composition in cattle, pigs, sheep and poultry," *Journal of Animal Science*, vol 39, no. 3: 493-499, 1974.

67. S. P. Nielsen, "The biological role of strontium," *Bone*, vol 35, no. 3: 583-588, 2005.

68. G. Oumaima, S. Thomas, C. Smith, and N. Birbilis. "Chromate replacement: what does the future hold?" *NPJ Materials Degradation*, vol 2, no. 1: 12, 2018.

69. G. Christian, H. N. McMurray, and G. Williams, "An Investigation of Zinc Based Polyphosphates as Corrosion Inhibitors for Use in Organically Coated Steel," *Meeting Abstracts*, no. 14, pp. 1348-1348, The Electrochemical Society, 2016.

70. L. Tiancheng, W. Liang, L. Li, X. Cui, X. Wei, H. Pan, and B. Li, "Novel calcitonin gene-related peptide/chitosan-strontium-calcium phosphate cement: Enhanced proliferation of human umbilical vein endothelial cells in vitro," *Journal of Biomedical Materials Research Part B: Applied Biomaterials*, vol 107, no. 1: 19-28, 2019.

71. N. Alexandru, V. Danila, E. Dragan, S. Pasca, A. Nemtoi, M. Constantin, A. Sava, and D. Haba, "The Effects of Insulin and Strontium Ranelate on Guided Bone Regeneration in Diabetic Rats," *Rev Chim (Bucharest)*. vol 68: 693-697, 2017.

72. A. Lode, C. Heiss, G. Knapp, J. Thomas, B. Nies, M. Gelinsky, and M. Schumacher, "Strontium-modified premixed calcium phosphate cements for the therapy of osteoporotic bone defects," *Acta biomaterialia*, vol 65: 475-485, 2018.

73. K. Ayesha, "Review on polymer/halloysite nanotube nanocomposite," *Polymer-Plastics Technology and Engineering*, vol 57, no. 6: 548-564, 2018.

74. P. Uresha, L. M. Pellizzeri, M. Kazi, Z. Hossain, E. Brigitte, Scammell, M. D. Grant, A. C. Scotchford, and A. C. Hannon, "In vitro cellular testing of strontium/calcium substituted phosphate glass discs and microspheres shows potential for bone regeneration," *Journal of tissue engineering and regenerative medicine*, 2019.

75. T. Ulrich, S. Ray, U. Sommer, T. ElKhassawna, T. Rehling, M. Hundgeburth, and A. Henb, "Bone formation induced by strontium modified calcium phosphate cement in critical-size metaphyseal fracture defects in ovariectomized rats," *Biomaterials*, vol 34, no. 34: 8589-8598, 2013.

76. K. Y. Chih, and C. W. Chen, "Neuroregeneration of induced pluripotent stem cells in polyacrylamide-chitosan inverted colloidal crystal scaffolds with poly (lactide-co-glycolide) nanoparticles and transactivator of transcription von Hippel-Lindau peptide," *Tissue Engineering*, vol Part A 23, no. 7-8: 263-274, 2017.

77. M. Massaro, C. G. Colletti, G. Lazzara, S. Milioto, R. Noto, and S. Riela, "Halloysite nanotubes as support for metal-based catalysts," *Journal of Materials Chemistry*, vol A 5, no. 26: 13276-13293, 2017.

78. P. Shraddha, U. Jammalamadaka, L. Sun, K. Tappa, and D. Mills. "Sustained release of antibacterial agents from doped halloysite nanotubes," *Bioengineering*, vol 3, no. 1: 1, 2016.

79. M. Ali, Z. Hajizadeh, and R. Firouzi-Haji, "Eco-friendly functionalization of magnetic halloysite nanotube with SO3H for synthesis of dihydropyrimidinones," *Microporous and Mesoporous Materials*, vol 259: 46-53, 2018.

80. Y. Zhang, A. Tang, H. Yang, and J. Ouyang, "Applications and interfaces of halloysite nanocomposites," *Applied Clay Science*, vol 119: 8-17, 2016.

81. J. Jiao, J. Ouyang, and H. Yang, "Pd nanoparticles and MOFs synergistically hybridized halloysite nanotubes for hydrogen storage," *Nanoscale research letters*, vol 12, no. 1: 240, 2017.

82. P. Pooria, R. DeSilva, V. Vahedi, and G. J. Churchman, "Halloysite nanotubes: prospects and challenges of their use as additives and carriers–A focused review," *Clay Minerals*, vol 51, no. 3: 479-487, 2016.

83. L. Geyuan, J. Zha, M. Niu, F. Hu, X. Hui, T. Tang, M. Fizir, and H. He, "Bifunctional monomer molecularly imprinted sol-gel polymers based on the surface of magnetic halloysite nanotubes as an effective extraction approach for norfloxacin," *Applied Clay Science*, vol 162: 409-417, 2018.

84. G. Danyi, J. Chen, K. Hou, S. Xu, J. Cheng, X. Wen, S. Wang, C. Huang, and P. Pi, "A facile preparation of superhydrophobic halloysite-based meshes for efficient oil–water separation," *Applied Clay Science*, vol 156: 195-201, 2018.

85. D. Papoulis, "Halloysite based nanocomposites and photocatalysis: A Review," *Applied Clay Science* vol 168: 164-174, 2018.

86. N. Reddy, K. S. Gangi, K. M. Rao, S. Y. Park, T. Kim, and I. Chung, "Fabrication of Aminosilanized Halloysite Based Floating Biopolymer Composites for Sustained Gastro Retentive Release of Curcumin," *Macromolecular Research*, vol 27, no. 5: 490-496, 2019.

87. Y. Zhang, X. He, J. Ouyang, and H. Yang. "Palladium nanoparticles deposited on silanized halloysite nanotubes: synthesis, characterization and enhanced catalytic property," *Scientific reports*, vol 3: 2948, 2013.

88. N. James, J. Weisman, C. Boyer, C. Wilson, and D. Mills, "Dry sintered metal coating of halloysite nanotubes," *Applied Sciences*, vol 6, no. 9: 265, 2016.

89. J. Udayabhanu, K. Tappa, and D. K. Mills, "Calcium phosphate/clay nanotube bone cement with enhanced mechanical properties and sustained drug release," *Current Topics in the Utilization of Clay in Industrial and Medical Applications*, IntechOpen, 2018.

90. G. Maria-Pau, M. Espanol, Y. Maazouz, V. Bergez, and D. Pastorino, "Bioceramics and bone healing," *EFORT open reviews*, vol 3, no. 5: 173-183, 2018.

91. M. Chris, and P. Dunnill, "A brief definition of regenerative medicine," pp 1-5, 2008.

92. T. Claire, T. M. Haanstra, C. S. Leichtenberg, S. H. Verdegaal, R. W. Ostelo, C. W. Henrica-deVet, R. Nelissen, and T. V. Vlieland, "Unfulfilled expectations after total hip and knee arthroplasty surgery: there is a need for better preoperative patient information and education," *The Journal of arthroplasty*, vol 31, no. 10: 2139-2145, 2010.

93. L. Tie, Z. Li, Q. Su, and Y. Hai, "Cement leakage in osteoporotic vertebral compression fractures with cortical defect using high-viscosity bone cement during unilateral percutaneous kyphoplasty surgery," *Medicine*, vol 96, no. 25, 2017.

94. K. S. Bong, Y. J. Kim, T. L. Yoon, S. A. Park, I. H. Cho, E. J. Kim, I. A. Kim, and J. W. Shin, "The characteristics of a hydroxyapatite–chitosan–PMMA bone cement," *Biomaterials*, vol 25, no. 26: 5715-5723, 2004.

95. B. Andreas, M. Bohner, P. Heini, S. Verrier, and E. Schneider, "Properties of an injectable low modulus PMMA bone cement for osteoporotic bone." *Journal of Biomedical Materials Research Part B: Applied Biomaterials: An Official Journal of The Society for Biomaterials, The Japanese Society for Biomaterials, and The Australian Society for Biomaterials and the Korean Society for Biomaterials*, vol 86, no. 2: 474-482, 2008.

96. W. Jeffery, U. Jammalamadaka, K. Tappa, and D. Mills, "Doped halloysite nanotubes for use in the 3D printing of medical devices," *Bioengineering*, vol 4, no. 4: 96, 2017.

97. K. Amelia, and M. Ahmad, "A review of cell adhesion studies for biomedical and biological applications," *International journal of molecular sciences*, vol 16, no. 8: 18149-18184, 2015.

98. C. Hsin-I, and Y. Wang, "Cell responses to surface and architecture of tissue engineering scaffolds," In *Regenerative medicine and tissue engineering-cells and biomaterials*, InTechOpen, 2011.

99. Z. Xingjie, P. Sitasuwan, S. Feng, and Q. Wang, "Effect of roughness on in situ biomineralized CaP-collagen coating on the osteogenesis of mesenchymal stem cells," *Langmuir*, vol 32, no. 7: 1808-1817, 2016.

100. D. K. Mills, "The role of polymer additives in enhancing the response of calcium phosphate cement," In *Orthopedic Biomaterials*, pp. 345-379, Springer, 2018.

101. D. Isabelle, and L. T. Kuhn, "Design and characterization of calcium phosphate ceramic scaffolds for bone tissue engineering," *Dental Materials*, vol 32, no. 1: 43-53, 2016.

102. M. J. Munita, and C. A. Arias, "Mechanisms of antibiotic resistance," *Microbiology spectrum*, vol 4, no. 2, 2016.

103. D. Ruiz, L. Koeinig, T. Dall, P. Gallo, A. Narzikul, P. Parvizi, and J. Tongue, "The direct and indirect costs to society of treatment for end-stage knee osteoarthritis," *J Bone Joint Surg Am*, vol 95: 1473-80, 2013.

104. D. Romano, N. Romano, L. Logoluso, and L. Drago, "Bone and joint infections in adults: a comprehensive classification proposal," *Eur Orthop Traumatol*, vol 1 no. 6, pp. 207–217, 2011.

105. P. Bejon, and E. Robinson, "Bone and joint infection," *Medicine*, vol 41, no. 12, pp. 719-722, 2013.

106. C. J. Ward, C. L. Romano, D. R. Hurtgen, S. K. Hardy, R. L. Woodbury, A. V. Trevino, C. R. Rathbone, and J. C. Wenke, "Staphylococcus aureus biofilms decrease osteoblast viability, inhibits osteogenic differentiation, and increases bone resorption *in vitro*," *BMC Musculoskel Dis*, vol 14:187, 2013.

107. J. Hatzenbueler, T. J. Pulling, "Diagnosis and management of osteomyelitis," *Am Fam Physician*, vol 84(9): 1027-1033, 2011.

108. L. Dijkshoorn, A. Nemec, and H. Seifert, "An increasing threat in hospitals: Multidrug-resistant Acinetobacter baumannii," *Nat. Rev. Microbiol*, vol 5, no. 12, pp 939, 2007.

109. R. J. Turner, "Metal-based antimicrobial strategies," *Micro Biotechnol*, vol. 10, no. 5, pp 1062–1065, 2017.

110. Y. N. Slavin, J. Asnis, U. O. Häfeli, and H. Bach, "Metal nanoparticles: Understanding the mechanisms behind antibacterial activity," *J. Nanobiotechnology*, vol 15, no. 1, pp 65, 2017.

111. F. Paladini, M. Pollini, A. Sannino, and L. Ambrosio, "Metal-based antibacterial substrates for biomedical applications," *Biomacromolecules*, vol. 16, no. 7, pp. 1873–1885, 2015.

112. A. Ewald, S. K. Gluckermann, R. Thull, and U. Gbureck, "Antimicrobial titanium/silver PVD coatings on titanium," *Biomed Eng Online*, vol 5, no. 1, pp 22, 2006.

113. H. Cheng, W. Xiong, Z. Fang, H. Guan, W. Wu, Y. Li, Y. Zhang, M. M. Alvarez, B. Gao, K. Huo, J. Xu, "Strontium (Sr) and silver (Ag) loaded nanotubular structures with combined osteoinductive and antimicrobial activities," *Acta Biomater*, vol 31, pp 388–400, 2016.

114. K. Memarzadeh, A. S. Sharili, J. Huang, S. C. F. Rawlinson, and R. P. Allaker, “Nanoparticulate zinc oxide as a coating material for orthopedic and dental implants,” *J Biomed Mater Res*, vol 103, no. 3, pp 981–989, 2015.

115. Y. Z. Wan, S. Raman, F. He, and Y. Huang, “Surface modification of medical metals by ion implantation of silver and copper,” *Vacuum*, vol 81, no. 9, pp 1114–1118, 2007.

116. C. S. Ciobanu, S. L. Iconaru, M. C. Chifiriuc, A. Costescu, P. LeCoustumer, D. Predoi, "Synthesis and antimicrobial activity of silver-doped hydroxyapatite nanoparticles," *Biomed Res Int 2013*, 2013.

117. J. A. Garza-Cervantes, A. Chávez-Reyes, and E. C. Castillo, “Synergistic antimicrobial effects of silver/transition-metal combinatorial treatments,” *Sci Rep*, vol 7(1): 903, 2017.

118. M. Y. Vaidya, A. J. McBain, J. A. Butler, C. E. Banks, and K. A. Whitehead, “Antimicrobial efficacy and synergy of metal ions against enterococcus faecium, klebsiella pneumoniae and acinetobacter baumannii in planktonic and biofilm phenotypes,” *Sci Rep*, vol 7(1): 5911, 2017.

119. P. A. Patil, B. R. Bhutkar, Y.D. Dange, and S. V. Kharat, “Screening of most effective nano metal between AgNP, CuNP and Ag-Cu NP’s synergistic by In vitro antibacterial comparison,” *J Nanomed Nanotechnol*, vol 7(353): 2, 2017.

120. S. Katva, S. Das, H. S. Moti, A. Jyoti, and S. Kaushik, “Antibacterial synergy of silver nanoparticles with gentamicin and chloramphenicol against Enterococcus faecalis,” *Pharmacogn Mag*, vol 13(Suppl 4): S828, 2017.

121. I. Hwang, J. H. Hwang, H. Choi, K. J. Kim, and D. G. Lee, “Synergistic effects between silver nanoparticles and antibiotics and the mechanisms involved,” *J Med Microbiol*, vol 61(12): 1719-1726, 2012.

122. M. Mohiti-Asli, B. Pourdeyhimi, and E. G. Loboa, “Novel, silver-ion-releasing nanofibrous scaffolds exhibit excellent antibacterial efficacy without the use of silver nanoparticles,” *Acta Biomater*, vol 10(5):2096-2104, 2014.

123. L. Yu, Y. Zhang, B. Zhang, and J. Liu J, “Enhanced antibacterial activity of silver nanoparticles/halloysite nanotubes/graphene nanocomposites with sandwich-like structure,” *Sci Rep*, vol 4:4551, 2014.

124. P. Ducheyne, R. L. Mauck, and D. H. Smith, “Biomaterials in the repair of sports injuries,” *Nat Mater*, vol 11: 652–654, 2012.

125. J. P. Issa, M. Bentley, V. M. Iyomasa, and R. F. Sebald, “Sustained release carriers used to delivery bone morphogenetic proteins in the bone healing process,” *Anat Histol Embryol*, vol 37: 181– 187, 2008.

126. P. P. Hensleea, D. M. Specera, M. B. Yoona, V. V. Naira, and Meretoja, “Biodegradable composite scaffolds incorporating an intramedullary rod and delivering bone morphogenetic protein-2 for stabilization in segmental long bone defects,” *Acta Biomater,* vol 7: 3627–3637, 2011.

127. N. Tiffany, F. K. Kasper, and A. G. Mikos, “Strategies for controlled delivery of growth factors and cells for bone regeneration,” *Adv Drug Deliv Rev,* vol 64(12): 1292–1309, 2012.

128. V. Petrovic, P. Zivkovic, D. Petrovic, and V. Stefanovic, “Craniofacial bone tissue engineering,” *Dent Clin N Am,* vol 50: 175–190, 2006.

129. S. Karnik, and D. K. Mills, “Nanoenhanced hydrogel system with sustained release capabilities,” *J Biomed Mat,* vol 103(7): 2416-26, 2007.

130. S. Karnik, U. Jammalamadaka, K. Tappa, and D. K. Mills, “Performance evaluation of nanoclay enriched antimicrobial hydrogels for biomedical applications,” *Heliyon,* 2016.

131. V. Uskokovic, “Mechanism of Formation Governs the Mechanism of Release of Antibiotics from Calcium Phosphate Nanopowders and Cements in a Drug-Dependent Manne,” *Journal of Materials Chemistry B,* 2019.

132. S. Patel, U. Jammalamadaka, L. Sun, K. Tappa and D. K. Mills, “Sustained Release of Antibacterial Agents from Doped Halloysite Nanotubes,” *Bioengineering (Basel),* vol 3(1): 1, 2015.

133. W. Wei, R. Minullina, E. Abdullayev, R. Fakhrullin, D. K. Mills, Y. Lvov, “Enhanced efficiency of antiseptics with sustained release from clay nanotubes,” *RSC Adv*, vol 4: 488–94, 2014.

134. D. K. Mills, K. Tappa, U. Jammalamadaka, P. A. Mills, J. S. Alexander, J. A. Weisman, “Medical Applications for 3D Printing. In Advances in manufacturing and processing of materials and structures,” Chapter 8: Yoseph Bar-Cohen, CRC Press - Taylor & Francis Group, Boca Rotan, FL. Publication April 2018.

135. P. Randjelovic, V. Slavimir, S. Nenad, S. Dusan, and I. Ivan, "Gentamicin nephrotoxicity in animals: current knowledge and future perspectives," *EXCLI journal,* vol 16: 388, 2017.

136. A. V. Bassenden, R. Dmitry, S. Kun, and A. M. Berghuis, "Structural analysis of the tobramycin and gentamicin clinical resistome reveals limitations for next-generation aminoglycoside design," *ACS chemical biology*, vol 11, no. 5: 1339-1346, 2015.

137. B. Kushner, D. Paul, D. Allen, and B. T. Cran, "Frequency and demographics of gentamicin use," *Otology & neurotology: official publication of the American Otological Society, American Neurotology Society [and] European Academy of Otology and Neurotology*, vol 37, no. 2: 190, 2016.

138. S. Samantha, H. Ipema, P. Hartke, C. Krueger, R. Rodriguez, A. E. Gross, and M. Gabay, "Intravenous push administration of antibiotics: literature and considerations," *Hospital pharmacy*, vol 53, no. 3: 157-169, 2018.

139. A. N. Malaviya, "Landmark papers on the discovery of methotrexate for the treatment of rheumatoid arthritis and other systemic inflammatory rheumatic diseases: a fascinating story," *International journal of rheumatic diseases*, vol 19, no. 9: 844-851, 2016.

140. I. Pountos, and P. V. Giannoudis, "Effect of methotrexate on bone and wound healing," *Expert opinion on drug safety*, vol 16, no. 5: 53, 2017.